



The Application of Layered Double Hydroxide Nanoparticles (LDHs) as Potential Anticancer Drug Delivery Systems

Ms. Zoleka Mncwabe

A thesis submitted to the School of Life Sciences, University of KwaZulu-Natal, Westville in
fulfilment of the degree of Master of Science in Biochemistry.

Supervisor

Professor Moganavelli Singh

2016 Durban-Westville

**The Application of Layered Double Hydroxide Nanoparticles (LDHs) as Potential
Anticancer Drug Delivery Systems**

Ms. Zoleka Mncwabe

2016

A thesis submitted to the School of Life Sciences, University of KwaZulu-Natal, Westville, for the degree of Master of Science in Biochemistry.

This is a thesis in which the chapters are written as discreet research papers with an overall introduction and literature and a final conclusion. These chapters are to be submitted for publishing in internationally recognized peer-reviewed journals.

As the candidate's supervisor I have approved this thesis for submission.

Supervisor. Professor Moganavelli Singh

Signature.....

This is to certify that this thesis is the original work of Ms. Zoleka Mncwabe

Signature.....

ABSTRACT

Chemotherapy being one of the principle techniques used in cancer treatment, has been applied in the treatment of a wide spectrum of cancers. However, this mode of treatment is fraught with a myriad of challenges, reducing its effectivity and inducing the need for repeated treatments. Poor drug delivery systems or lack thereof, have led to patients suffering unpleasant side effects that not only cause collateral damage to their bodies but also reduces the quality of their lives. The current array of chemotherapeutic drugs available may be effective in certain cancers, nevertheless the need for their optimization is still necessary for better safety, stability and efficiency of treatment. Thus the current study was designed to investigate the potential of layered double hydroxide (LDH) nanoparticles in the delivery of the broad spectrum anticancer drug, 5-Fluorouracil (5-Fu). Four LDH nanoparticles, MgAl 2:1, MgAl 3:1, ZnAl 2:1 and ZnAl 3:1 were successfully synthesized and intercalated with 5-Fu using the calcination reconstruction process to form nanohybrids. The LDHs and their nanohybrids, MgAl 2:1-5-Fu, MgAl 3:1-5-Fu, ZnAl 2:1-5-Fu and ZnAl 3:1-5-Fu were structurally confirmed using XRD, FTIR, UV-Vis, ICP-OES; with size, zeta potential and ultrastructural morphology investigated using nanoparticle tracking analysis (NTA) and electron microscopy (TEM and SEM). LDHs were characteristically hexagonal in shape with sizes ranging from 100 -150 nm, and high zeta potentials enforcing their colloidal stability. The successful intercalation of 5-Fu was confirmed from drug encapsulation efficiency studies to be between 40-60% in the respective LDHs. Furthermore, drug release studies revealed a steady controlled release of the drug over a 7-hour period at pH 4-7, with more than 60% of the drug being released by the end of this period. *In vitro* MTT [3-(4,5-dimethylthiazol-2-yl)-2,5-diphenyltetrazolium bromide] and SRB (Sulphorhodamine B) cytotoxicity studies on free 5-Fu and LDH bound 5-Fu in human cell lines, breast adenocarcinoma cell line (MCF-7), hepatocellular carcinoma (HepG2), colorectal adenocarcinoma (CaCo-2) and embryonic kidney (HEK293), showed a dose dependent cytotoxicity profile with the free 5-Fu being more toxic to the cells than the bound drug. This was further confirmed in fluorescent apoptotic studies (dual acridine orange and ethidium bromide staining method), where free 5-Fu had a higher apoptotic index than the LDH bound 5-Fu

Key words: LDH, cancer, drug delivery, 5-fluorouracil, nanoparticles, cytotoxicity, apoptosis

DECLARATION 1- PLAGIARISM

I, Zoleka Mncwabe declare that:

- i. The research reported in this thesis, except where otherwise indicated or acknowledged, is my original work.
- ii. This dissertation has not been submitted in full or in part for any degree or examination to any other university prior.
- iii. This dissertation does not contain other persons' data, pictures, graphs or other information, unless specifically acknowledged as being sourced from such persons.
- iv. This dissertation does not contain other persons' writing, unless specifically acknowledged as being sourced from other researchers. Where other written sources have been quoted, then:
 - a) Their words have been re-written but the general information attributed to them has been referenced accordingly.
 - b) Where their exact words have been used, their writing has been placed inside quotation marks, and referenced accordingly.
- v. Where I have used material for which publications followed, I have indicated in detail my role in the work;
- vi. This thesis is primarily a collection of material, prepared by myself through scientific experimentation and presented as an oral presentation at conferences
- vii. This thesis does not contain text, graphics or tables copied and pasted from the Internet, unless specifically acknowledged, and the source being detailed in the dissertation and in the references sections.

.....
Signed

Date

DECLARATION 2-PUBLICATIONS

My role in each paper and presentation is indicated. The * indicates corresponding author.

Publication 1:

Zoleka Mncwabe¹ and Moganavelli Singh*. The application of MgAl-LDHs as Potential Anticancer drug delivery vehicles. *To be submitted for publication.*

Publication 2:

Zoleka Mncwabe¹ and Moganavelli Singh*. The application of ZnAl-LDHs as Potential Anticancer drug delivery vehicles. *To be submitted for publication.*

Conferences Attended

1. Oral Presentation – The Application of Layered Double Hydroxides (LDHs) as Anticancer Drug Delivery Vehicles. South African Society for Biochemistry and Molecular Biology (SASBMB) congress. East London 14 July 2016

ACKNOWLEDGEMENTS

I would like to thank God for keeping me head strong and for all the blessings He has bestowed me throughout my Masters experience.

I would like to especially thank my Supervisor, Professor Moganavelli Singh, for overseeing my work, helping me to design and shape my MSc. project to and for allowing my curious mind to venture into the field of cancer research.

I send my sincerest gratitude to Dr Sooboo Singh at the University of KwaZulu-Natal, Chemistry Department for helping me in all aspects of chemistry with my work, you truly revealed a love for chemistry I never thought I had to such an extent. I would also like to thank Drushan Padayachee, Harinarayana Bandaru and Samuel Aremu for their assistance with chemistry analyses. I am eternally grateful to the National Research Fund for funding this project.

I would also like to thank my colleagues at the Non-viral Gene Delivery Lab at the University of KwaZulu-Natal Westville. All of you guys have made my MSc experience quite fun-filled and I especially would like to thank you for scientific insights that shaped my project.

Lastly, but most certainly not the least, I would like to thank the Njilo family for believing and being there for me every step of the way even when I couldn't manage to cheer myself on dark days, you managed to do that for me and I will always hold you dear.

DEDICATION

I would like to dedicate this to all the Cancer victims, both still living and those who are in a better place now (Miss Bazamile Owasembo Mkhize), as well as their families who are facing this disease. Hopefully my work can serve as a template for more practical measures to be taken to ensure that efficient and rapid treatment systems are developed and made available.

Table of Contents

ABSTRACT	iii
DECLARATION 1- PLAGIARISM	iv
DECLARATION 2-PUBLICATIONS	v
ACKNOWLEDGEMENTS	vi
DEDICATION	vii
LIST OF TABLES	xii
LIST OF FIGURES	xiii
1.1 Introduction	19
1.2 Background of Study	19
1.3 Significance and Novelty of Study	20
1.4 Aims	20
1.5 Objectives	20
1.6 Outline of the Dissertation.	21
1.6.1 Chapter 1	21
1.6.2 Chapter 2	21
1.6.3 Chapter 3	21
1.6.4 Chapter 4	22
1.6.5 Chapter 5	22
1.7 References	23
CHAPTER 2	24
2. LITERATURE REVIEW	24
2.1 Introduction	24
2.2 Anticancer Drugs	25
2.2.1 Alkylating Agents	27
2.2.2 Antimetabolites	28
2.2.3 Hormones and Antibiotics	28
2.2.4 Nucleic acids	28
2.2.5 Side Effects of Chemotherapeutic agents	29
2.3 Anticancer Drug: 5-Fluorouracil (5-Fu)	30
2.3.1 Mechanism of Action of 5-Fluorouracil	31
2.3.2 Side Effects of 5-Fluorouracil	32
2.3.3 Delivery of 5-Fluorouracil	32
2.4 Nanotechnology in Medicine	33
2.5 Drug Delivery Systems (DDS)	34
2.6 Layered Double Hydroxides (LDHs)	35

2.6.1 Applications of Layered Double Hydroxides.....	37
2.6.3 LDHs for drug delivery	39
2.6.4 LDH nanoparticle cellular uptake and release mechanisms.....	41
2.7 Intercalation of Chemotherapeutic drugs in LDHs	42
2.7.1 Alkalisiation of 5-Fluorouracil.....	42
2.7.2 Co-Precipitation	43
2.7.2 Ion-Exchange route.....	43
2.7.3 Calcination / Reconstruction.....	44
2.7.4. Other methods of encapsulation	44
2.8 Experimental Techniques.....	44
2.8.1 Powder X-Ray Diffraction (XRD).....	44
2.8.3 Microscopy.....	45
2.8.3.1 Scanning Electron Microscopy.....	45
2.8.3.2 Transmission Electron Microscope.....	46
2.8.4 Nanotracking analysis (NTA)	46
2.8.5 Cytotoxicity Studies	47
2.8.5.1 MTT Assay	47
2.8.5.2 Sulphorhodamine B Assay (SRB).....	47
2.9 Novelty of study.....	48
2.9 References.....	49
CHAPTER 3.....	61
Abstract.....	62
3.1 Introduction.....	63
3.2 Materials	64
3.3 Methods.....	65
3.3.1 Synthesis of the MgAl layered double hydroxides	65
3.3.2 Calcination.....	65
3.3.3 MgAl-LDH: 5-Fu conjugate synthesis.....	66
3.3.4 Drug encapsulation efficiency	66
3.3.5 Powder X-Ray diffraction	66
3.3.6 Fourier Transform Infrared Spectroscopy (FTIR)	67
3.3.7 Inductively Coupled Plasma Analysis-Optical Emission Spectroscopy (ICP-OES)	67
3.3.8 Electron Microscopy	67
3.3.9 Nanoparticle Tracking Analysis (NTA)	67
3.3.10 Drug release Studies	68
3.3.11 <i>In vitro</i> cell culture studies.....	68

3.3.12 MTT Cytotoxicity assay.....	68
3.3.13 Sulphorhodamine B (SRB) Cytotoxicity assay	69
3.3.14 Apoptosis.....	69
3.3.15 Statistical analyses	70
3.4 Results and Discussion.....	70
3.4.1 Syntheses of LDHs	70
3.4.2 UV-Vis spectroscopy.....	71
3.4.3 Powder X-ray Diffraction Spectroscopy.....	72
3.4.4 Fourier Transform Infrared Spectroscopy.....	72
3.4.5 Inductively coupled plasma-optical emission spectroscopy (ICP-OES).....	73
3.4.6 Electron Microscopy (TEM and SEM)	73
3.4.6 Nanoparticle Tracking Analysis (NTA)	75
3.4.7 Drug release studies	76
3.4.8 Cytotoxicity studies.....	77
3.4.8.1 MTT assay	77
3.4.8.2 Sulphorhodamine B (SRB) assay.....	80
3.4.9 Apoptosis studies.....	81
3.5 Conclusion	84
3.6 References.....	86
CHAPTER 4.....	90
Abstract.....	91
4.1 Introduction.....	92
4.2 Materials	93
4.3 Methods.....	94
4.3.1 Synthesis.....	94
4.3.3 ZnAl-LDH: 5-Fu synthesis	94
4.3.4 UV-Vis Spectroscopy.	94
4.3.5 Powder X-Ray diffraction	95
4.3.6 Fourier Transform Infrared Spectroscopy (FTIR)	95
4.3.7 Inductively Coupled Plasma Analysis-Optical Emission Spectroscopy (ICP-OES)	95
4.3.8 Electron Microscopy	95
4.3.9 Nanoparticle Tracking Analysis (NTA)	96
4.3.10 Drug release Studies	96
4.3.11. <i>In vitro</i> Cell Culture studies	96
4.3.12 MTT Cytotoxicity Assay.....	96
4.2.13 Sulphorhodamine B (SRB) assay.....	97
4.3.14 Apoptosis Study.....	98

4.3.15 Statistical Analyses.....	98
4.4 Results and Discussion.....	98
4.4.1 Synthesis of ZnAl-LDH	98
4.4.2 UV-Vis spectroscopy	99
4.4.3 XRD Analysis.	100
4.4.4 Fourier Transform Infrared Spectroscopy.....	101
4.4.5 Inductively coupled plasma-optical emission spectroscopy (ICP-OES).....	101
4.4.6 Electron Microscopy (SEM and TEM)	101
4.4.7 Nanoparticle tracking analysis (NTA)	103
4.3.8 Drug release studies	104
4.4.9 MTT Cytotoxicity Assay.....	105
4.4.10 Sulphorhodamine B (SRB) assay	108
4.4.11 Apoptosis studies	110
4.4 Conclusion	114
4.6 References	115
CHAPTER 5.....	120
5.1 Conclusion	120
5.2 Future improvements and prospects.....	121
APPENDIX.....	122

LIST OF TABLES

- Table 2.1** Illustration of LDH-Drug formulations and their various applications.
- Table 3.1** MgAl-LDH Encapsulation efficiencies.
- Table 3.2** Net zeta potentials of MgAL 2:1, MgAl 2:1-5-Fu, MgAl 3:1 And MgAl 3:1-5-Fu.
- Table 3.3** IC₅₀ (in µg/m L) Values for MgAl 2:1-5-Fu vs pure 5-Fu vs. MgAl 3:1-5-Fu versus pure 5-Fu respectively.
- Table 3.4** IC₅₀ (in µg/m L) Values for MgAl 2:1-5-Fu vs pure 5-Fu vs. MgAl 3:1-5-Fu vs pure 5-Fu.
- Table 3.5** Apoptotic Index (AI) of cells exposed to MgAL-2:1-5-Fu vs. Free 5-Fu and MgAl 3:1-5-Fu vs. Free 5-Fu.
- Table 4.1** ZnAl-LDHs Encapsulation Efficiencies (% EE).
- Table 4.2** IC₅₀ (in µg/m L) Values for ZnAl 2:1-5-Fu vs pure 5-Fu vs. ZnAl 3:1-5-Fu vs. Free 5-Fu.
- Table 4.3** IC₅₀ (in µg/m L) Values for ZnAl 2:1-5-Fu vs pure 5-Fu vs. ZnAl 3:1-5-Fu vs pure 5-Fu.
- Table 4.4** Apoptotic Index (AI) of cells exposed to ZnAL-2:1-5-Fu vs. Free 5-Fu and ZnAl 3:1-5-Fu vs. Free 5-Fu.

LIST OF FIGURES

- Figure 2.1** Data from the United States Centre for Disease Control illustrating the expected increase in cancer till 2030 (CaseyResearch, 2012).
- Figure 2.1** Illustration of the most common types of cancers in various organs (CDC, 2016).
- Figure 2.1** Chemotherapeutic drugs and their mechanisms of action (Pharmafactz, 2016).
- Figure 2.4** (a) 3D and (b) 2D structures of the anticancer drug 5-Fluorouracil (Chemistry, 2016).
- Figure 2.5** The mechanism of action of 5-Fluorouracil adapted from (Fitzakerley, 2015).
- Figure 2.6** Schematic illustration of the hierarchical organisation of the layered double hydroxide structure and its chemical components (Gu *et al.*, 2015).
- Figure 2.7** Various applications of hydrotalcite-like clays.
- Figure 2.8** Illustration of the cellular uptake of LDH-drug Nanocomplexes LDH drug nanocomplexes attach to the membrane, followed by clathrin mediated endocytosis (2-4). proton sponge effects (Rojas *et al.*, 2015).
- Figure 2.9** Schematic illustration of the orientation of 5-Fu intercalates in LDHs (Wang *et al.*, 2005a).
- Figure 3.1** (a) Pristine MgAl 2:1 and MgAl₃:1 (b) Calcined MgAl 2:1 and MgAl₃:1.
- Figure 3.2** UV-Vis spectroscopy of 5-Fu, MgAl 2:1-5-Fu and MgAl 3:1 5-Fu.

- Figure 3.3** TEM images of (a) MgAl 2:1, (b) Calcined MgAl 2:1 (c) and MgAl 2:1-5-Fu (Scale bar \leq 200).
- Figure 3.4** TEM of (a) MgAl 3:1, (c) Calcined MgAl 3:1 and (c) MgAl 3:1-5-Fu (Scale Bar \leq 200 nm).
- Figure 3.5** SEM micrographs of (a) MgAl 2:1 pure (b) calcined MgAl 2:1 (c) MgAl 2:1-5-Fu (Scale Bar \leq 150 nm).
- Figure 3.6** SEM micrographs of (a) MgAl 3:1 pure (b) calcined MgAl 3:1 (c) MgAl 3:1-5-Fu (Scale Bar \leq 150 nm).
- Figure 3.7** Drug release profiles of MgAl 2:1-5-Fu (a) and MgAl 3:1-5-Fu (b) at pH \sim 4 and pH \sim 7 respectively.
- Figure 3.8** MTT Assay with MgAl-2:1-5-Fu vs. Free 5-Fu at concentrations 12.5 μ g/mL, 25 μ g/mL, 50 μ g/mL and 100 μ g/mL on HEK293, MCF-7, / HepG2 CaCo-2 cell lines [data presented in mean standard deviation (n=3) ($p^* < 0.05$)].
- Figure 3.9** MTT Assay with MgAl-3:1-5-Fu vs. Free 5-Fu at concentrations 12.5 μ g/mL, 25 μ g/mL, 50 μ g/mL and 100 μ g/mL on HEK293, MCF-7, / HepG2 CaCo-2 cell lines [data presented in mean standard deviation (n=3) ($p^* < 0.05$)].
- Figure 3.10** Sulphorhodamine B Assay with MgAl-2:1-5-Fu vs. Free 5-Fu at concentrations 12.5 μ g/mL, 25 μ g/mL, 50 μ g/mL and 100 μ g/mL on HEK293, MCF-7, HepG2 CaCo-2 cell lines [data presented in mean standard deviation (n=3) ($p^* < 0.05$)].
- Figure 3.11** Sulphorhodamine B assay for MgAl-3:1-5-Fu vs. Free 5-Fu at concentrations 12, 5 μ g/mL, 25 μ g/mL, 50 μ g/mL and 100 μ g/mL on HEK293, MCF-7, HepG2 and CaCo-2 cell lines [data presented in mean standard deviation (n=3) ($p^* < 0.05$)].

- Figure 3.12** Micrograph images of apoptosis induced by MgAl 2:1-5-Fu vs. Free 5-Fu on HEK293, MCF- HepG2 and CaCo-2 cell lines (L=Live cells, A=Apoptotic cells, LA= Late Apoptotic cells and EA= Early Apoptotic cells).
- Figure 3.13** Micrograph images of apoptosis induced by MgAl 3:1-5-Fu vs. Free 5-Fu on HEK293, MCF- HepG2 and CaCo-2 cell lines (L=Live cells, A=Apoptotic cells, LA= Late Apoptotic cells and EA= Early Apoptotic cells).
- Figure 4.1** Synthesized LDHs (a) ZnAl 2:1 pristine (b) ZnAl 3:1 pristine (c) ZnAl 3:1-5-Fu calcined (d) ZnAl 3:1 calcined.
- Figure 4.2** TEM images of (a) MgAl 3:1, (c) Calcined ZnAl 3:1 and (c) ZnAl 3:1-5-Fu (scale \leq 150nm).
- Figure 4.3** TEM images of (a) ZnAl 3:1, (c) Calcined ZnAl 3:1 and (c) ZnAl 3:1-5-Fu (scale \leq 150nm).
- Figure 4.4** SEM micrographs of (a) ZnAl 3:1, (c) Calcined ZnAl 3:1 and (c) ZnAl 3:1-5-Fu (scale \leq 250nm).
- Figure 4.5** SEM micrographs of (a) ZnAl 3:1, (c) Calcined ZnAl 3:1 and (c) ZnAl 3:1-5-Fu (scale \leq 200nm).
/
- Figure 4.6** UV-vis spectrum of 5-Fu, ZnAl 2:1-5-Fu and ZnAl 3:1-5-Fu.
- Figure 4.7** (a) Drug release profiles of ZnAl 2:1-5-Fu and (b)ZnAl 3:1-5-Fu at pH ~4 and pH ~7 respectively.

Figure 4.8 MTT Assay with ZnAl-2:1-5-Fu vs. Free 5-Fu at concentrations 12, 5µg/ mL, 25µg/ mL, 50µg/ mL and 100µg/ mL on HEK293, MCF-7 HepG2 CaCo-2 cell lines [data presented in mean standard deviation (n=3) ($p^* < 0.05$).

Figure 4.9 MTT Assay with ZnAl-3:1-5-Fu vs. Free 5-Fu at concentrations 12, 5µg/ mL, 25µg/ mL, 50µg/ mL and 100µg/ mL on HEK293, MCF-7, HepG2 CaCo-2 cell lines [data presented in mean standard deviation (n=3) ($p^* < 0.05$).

Figure 4.10 Sulphorhodamine B assay for ZnAl-2:1-5-Fu vs. Free 5-Fu at concentrations 12, 5µg/ mL, 25µg/ mL, 50µg/ mL and 100µg/ mL). on HEK293, MCF-7, HepG2 and CaCo-2 cell lines [data presented in mean standard deviation (n=3) ($p^* < 0.05$).

Figure 4.11 Sulphorhodamine B assay for ZnAl 3:1-5-Fu vs. Free 5-Fu at concentrations 12, 5µg/ mL, 25µg/ mL, 50µg/ mL and 100µg/ mL). on HEK293, MCF-7, HepG2 and CaCo-2 cell lines [data presented in mean standard deviation (n=3) ($p^* < 0.05$).

Figure 4.12 Micrograph images of apoptosis induced by ZnAl 2:1-5-Fu vs. Free 5-Fu on HEK293, MCF- HepG2 and CaCo-2 cell lines (L=Live cells, A=Apoptotic cells, LA= Late Apoptotic cells and EA= Early Apoptotic cells. [Scale bar at 100 µm].

Figure 4.13 Micrograph images of apoptosis induced by ZnAl 3:1-5-Fu vs. Free 5-Fu on HEK293, MCF- HepG2 and CaCo-2 cell lines (L=Live cells, A=Apoptotic cells, LA= Late Apoptotic cells and EA= Early Apoptotic cells. [Scale bar at 100 µm].

ABBREVIATIONS

LDH	Layered Double Hydroxide
DDS	Delivery System
MgAl	Magnesium Aluminium
ZnAl	Zinc Aluminium
MgAl-5-Fu	Magnesium Aluminium-5-Fluorouracil
ZnAl-5-Fu	Zinc Aluminium-5-Fluorouracil
TEM	Transmission Electron Microscopy
SEM	Scanning Electron Microscopy
NTA	Nanoparticle Tracking Analysis
ICP-OES	Inductively Coupled Plasma Optical Emission Spectroscopy
FTIR	Fourier Transform Infrared
XRD	X-Ray Diffraction
UV	Ultra Violet
EE	Encapsulation Efficiency
AI	Apoptosis Index
HEK293	Human Embryonic Kidney 293
MCF-7	Human breast adenocarcinoma cell line-7
CaCo-2	Colorectal adenocarcinoma cells-2
HepG2	Hepatocarcinoma Cell line
MTT	(3-(4,5-dimethyl-2-thiazolyl)-2,5-diphenyltetrazolium bromide) tetrazolium reduction assay

SRB	Sulphorhodamine B assays (SRB assay)
MEM	Minimal Essential Medium
PBS	Phosphate buffer Saline
CDC	Centers for Disease Control
WHO	World Health Organization
CANSA	Cancer Association of South Africa

CHAPTER 1

1.1 Introduction

The background of the study provides a brief introduction to the study. It further describes the challenges faced in anticancer drug delivery systems and how this study will serve to try to overcome some of these hurdles. The significance and novelty, including the aims, objectives and outlines of the study are outlined.

1.2 Background of Study

The battle against cancer in recent years has presented the scientific world with the challenge of finding a safe and effective drug delivery system to deliver anticancer drugs effectively to the appropriate affected sites (Tiwari *et al.*, 2012). Although, many drug systems have been developed and utilized, there still exists the need for safer and target specific delivery systems for anticancer drugs. Administration of anticancer drugs such as 5-Fluorouracil (5-Fu), although effective, does present with the problem of collateral damage to unaffected areas in the body, leading to unpleasant side effects (Holohan *et al.*, 2013, Tiwari *et al.*, 2012). Nanoparticles in recent years have shown potential as drug delivery carriers, due to their nanoscale and chemical properties which enables effective encapsulation of drugs. Amongst the various inorganic nanoparticles being used, the layered double hydroxide nanoparticles have also shown some potential in drug delivery (Aguzzi *et al.*, 2007, Haley and Frenkel, 2008). Hence, LDHs have been researched as both gene and drug delivery vehicles, successfully showing the nanoparticle's ability to protect, sustain and improve on the limitations of many previously studied nanoparticles (Choi and Choy, 2011). The ability of LDHs to deliver the hydrophobic drug raloxifene hydrochloride (RH), using the co-precipitation method to intercalate the drug, showed the controlled release of RH from the LDH revealing a sustained system of drug delivery (Senapati *et al.*, 2016). From the myriad of drug delivery vehicles that have been synthesized to date for the purposes of drug delivery, many fail to completely eliminate nanoparticle carrier from the body and leading to accumulation of the carrier, with adverse effects on the body.

1.3 Significance and Novelty of Study

Most nanoparticle drug delivery systems do not provide adequate protection or cellular uptake of certain drugs. Hence, LDHs are being investigated as a possible alternative option. This study examines the potential of two layered double hydroxide nanoparticles (or LDHs) viz. magnesium aluminium (MgAl 2:1-LDH and MgAl 3:1-LDH) and zinc aluminium (ZnAl 2:1-LDH and ZnAl 3:1-LDH), to deliver the anticancer drug, 5-Fluorouracil, a primary drug for targeting colorectal cancer, to mammalian cancer cells *in vitro*. This study further seeks to understand the chemistry of these nanostructures, and how their morphology favours protection and controlled release of the drug in the desired cells or tissue. These two LDHs are further compared with regards to their limitations and advantages. Thus the roadmap of this thesis is such that past literature and research findings are critically evaluated to help improve on the knowledge of the LDHs' applicability as drug delivery systems. Comparative studies look at how the two synthesized LDHs, namely, MgAl-LDH and ZnAl-LDHs differ in their respective characteristics and this is done in individualized chapters with the aim to publish the research findings.

1.4 Aims

The principle aim of our study is to first synthesise and subsequently evaluate the ability of two distinctly different layered double hydroxides (MgAl 2:1-LDH, MgAl 3:1-LDH, ZnAl 2:1-LDH and ZnAl 3:1-LDH) to encapsulate a very hydrophilic drug, 5-Fluorouracil (5-Fu), and deliver it efficiently to mammalian cancer cells. We also examine their drug binding and release properties to ascertain their suitability as drug carriers.

1.5 Objectives

- To synthesize and fully characterize the MgAl-LDH and ZnAl-LDHs using ICP-OES, FTIR, UV-spectroscopy, TEM, SEM, and Nanoparticle Tracking Analysis (NTA)
- To intercalate the drug, 5-Fu, into the LDHs and fully characterize the binding.
- To determine the physicochemical and morphological characteristics of the LDH–Drug complexes.

- To determine the advantages, if any, of LDH bound 5-Fu versus the freely delivered 5-Fu, with regards to cellular uptake, anticancer activity and apoptosis.

1.6 Outline of the Dissertation.

This dissertation is made up of 5 chapters, with Chapters 3 and 4 written in the form of two papers.

1.6.1 Chapter 1

This chapter provides a brief background to the study, rationale and significance for the study of LDHs as potential drug delivery vehicles, as well the outline of the whole thesis. A note is made as to the novelty of the research. Within this chapter the primary aims and objectives are stated as well. References are stated accordingly at the end for this chapter.

1.6.2 Chapter 2

The detailed literature survey forms the basis of this chapter. Subtopics leading to a better understanding of the past to present research on layered double hydroxides (LDHs) are discussed. This is to introduce the nanoparticle and its role over the past years in medicine and in general. Limitations encountered by researchers are outlined, including possible methods for improving this drug delivery system. Background to the analytical techniques used in this project are detailed and their necessity for the understanding of the LDH as well as the LDH: Drug nanocomplexes are explained.

1.6.3 Chapter 3

This chapter, is written in paper format. The title of the article is “The Application of MgAl Layered Double Hydroxides as Potential Anticancer Drug Delivery Vehicles”. This article

examines the two synthesised magnesium aluminium layered double hydroxides (namely, MgAl 2:1-LDH and MgAl 3:1-LDH) and their application in the effective delivery of 5-Fu. Conclusions and future prospects for these LDHs in drug delivery are discussed.

1.6.4 Chapter 4

This chapter is written in paper format similar to chapter 3, but looks at the zinc and aluminium LDHs. The title of the article is “The Application of ZnAl Layered Double Hydroxides as Potential Anticancer Drug Delivery Vehicles”. This article looks at ZnAl 2:1-LDH and ZnAl 3:1-LDH, and their application in the effective delivery of 5-Fu. Conclusions and future prospects for these LDHs in drug delivery are discussed.

1.6.5 Chapter 5

This chapter provide the conclusions deduced from the study, and highlights further recommendations or areas for improvement or optimizations to make these LDHs suitable drug delivery vehicles.

1.7 References

- Aguzzi, C., Cerezo, P., Viseras, C. & Caramella, C. 2007. Use of clays as drug delivery systems: possibilities and limitations. *Applied Clay Science*, 36, 22-36.
- Choi, S.-J. & Choy, J.-H. 2011. Layered double hydroxide nanoparticles as target-specific delivery carriers: uptake mechanism and toxicity. *Nanomedicine*, 6, 803-814.
- Haley, B. & Frenkel, E. Nanoparticles for drug delivery in cancer treatment. *Urologic Oncology: Seminars and original investigations*, 2008. Elsevier, 57-64.
- Holohan, C., Van Schaeybroeck, S., Longley, D. B. & Johnston, P. G. 2013. Cancer drug resistance: an evolving paradigm. *Nature Reviews Cancer*, 13, 714-726.
- Senapati, S., Thakur, R., Verma, S. P., Duggal, S., Mishra, D. P., Das, P., Shripathi, T., Kumar, M., Rana, D. & Maiti, P. 2016. Layered double hydroxides as effective carrier for anticancer drugs and tailoring of release rate through interlayer anions. *Journal of Controlled Release*, 224, 186-198.
- Tiwari, G., Tiwari, R., Sriwastawa, B., Bhati, L., Pandey, S., Pandey, P. & Bannerjee, S. K. 2012. Drug delivery systems: An updated review. *International journal of pharmaceutical investigation*, 2, 2.

CHAPTER 2

2. LITERATURE REVIEW

2.1 Introduction

Cancer is a disease characterized by uncontrollable cell growth resulting in the formation of cancerous cellular clusters referred to as tumours. Tumours grow and inhibit the normal functioning, among many other factors, of various organs in the body through the release of hormones that significantly alter organ function (Cole, 1973, Kamb *et al.*, 2007, Karpanen *et al.*, 2001). Through a process of metastasis, the cancerous cells spread throughout the body via the blood or lymphatic systems (Kucia *et al.*, 2005). Various factors, many of which are known, contribute to the development and subsequent spread of cancer. Mutational errors during cell division, aging, tobacco intake, sun exposure, radiation exposure, potential carcinogenic chemicals, viruses and bacteria, certain hormones, alcohol, poor diet, and lack of physical activity are just some of the known causes of cancer (Cancer.Net, 2015, MedicineNet.com, 2016). The genes commonly implicated in cancer initiation and development, are the oncogenes that are activated and tumour suppressor genes that become inactivated, resulting in these genes not performing their normal functions in the body. Figure 2.1 provides a projection for the increase in cancer incidents till 2030.

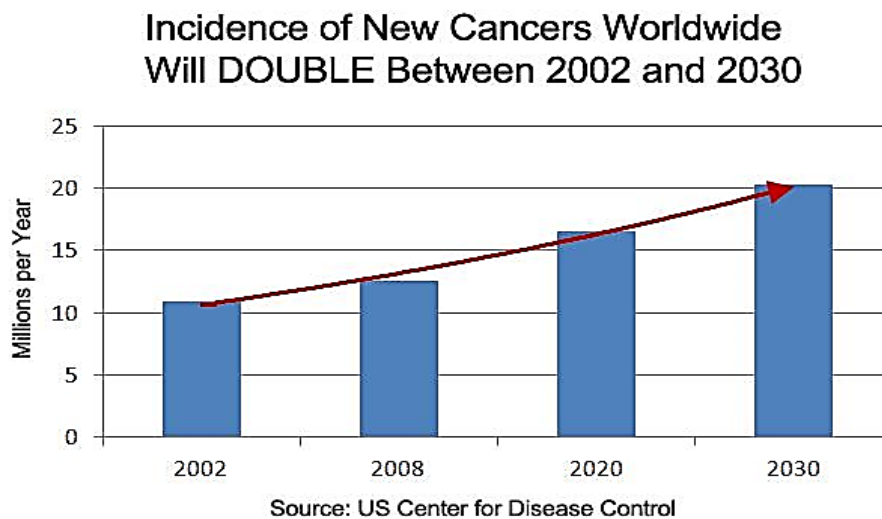


Figure 2.1 Data from the United States Centre for Disease Control illustrating the expected increase in cancer till 2030 (CaseyResearch, 2012).

From the data compiled by the Centre for Diseases Control and Prevention (CDC) on the prevalence of cancer worldwide, approximately 14.1 million cases of cancer are diagnosed each year and a staggering 8.2 million people die from cancer annually. In 2015 the number of reported cancer cases rose to 19.3 million. Of the various types of cancers diagnosed worldwide, (Figure 2.2), the most prominent of these were lung cancer (13%), breast cancer (12%), colorectal cancer and other stomach cancers (17% combined), prostate cancer (8%), liver cancer (6%) and cervical cancer (4%) (CDC, 2016). A challenge facing researchers is in finding an appropriate drug delivery system to allow for the safe delivery of the existing drugs, while minimizing the cost and time needed for these drugs to be effective.

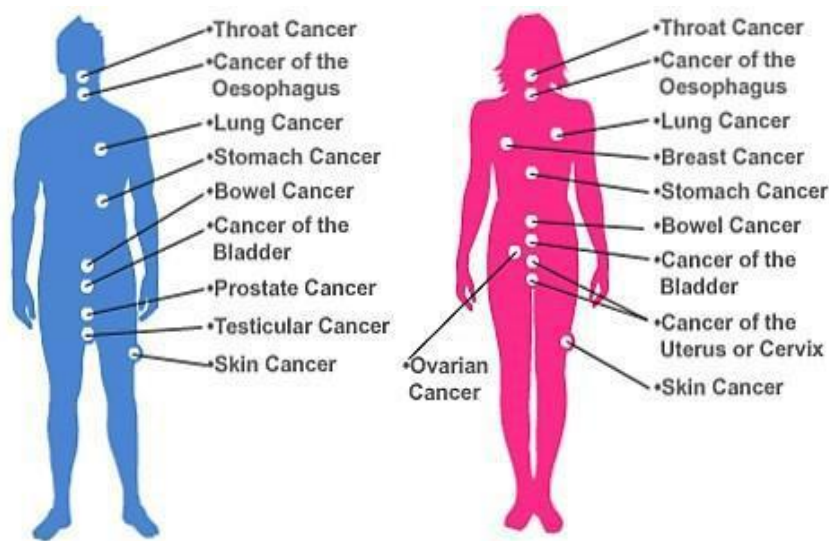


Figure 2.2: Illustration of the most common types of cancers in various organs (CDC, 2016).

2.2 Anticancer Drugs

Chemotherapy is one of the common modes of cancer treatment involving the use of one or more anticancer drugs or chemicals for the purposes of destroying cancer cells. Research has shown that cancerous cells present a satisfactory apoptotic response after exposure to various chemotherapeutic drugs (Liu, 2009). The term “anticancer drugs” or “antineoplastic drugs” refers

to a number of drugs developed for the effective treatment of cancer. The application of these anticancer drugs or chemicals in treatment against cancers is therefore termed chemotherapy (Rang *et al.*, 2016). It is worth noting that chemotherapy is a very aggressive and systemic form of chemical drug therapy which has various implications for the patient (Chen, 2016). The main reason this form of therapy is applied is primarily because it lowers the total number of cancer cells significantly, in addition to reducing the spread of the cancer and reduction of tumour sizes. This method of treatment is also advantageous in a sense that it is non-invasive and limits the risk of infection. However, patients do have to consider a number of implications accompanying the use of chemotherapy, such as the high cost of the treatment, time spent on sessions, unpleasant side effects, and as well as the need to use other drugs to suppress some of these side effects (Chen, 2016).

Anticancer or chemotherapeutic drugs can be categorized into several major classes: alkylating agents, antimetabolites, natural products, and hormones (Rang *et al.*, 2016). However, some drugs developed with the purpose of combating cancers may not fall under the above mentioned classes of drugs although they are applied in chemotherapy. Figure 2.3 outlines the various drugs currently in use and their mechanism of action.

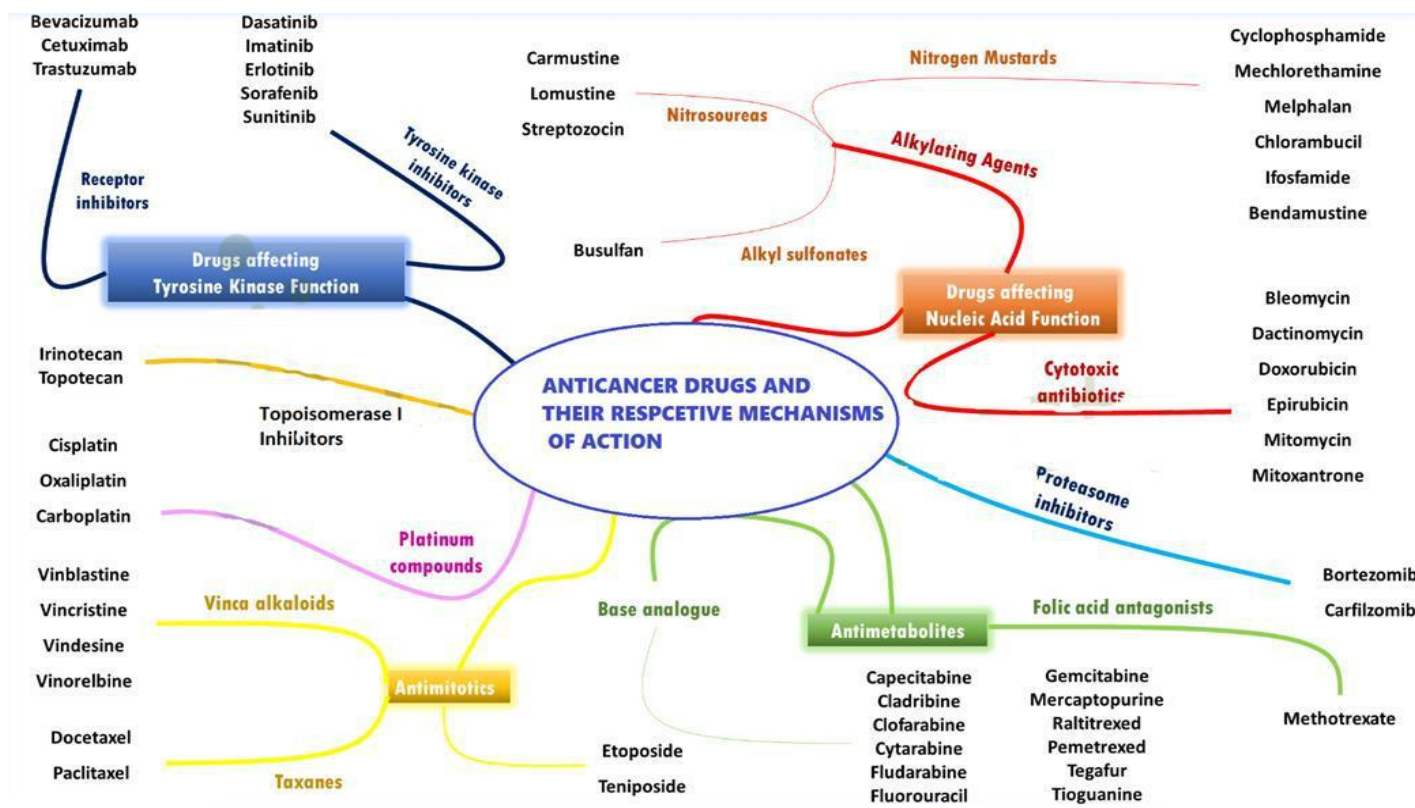


Figure 2.3 Chemotherapeutic drugs and their mechanisms of action (Pharmafactz, 2016)

2.2.1 Alkylating Agents

Alkylating agents are the one of the oldest group of drugs used in chemotherapy. They are genotoxic drugs (i.e. toxic to nucleic acids). These agents bind to the DNA and interrupt its replication and transcription. The purpose of these drugs is to induce DNA damage in cancerous cells leading to their apoptosis. Alkylating agents act by replacing a hydrogen atom by an alkyl radical through an electrolytic attack. However, this compound can then also react with molecules containing an atom in a lower valence state that will can also undergo an electrolytic attack (dos Santos Guimarães *et al.*, 2013). Alkylating agents can work at any point during the cell cycle and are thus known as cell cycle-independent drugs (dos Santos Guimarães *et al.*, 2013, Lind, 2008). Some examples of alkylating agent are mustard gas, nitrosoureas and alkyl sulfonates (dos Santos Guimarães *et al.*, 2013). However, a study conducted by (Hawkins *et al.*, 1992) showed an association of secondary leukaemias with patients that had been treated for cancer previously. In this study, of a cohort of 16 422 one year survivors of childhood cancer diagnosed in Britain between the years 1962 and 1983, 22 patients showed the development of secondary leukaemia.

Hence, it was concluded that the accumulation of the alkylating agents as well as other drugs led to this secondary cancer development (Hawkins *et al.*, 1992).

2.2.2 Antimetabolites

Antimetabolites are cell cycle dependent cytotoxic agents, which were developed more than 65 years ago, and are hence among the initially used chemotherapy agents. They can be divided according to their structure and function, as folic acid analogs, purine analogs, pyrimidine analogs and cytidine analogs (Abraham *et al.*, 2007, Lind, 2008). These antimetabolites work by halting DNA or RNA synthesis and replication, and by inhibiting essential enzymes needed to carry out these processes. Through disincorporation, apoptosis is induced as the damage to DNA leads to programmed cell death. Unlike their cell cycle independent counterparts (alkylating agents), antimetabolites work only during the DNA synthesis phase or the S-Phase. Prominent examples of antimetabolite chemotherapeutic agents include 5-Fluorouracil which is a pyrimidine analog (Abraham *et al.*, 2007), and methotrexate (Praetorius and Mandal, 2007)

2.2.3 Hormones and Antibiotics

Hormones such as glucocorticoids, progestins, antioestrogens, antiandrogens, and Selective Estrogen Receptor Modulators (SERMs), are just a few of the variety of hormones used in the fight against cancer, through systematic and dose dependent delivery to patients (Brunton *et al.*, 2011). Antibiotics such as anthracyclines, bleomycin, antracenediones and doxorubicin have also been widely used in cancer therapy (Thorn *et al.*, 2011).

2.2.4 Nucleic acids

Gene therapy is a term used to describe the application of nucleic acids for therapeutic purposes (Flotte and Carter, 1995, Niidome and Huang, 2002). Various genetic diseases that have been addressed using this form of therapy, especially, cystic fibrosis (Colledge and Evans, 1995, Griesenbach and Alton, 2013), Parkinson's disease (Mittermeyer *et al.*, 2012, Palfi *et al.*, 2014), as well as other forms of inherited or acquired genetic diseases such as cancer. Nucleic acids have

been applied in monotherapy or in combination with other regimens such as radiation and chemotherapy (Balasubramanian and Neidle, 2009, Schwarzenbach *et al.*, 2011).

Nucleic acids that have been applied in cancer therapy specifically include plasmid DNA (pDNA), synthetic nucleic acids such as antisense oligonucleotides, small interfering RNAs (siRNA), micro RNA (miRNA), messenger RNA (mRNA), and other double stranded RNAs such as polyinosine-cytosine (pIC) (Sajeesh *et al.*, 2014). Nucleic acids work in various ways intracellularly; some may render gene knockdown or silencing (siRNAs), while others deal with the replacement or substitution of the defective genes (pDNA) with a normal one. Therefore, pDNA vectors are utilized for intra-nuclear delivery to replace or to substitute specific genetic functions in the targeted cell resulting in an addition of a gene function. On the other hand, loss of gene function is often achieved through intra-cytoplasmatic delivery of synthetic antisense oligonucleotides, or siRNA reducing the expression of endogenous genes in a sequence-specific manner (Kim *et al.*, 2006). Thus, the mechanisms of the therapeutic effects of nucleic acids are diverse and include (among many actions) the inhibition of neoangiogenesis, activation of cytokines or immunostimulatory responses (Wagner *et al.*, 2004), induction of apoptosis.

Reduction of tumor cell proliferation or strategies to replace deleted genes or to over-express beneficial genes (Kim *et al.*, 2006, Russ and Wagner, 2007).

2.2.5 Side Effects of Chemotherapeutic agents

Chemotherapy drugs on their own, although effective in many cases, present adverse side effects due to various factors that affect their efficiency (de Mol *et al.*, 2016, Monje and Dietrich, 2012). Lack of cell / tumour specific targeting (Pabla and Dong, 2012), unknown doses or concentrations of the drug once inside the body, and over expression of the functions of the specific chemotherapeutic agents, (Song *et al.*, 2014), can all produce unwelcome side effects.

Side effects commonly experienced by patients include (but are not limited to), hair loss, decreased blood cell count, cardiac dysfunction, diarrhoea, hyperglycaemia, vomiting, skin irritation, decrease in fertility and libido, immunosuppression and myelosuppression (in the case of bone marrow paralysis leading to a decrease in white blood cell count or a total destruction of the bone marrow), typhlitis (an intestinal infection), anaemia which can ultimately lead to fatigue, and the possibilities of secondary neoplasms (Gill *et al.*, 2006).

2.3 Anticancer Drug: 5-Fluorouracil (5-Fu)

This research project examines the delivery of 5-Fluorouracil (5-Fu) (trade name Adrucil) using layered double hydroxides (LDHs) as the drug carriers. 5-Fluorouracil (5-Fu) is a widely used anticancer drug. It has been used in cancer treatment since 1959, when it was officially recommended as an anticancer drug (van Kuilenburg and Maring, 2013). However, its discovery goes back to the year, 1954, when Abraham Cantarow and Karl Paschkis discovered that liver tumours absorbed radioactive uracil more easily than normal liver cells. Earlier discoveries showed that fluorine in fluoroacetic acid inhibited a vital enzyme, leading to the synthesis of fluorouracil, and the discovery of the drug, 5-Fluorouracil. Since then 5-Fu has been utilized for the treatment of colorectal, breast, head and neck, thymus, bladder, and gastrointestinal cancers, in addition to neuroendocrine tumors among others (Folprecht *et al.*, 2004, Prado *et al.*, 2007, van Kuilenburg and Maring, 2013).

With respect to its chemistry, 5-Fu is a heterocyclic aromatic organic compound. Its structure is similar to that of the pyrimidine bases of deoxyribonucleic acid (DNA) and ribonucleic acid (RNA). 5-Fluorouracil is an analogue of uracil with a fluorine atom at carbon-5, replacing hydrogen. It is highly hydrophilic and has a high solubility in basic water (Li *et al.*, 2008). Figure 2.4 shows the (a) 3D and (b) 2D structures of 5-Fluorouracil.

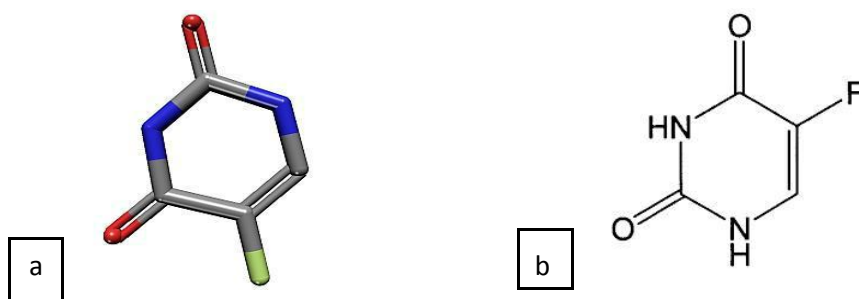


Figure 2.4: (a) 3D and (b) 2D structures of the anticancer drug 5-Fluorouracil (Chemistry, 2016)

2.3.1 Mechanism of Action of 5-Fluorouracil

The mechanism of action of 5-Fu has been proposed by several researchers. It has been found that 5-Fu rapidly enters the cancerous cell using the same facilitated transport mechanism as uracil, where it is converted intracellularly into the following metabolites: fluorodeoxyuridine monophosphate (FdUMP), fluorodeoxyuridine triphosphate (FdUTP), and fluorouridine triphosphate (FUTP) (Maxwell *et al.*, 2003). These active metabolites then disrupt ribonucleic acid synthesis and the action of thymine synthase (TS), an essential enzyme involved in the catalysis and biosynthesis of thymidylate. This enzyme also plays a role in the regulation of protein synthesis and other apoptotic processes that occur within the cell (Li *et al.*, 2013, Longley *et al.*, 2003)

It has been observed that the rate-limiting enzyme in 5-Fu catabolism, dihydropyrimidine dehydrogenase (DPD), converts 5-Fluorouracil to dihydrofluorouracil (DHFU). More than 80% of the administered 5-Fu is catabolized primarily in the liver, where DPD is abundantly expressed (Longley *et al.*, 2006). Figure 2.5 below outlines the mechanism of action of 5-Fluorouracil in detail.

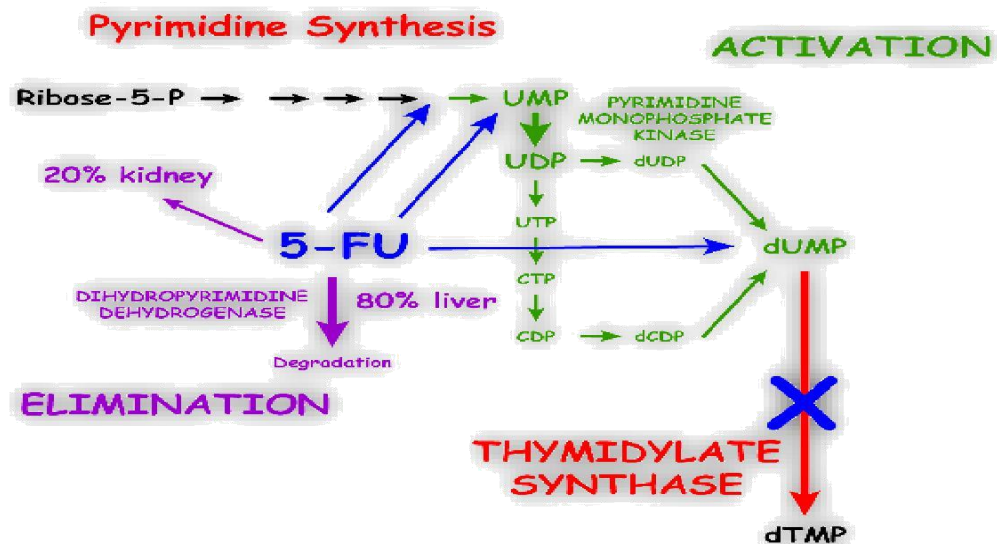


Figure 2.5: The mechanism of action of 5-Fluorouracil adapted from (Fitzakerley, 2015)

2.3.2 Side Effects of 5-Fluorouracil

Some of the noted general side effects of administered 5-Fu, include diarrhoea, nausea and possible occasional vomiting, mouth sores, poor appetite, watery eyes, sensitivity to light (photophobia), taste changes, metallic taste in mouth during infusion, discoloration along the vein through which the medication is given, and low blood cell counts (Navigating Cancer, 2016). The 5-Fu which is available commercially usually as Efudex solution (2-5%) and a topical cream (2-5%), also comes with various side effects when used by the patient (Weinreb, 1987). These include burning, crusting of skin, allergic contact dermatitis, erosions, erythema, hyperpigmentation, irritation, pain, photosensitivity, pruritus, scarring, rash, soreness and ulcerations (Weinreb, 1987). Cases of miscarriage and birth defects such as ventricular septal defects have also been reported when Efudex was applied to areas of the mucous membrane (Cardonick and Iacobucci, 2004). Leucocytosis is another haematological side effect commonly observed (Cardonick and Iacobucci, 2004, Navigating Cancer, 2016).

2.3.3 Delivery of 5-Fluorouracil

Studies conducted both *in vitro* and *in vivo* in the delivery of deliver 5-Fu using poly (lactide-co-glycolide) (PLGA) nanoparticles, have shown that PGLA helps to improve 5-Fu's oral bioavailability. Kumari *et al.*, 2016). Furthermore, chitosan nanospheres have also been successfully used in the delivery of 5-Fu (Cavalli *et al.*, 2014). These drug loaded nanospheres were prepared using a technique derived from a combination of the coacervation and the emulsion droplet coalescence methods. The encapsulation efficiency achieved was approximately 70% (Cavalli *et al.*, 2014). Cytotoxicity profiles in the cancer cell lines HT-29 and PC-3, revealed that in comparison to freely delivered 5-Fu, the chitosan encapsulated 5-Fu produced lowered cytotoxicity (Cavalli *et al.*, 2014). 5-Fu was also successfully delivered using non-ionic surfactant vesicles (niosomes), prepared by the hand shaking method (HSM) (Marwa *et al.*, 2013), as an alternative to delivery using liposomes (Ahmad *et al.*, 2014). Antibodies have also been used to deliver 5-Fu. Antibody systems such as the Monoclonal Antibody Modified Bovine Serum Albumin Nanoparticles (MAMBSA), were used in the delivery of 5-Fu (Fadaeian *et al.*, 2015), which showed a more targeted mode of delivery of the drug, thereby lowering the risk of collateral cell death. Other nanoparticles such as gold nanoparticles (GNPs) have also been used in the delivery of 5-Fu (Dianzani *et al.*, 2014). Current research looking into the delivery of 5-Fu using

Layered Double Hydroxides has also emerged, and presents with higher possibilities a simplistic yet effective method of 5-Fu delivery (Kim *et al.*, 2014).

Combination therapy with 5-Fluorouracil co-delivered along with methotrexate, another anticancer drug has also been accomplished. Nanocomplexes comprising MTX/LDH (ML), 5-Fu/LDH (FL), and (MTX + 5-Fu)/LDH (MFL) were also successfully synthesised (Kim *et al.*, 2014). Using the HeLa and HEK293 cell lines, the study indicated that not only was the cytotoxicity of 5-Fu significantly reduced due to encapsulation within the LDH, but that its combination with methotrexate resulted in higher apoptosis in the cancerous cells (HeLa) whilst significantly reducing toxicity to the control cell line (HEK293) (Kim *et al.*, 2014, Li *et al.*, 2004, Wang *et al.*, 2005b).

Over the past 50 years, despite its many advantages, clinical applications have been greatly limited due to drug resistance to 5-Fu. The overall response rate for advanced colorectal cancer has been reported to be only 10–15% for the 5-Fu alone, but the combination of 5-Fu with other anticancer drugs improved the response rates to 40–50% which is still needs improvement (Zhang *et al.*, 2008a). A myriad of pharmaceutical companies has conducted studies examining the possibilities of combination therapy of various other anticancer drugs with 5-Fu. One such study, conducted by the company Sanofi-Aventis, looked into the effects of the combination therapy of oxaliplatin /5-Fluorouracil/ leucovorin for the treatment of metastatic colon or rectum carcinomas that had progressed for six months, following the first time treatment with a combination drug called eloxatin. An injection containing infusional 5-Fu and leucovorin (LV) was then administered (Sanofi-Avecntis, 2002). Eloxatin or otherwise known asoxaliplatin, is an organoplatinum alkylating agent, which increased the tumour response overall. This drug is FDA (Federal Drug Agency) approved, and was first introduced in France in 1996 and in Europe in 1999, and has since been widely used throughout the world (Sanofi-Avecntis, 2002).

2.4 Nanotechnology in Medicine

Nanotechnology, a multidisciplinary science presents a cutting edge form of technology with opportunities for broader and more efficient modes of drug delivery. The application of nanotechnology in medicine is referred to as nanomedicine. Nanotechnology is defined as the

understanding, control and tolerance of matter (nanomaterials or nanoparticles) generally within the 1-100 nm dimension range, and their application in various functions (Sanofi-Avecntis, 2002, Zhang *et al.*, 2008a). Nanoparticles have unique physicochemical properties such as ultra-small size, large surface area to mass ratio, and high reactivity that allows for more efficient use. These properties can be exploited to improve on the limitations found in current and previously existing traditional therapeutic and diagnostic agents. Furthermore, many nanoparticles have shown lower cytotoxicity, an efficient and non-invasive form of administration, extended half-life of any biomaterial they carry, and the potential to reduce the cost of health-care (Zhang *et al.*, 2008b). Organic and inorganic nanoparticles have been utilized in a myriad of therapeutic applications, viz. fluorescent biological labels, drug and gene delivery vehicles, protein detectors, DNA structure probes, in-tissue engineering, tumour destruction via heating (hyperthermia), separation and purification of biological molecules and cells, as MRI contrast enhancers and in phagokinetic studies (Huang *et al.*, 2007, Lohse and Murphy, 2012, Novio *et al.*, 2013, Salata, 2004). Some of the commonly used nanoparticles to date include lipid and polymers nanostructures, such as liposomes, dendrimers and chitosan (Fu and Yao, 2001, Novio *et al.*, 2013, Zhang *et al.*, 2014). Inorganic nanoparticles that have been used include carbon nanotubes, gold, silver, calcium phosphate, silicon oxides, iron oxides, and layered double hydroxides (LDHs) (Bhattacharyya *et al.*, 2011, Na *et al.*, 2009, Zhang *et al.*, 2014).

2.5 Drug Delivery Systems (DDS)

Chemotherapy requires the delivery of the drug to the site of cancer growth, to reduce and or halt the further spread of the cancerous cells. One of the main challenges facing drug delivery is the concept of "targeted delivery". Over a century ago researchers had already asked the major question: Can a drug be developed such that it can be targeted to the site but not cause collateral damage to healthy cells as a "Magic Bullet"? (Pettrak, 2005, Tiwari *et al.*, 2012). Hence, this was a clear concern from the early years, but with the recent developments in the synthesis of new and appropriate targeted drug delivery system (DDS or TDDS), the dream of targeted delivery could become a reality (Pettrak, 2005). Developing a new drug molecule that is site specific, is not only expensive but also time consuming. This has hence driven the need to develop efficient delivery systems for the existing therapeutic drugs as well (De Jong and Borm, 2008). A drug delivery

system must, along with its other properties, be able to target the drug to the specific site where required, reduce the collateral toxicity of the drug being delivered and offer bioavailability of the drug. The drug delivery system must also comprise: (i) high drug encapsulation and sustained controlled release (ii) appropriate formulation and shelf-life (iii) biocompatibility (iv) biodistribution and targeting, and lastly (v) functionality (De Jong and Borm, 2008). Another essential factor to consider in a DDS is the rate of the drug elimination from the body (Petрак, 2005). It is important that the carrier must not release the drug prematurely (Hashida *et al.*, 2002), but on the other hand, it should not bind the drug too tightly that it prevents its easy release. If it is eliminated from systemic circulation rapidly and before it can be delivered to the target site, the amount of conjugate at the target site might be insufficient to provide the required concentration of the free (unbound) drug, and to elicit the desired therapeutic effect. The design and the production of the drug carrier system needs to remove all nonspecific interactions occurring between the DDS and the environment of the systemic compartment (De Jong and Borm, 2008, Hashida *et al.*, 2002). One of the advantages of using nano-DDSs for the delivery of drugs is that these nanocarriers can become readily attracted to and concentrated at tumour, inflammatory and antigen sampling sites, through the enhanced permeability and retention (EPR) effect of the vasculature (Prabhakar *et al.*, 2013). Some hydrophobic polymeric nanoparticles can act as drug depots, which is largely dependent on the carrier design, and its ability to allow for greater bioavailability of the drug. Drug loading and release are of the utmost importance in drug delivery (Singh and Lillard, 2009). Loading characteristics of a nanoparticle are usually predetermined depending on the methods of formulation. The first method, is the incorporation of the drug at the time of nanoparticle formulation or secondly, the encapsulation of the drug after formulation of the nanoparticle (Singh and Lillard, 2009). These methods will determine the rate of release of the drug, its concentration in the nanoparticle, as well as the degree of protection conferred by the nanoparticle to the drug (Prabhakar *et al.*, 2013, Singh and Lillard, 2009, Soppimath *et al.*, 2001)

2.6 Layered Double Hydroxides (LDHs)

Layered double hydroxides (LDHs), better known as hydrotalcite-like compounds (HTCs) were first introduced to the scientific world in 1842 in Sweden as hydroxycarbonates of magnesium and aluminium that occur naturally from contorted plates and fibrous masses. The first formula ($[\text{Mg}_6\text{Al}_2(\text{OH})_{16}\text{CO}_3 \cdot 4\text{H}_2\text{O}]$) for these layered double hydroxides was then presented at the

University of Florence, Italy by Professor Mannase (Rahman and Al-Deyab, 2011). Layered double hydroxides (LDHs) can be better described using the general formula $[M^{II}_{1-x}M^{III}_x(OH)_2 \cdot x/m \cdot nH_2O] (A^{m-})_{x/m}$ ($x = 0.2-0.4$; $n = 0.5-1$), where M^{II} represents a divalent metal cation such as Mg^{2+} and Ca^{2+} , M^{III} a trivalent metal cation such as Al^{3+} , Cr^{3+} and Fe^{3+} , and A^{m-} an anion (Zhang *et al.*, 2014). Each cation in the LDH layers is surrounded by six OH^- ions, forming an octahedral subunit that share edges which can be expanded forming a two-dimensional layer, which in turn can expand infinitely (Rahman and Al-Deyab, 2011, Zhang *et al.*, 2014). Figure 2.6 provide an illustration of the LDH structure and its chemical components. The magnesium and aluminium composed LDHs have structural similarities to brucite. In brucite, magnesium cations are located at the centre of the octahedral, which contain hydroxyl anions on their vertices (Rahman and Al-Deyab, 2011). These sections are organised into neutral layers forming a honeycomb-like structure that is hydrogen bonded (Arruda *et al.*, 2013). The LDH structure is positively charged due to the presence of anions and water molecules between the cationic layers, giving the structure an ordered interlayer domain. Electrostatic interaction holds the layers of the LDH, unlike the hydrogen bonding seen in the brucite structure (Rahman and Al-Deyab, 2011). Any anion can be intercalated between the cationic layers of the LDH as long as those anions do not disturb the metal ions that form the brucite like structure, and they have sufficient charge density. Some examples of anions that have been intercalated include carbonates, nitrate chlorides and fluoride anions (Bao *et al.*, 2011). Numerous studies have also reported the intercalation of large organic anionic substances such as DNA and RNA, as seen in some recent applications of LDHs as gene delivery vehicles (Balcomb *et al.*, 2015, Ladewig *et al.*, 2010); and also carboxylates, dicarboxylates, alkylsulfates and alkanesulfonates (Bao *et al.*, 2011). These molecules often range in size from 20 nm to 150 nm depending on the mode of synthesis. This varied range allows for the versatility of the type of applications for the LDH (Bao *et al.*, 2011, Gu *et al.*, 2015).

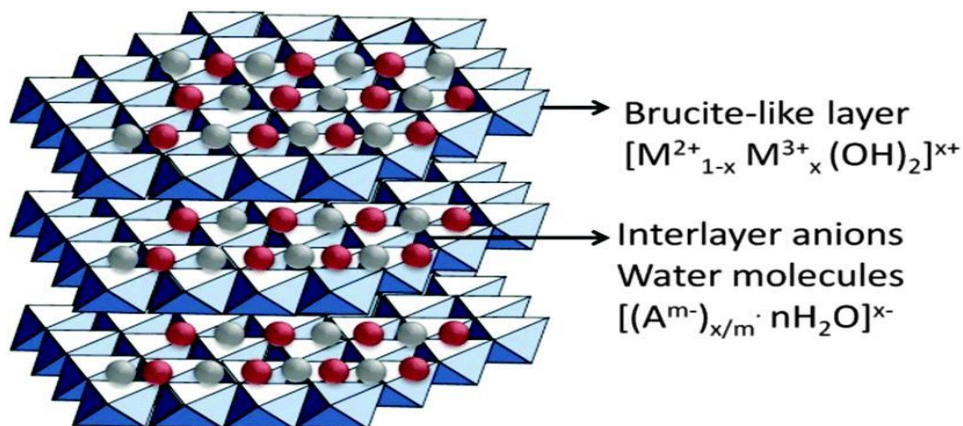


Figure 2.6: Schematic illustration of the hierarchical organisation of the layered double hydroxide structure and its chemical components (Gu *et al.*, 2015)

2.6.1 Applications of Layered Double Hydroxides

For many centuries LDHs have been used as ceramic precursors and often used to make clay pots, etc. Their recent introduction in the world of nanotechnology came when at the time when they were first being utilized as catalysts for hydrogenation, polymerization and steam reforming, and further as ion exchangers, molecular sieves, absorbance molecules, halogen scavengers, PVC stabilizers, and in waste water treatment applications among others (Ladewig *et al.*, 2010). Figure 2.7 highlights some of the commercial applications of LDHs. The environmental applications of LDHs can be extended by various modifications. Modification of LDHs with organic anions allows adsorption of neutral or even positively charged apolar species in the interlayer (gallery space) or on the surface of the solids, while the intercalation of polydentate ligands such as citrate, malate and ethylenediaminetetraacetate (EDTA) modifies the metal ions uptake capacity of the hydroxylated layer (Rojas, 2014).

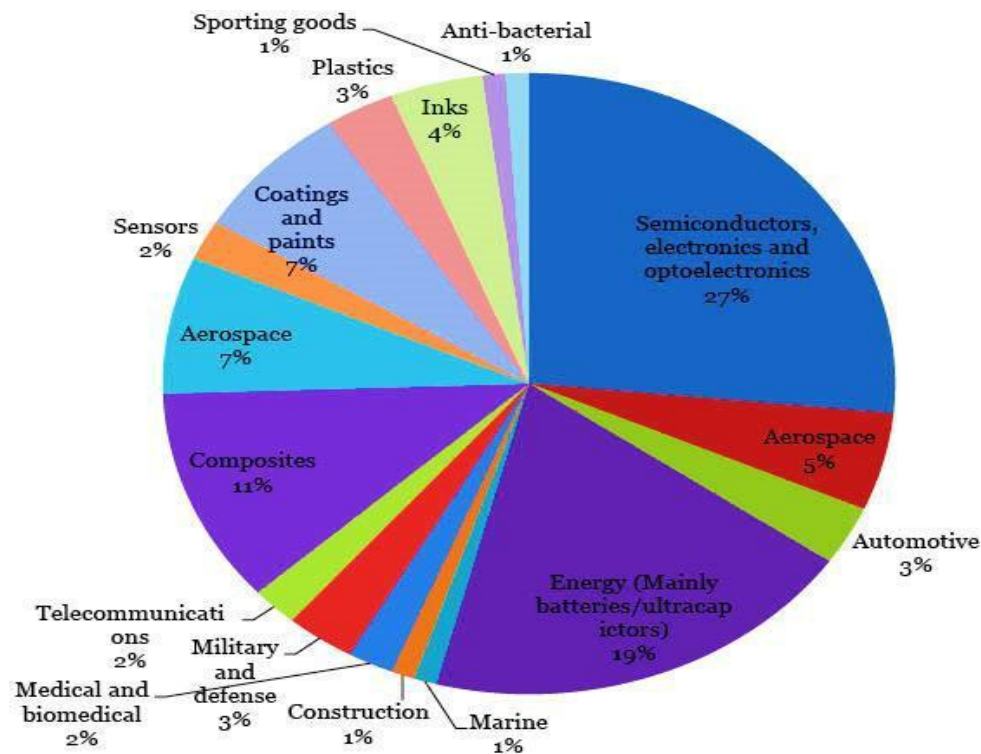


Figure 2.7: Various applications of hydrotalcite-like clays.

2.6.2 Properties of Layered double hydroxides

LDHs exhibit properties such as a high specific surface area ($300 \pm 100 \text{ m}^2/\text{g}$), and a "memory effect" which allows for reconstruction under mild conditions. It has been reported that the calcination of synthetic hydrocalumite (a calcium aluminium LDH) at temperatures ranging from 500-900 °C, led to the formation of crystal mayenite ($\text{Ca}_{12}\text{Al}_{14}\text{O}_{33}$) and lime (CaO). However, after exposure to deionized water the structure of hydrocalumite was completely recovered at room temperature (Del Hoyo, 2007, Mascolo and Mascolo, 2015). Layered double hydroxides also have a buffering property, as mentioned earlier, which is due to the anion exchange property that they have. Hence, the main features of these solids are, a high anion exchange capacity (around 3 meq/g), the instability of the layers at low pH, and the capacity to reconstruct its lamellar structure from the oxides obtained by their calcination (Rojas, 2014).

2.6.3 LDHs for drug delivery

There have been recent reports on the pharmaceutical application of LDHs as drug delivery vehicles, which have proposed that LDHs are great vehicles in drug delivery, in the sense that they can intercalate and deintercalate anionic substances providing a system that allows for controlled release of drugs (Del Hoyo, 2007). Some of the drugs that have been intercalated thus far within LDHs, include ibuprofen, isofamide, camptothecin, protocatechuic acid, etoposide, ciprofloxacin (Gu *et al.*, 2014), α -methyl-4-(2-methylpropyl) benzene acetic acid, diclofenac (Khan *et al.*, 2001) and [2-(2, 6-dichloro-phenylamino)-phenyl] acetic acid (Rives *et al.*, 2014). These drugs are often used for treatment of acute flares and inflammation, but present limitations in the sense that they affect the normal functioning of the central nervous system (CNS) in some patients, as well as a host of other detrimental effects, mostly seen in chemotherapy patients (Rives *et al.*, 2014). When intercalated into LDHs, these drugs exhibited a controlled system of release, resulting in the lowering of some of the side effects of “free” drug delivery (Del Hoyo, 2007). This recent surge toward drug intercalation has therefore led to numerous experiments that aim to intercalate different types of anticancer drugs into the LDHs e.g. methotrexate (MTX) (Bullo Saifullah, 2015, Lindgren *et al.*, 2006). Some of the drugs that have been previously intercalated within LDHs for biomedical purposes are listed in Table 2.1. For the purposes of this project we looked at the two major LDH types, namely MgAl and ZnAl LDHs, for the delivery of 5-Fluorouracil.

Table 2:1 Illustration of LDH-drug formulations and their various applications

Type of formulation	Name of Formulation	Type of Disease
Anticancer formulation	Methotrexate LDHs (MgAl)	Bone cancer, leukaemia
	Ifosfamide LDHs (MgAl)	paediatric, adult tumours and lymphomas
	camptothecin LDHs (MgAl)	lung cancer , ovarian cancer , stomach cancer
	Protocatechuic acid LDHs(ZnAl)	cervix, breast ,human leukaemia
	Etoposdie Mg/Al LDHs	small-cell lung carcinoma, gastric cancers, malignancies
	Ciprofloxacin LDHs (MgAl and ZnAl)	Adenocarcinomic, Epithelial cancer cell line
Antimicrobial	Ciprofloxacin LDHs (MgAl)	pseudomonas aeruginosa
Formulation	hippuric acid ZnAl	P. Aeruginosa, staphylococcus
	Benzylpenicillin-MgAl LDHs	Micrococcus lysodeikticus
	amino acid -MgAl LDHs	P. Aeruginosa, staphylococcus
	AgNpbio-MgAl LDHs	Escherichia Coli, S.aureus
	AgNpbio-ZnAl LDHs	A. aureus (ACTCC 25923)
	Zn-Ti LDHs	Saccharomyces cereviciae
Antituberculosis formulation	PAS ZnLH	M. tuberculosis
	Cinnamic acid ZnLDH	Protection form UV Radiation
	Cinnamic acid Zn/Al	Protection form UV Radiation
	Benxophenone-4-ZnAl	Protection form UV Radiation
Gene delivery formulation	DNA LDHs (MgAl)	DNA Protection
Gene delivery formulation	plasmid DNA LDHs (MgAl)	enhanced siRNA stability
	siRNA LDHs (ZnAl)	cancer treatment
	siRNA-5-Fu LDHs (ZnAl)	transfected into cytoplasm

2.6.4 LDH nanoparticle cellular uptake and release mechanisms

The cellular uptake of LDHs and LDH nanohybrids have d endocytosis is the main pathway in which the LDHs are internalised in mammalian cells (Figbeen the focus of some studies (Choy *et al.*, 2000). This has led to the proposal that clathrin-mediateure 2.8). Further research endeavours have also demonstrated that in both cell bodies and neurons (PC12 cells), the internalisation of siRNA-LDHs is through clathrin mediated endocytosis, with subsequent retrograde transport to the cell body followed by efficient release into the cytoplasm (Wong *et al.*, 2010). LDHs exhibit a property called the proton sponge effect, due to their high buffering capacity. This plays a crucial role in the release of the LDH's contents into the cell, since due to this proton sponge effect, the endosomal compartment containing the nanoparticle ruptures and exposes the biomolecules within the LDH (Figure 2.8). It was also demonstrated that in tumours or other immortalized cell lines, internalized LDH nanoparticles move from the early endosomes (pH 6.2) to the late endosomal compartment (pH 5–6) throughout various stages in the cell, further confirming the pH dependent release of biomolecules (Wong *et al.*, 2010). LDHs are excocytosed from the cell after their intended function is completed. (Wong *et al.*, 2010).

Figure 2.8 provides an overview of how the mechanism of both internalization and release of encapsulated contents takes place with LDHs. The huge advantage of LDHs is that due to cancer cells having anaerobic cellular conditions they easily release their contents when the pH is lowered in these cells (Del Hoyo, 2007, Rojas *et al.*, 2015). The lowered pH of cancer cells is due to the Warburg effect (Gatenby and Gillies, 2004), which refers to the observation that most cancer cells predominantly produce energy by a high rate of glycolysis, followed by lactic acid production in the cytosol, rather than by a comparatively low rate of glycolysis followed by oxidation of pyruvate in mitochondria as in most normal cells (Alfarouk *et al.*, 2011, Kim and Dang, 2006, Vander Heiden *et al.*, 2009).

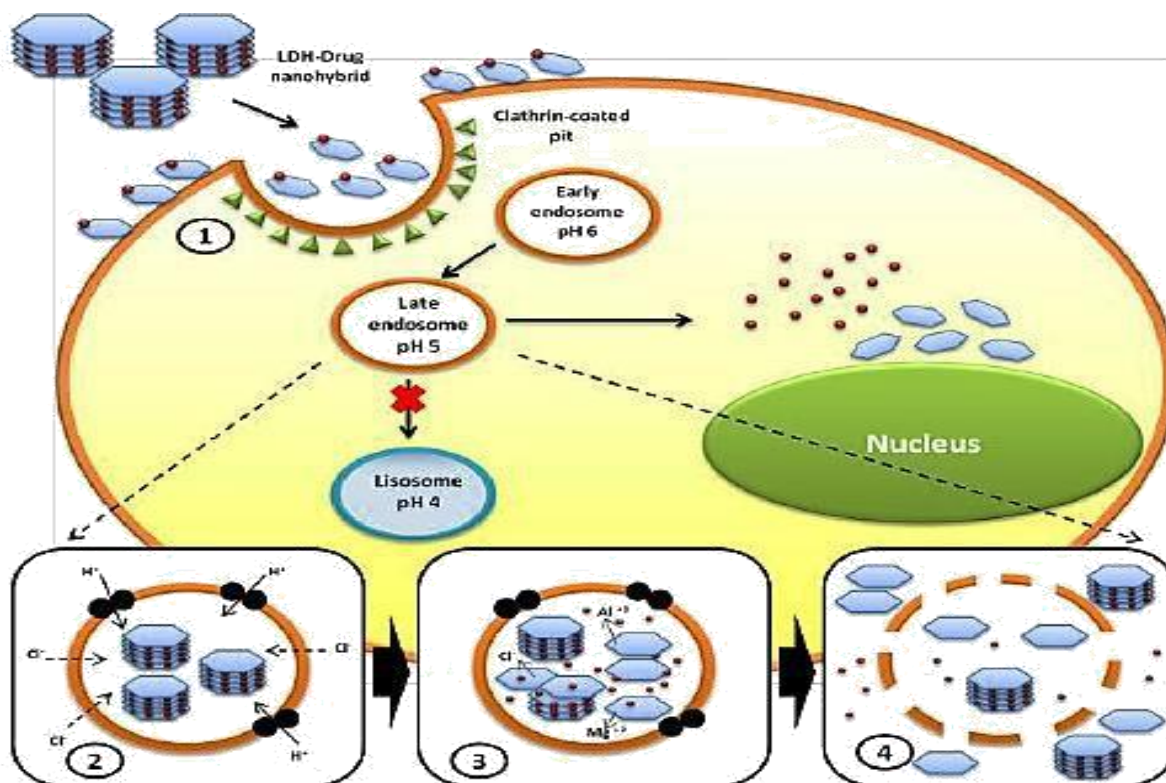


Figure 2.8: Illustration of the cellular uptake of LDH-drug nanocomplexes (1) LDH-drug nanocomplexes attach to the membrane, followed by clathrin mediated endocytosis (2-4) proton sponge effects (Rojas *et al.*, 2015).

2.7 Intercalation of Chemotherapeutic drugs in LDHs

2.7.1 Alkalisiation of 5-Fluorouracil

5-Fu is a neutral weak acid and several studies have reported on the difficulty of intercalating it into various host nanoparticles. One study, however, showed that following treatment with alkali, interestingly, the resulting conjugate base was anionic and could be intercalated in the MgAl-LDH (Wang *et al.*, 2005b). For the purpose of this project the main nanocomplex synthesis route taken was the reconstruction route, together with treating the drug with alkali. Many other factors may influence the orientation of the 5-Fu in the LDH (Figure 2.9).

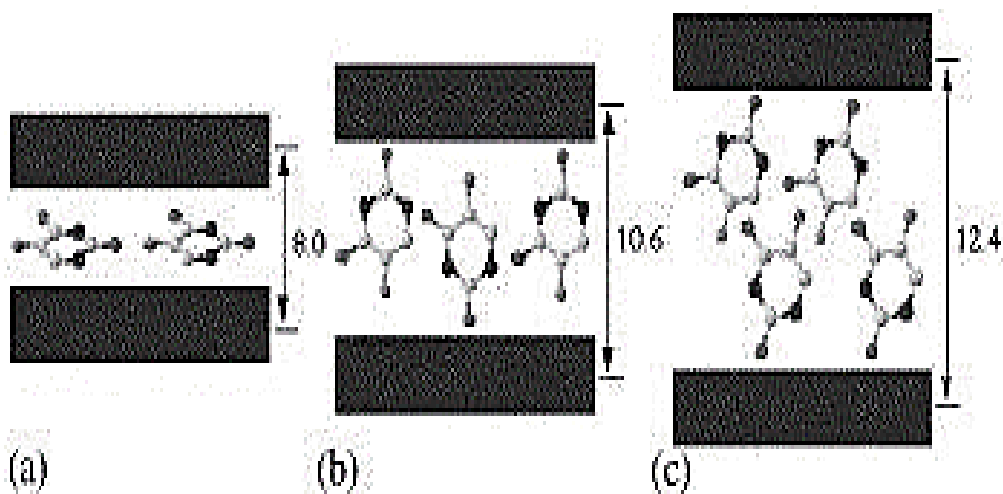


Figure 2.9 Schematic illustration of the orientation of 5-Fu intercalates in LDHs (Wang *et al.*, 2005a)

2.7.2 Co-Precipitation

The co-precipitation technique is perhaps the most commonly used, and the simplest method of drug encapsulation within LDHs. In this procedure, the drug solution is added drop-wise to an aqueous solution of two different metals that are used as precursors. This is followed by the gradual addition of an alkaline solution to the mixture with vigorous stirring under a nitrogen atmosphere, until a final pH of 10 is reached (Barahuie *et al.*, 2014). The mixture is then aged at 80 °C and the resultant slurry was filtered, washed with deionized water, and finally dried in an oven at 60 °C (Barahuie *et al.*, 2014). This method produces large quantities of LDH nanoparticles and the packing density of the interlayer anion is diverse due to variable M^{+2}/M^{+3} . Although a large number of molecules can be incorporated using this method, there is a significantly higher uptake of carbon dioxide and incorporation of unwanted hydroxide anions from the reaction mixture (Alcantara *et al.*, 2010, Barahuie *et al.*, 2014).

2.7.2 Ion-Exchange route

For unstable metal cations or intercalated anions, methods such as the co-precipitation method are not effective. For these species the ion-exchange method is more effective and is usually favoured. A solution containing the anionic species is added to an aqueous solution containing the LDH. The reaction mixture is kept at pH 7–10 by simultaneous addition of an alkaline solution, and the

suspension formed is vigorously stirred at room temperature. The slurry is then aged at 80 °C and washed as in the co-precipitation method (Barahuie *et al.*, 2014). Factors such as anion affinity, exchange medium, pH and chemical composition can affect the encapsulation of species using this ion-exchange procedure.

2.7.3 Calcination / Reconstruction

For our study we used the calcination or reconstruction method to encapsulate 5-Fu within the two types of LDH synthesized. For this route, LDHs are synthesized through precipitation without adding the alkalized drug. The LDHs are then calcined at 400 °C. Thereafter, the drug solution is vigorously mixed whilst adding the respective LDH powders, to form the drug containing nanocomplexes. These are usually stored in their slurry form for later usage.

2.7.4. Other methods of encapsulation

Hydrothermal and urea hydrolysis methods have also been previously used to incorporate anionic species such as drugs into LDHs. The LDH prepared by urea hydrolysis and hydrothermal methods have homogeneous sizes, and platelet-like primary particles with well-defined hexagonal shapes and good crystal quality (Barahuie *et al.*, 2014)

2.8 Experimental Techniques

2.8.1 Powder X-Ray Diffraction (XRD).

X-Ray Powder Diffraction (XRD) is an analytical technique used for identification of the phases of crystalline material formation and provides essential information on the unit cell dimensions of such a structure (Afyon *et al.*, 2013). The material to be analysed has to be in powdered form, it is then homogenized and its average bulk composition is determined. Max Von Laue discovered. This method of crystal analysis in 1912. He noticed that crystalline substances act as three dimensional diffraction gratings for X-Ray wavelengths, these were similar to spacing planes

LDHs, it has allowed for the proper characterisation and affirmation of the proper structure of the LDH and thus we have applied this method to analyse both the MgAl-LDHs as well as the ZnAl-LDHs in a crystal lattice structure (Bartholomew, 2013). XRD has been used extensively to analyse.

2.8.3 Microscopy

Electron Microscopy is an important analytical technique in nanotechnology. Nanoparticles generally being small particles (nm scaled) to analyse usually are better characterized using the different electron microscopies available. The most common types of electron microscopies available are Scanning Electron Microscopy (SEM) as well as Transmission Electron Microscopy (TEM). Electron Microscopes apply the principle that because the wavelength of an electron is up to 100,000 times shorter than that of visible light photons, the electron microscope is enabled a much higher resolving power than a conventional light microscope (Erni et al., 2009). The SEM and TEM microscopy techniques were used in the characterisation of the MgAl-LDHs and ZnAl-LDHs, their calcined derivatives as well as the drug nanohybrids.

2.8.3.1 Scanning Electron Microscopy.

The basic principle of S.E.M is that electrons are accelerated in an SEM and carry large amounts of kinetic energy. This energy is dissipated as a variety of signals produced by the electron-sample interactions when the incident electrons are decelerated in the sample (Erni et al., 2009). These signals include secondary electrons (that produce S.E.M images), backscattered electrons (BSE), diffracted backscattered electrons (EBSD that are used to determine crystal structures and orientations of minerals), photons (characteristic X-rays that are used for elemental analysis and continuum X-rays), visible light (cathodoluminescence–CL), and heat. The SEM scans the surface of the sample giving the profile of its surface morphology, size range, aggregation characteristics as well as other essential information about the analysed sample Layered double hydroxides form hexagonal or pentagonal structures that can easily be detectable through scanning electron microscopy (Swapp, 2016). This information is essential for confirmation of true LDH formation after its synthesis and to confirm intercalation of the drug into the respective LDH and monitor any morphological and size change.

2.8.3.2 Transmission Electron Microscope.

In transmission electron microscopy (TEM), the source of illumination is a beam of electrons of very short wavelength, emitted from a tungsten filament at the top of a cylindrical column of about 2m in height. The whole optical system of the microscope is enclosed in vacuum. Air must be evacuated from the column to create a vacuum so that the collision of electrons with air molecules and hence the scattering of electrons are avoided. At specific intervals along the column specific intervals magnetic coils are placed(Reimer, 2013). Just as the light is focused by the glass lenses in a light microscope, these magnetic coils in the electron microscope focus the electron beam. The magnetic coils placed at specific intervals in the column acts as an electromagnetic condenser lens system(Reimer, 2013). TEM was applied in the analysis and imaging of the respective LDHs, their calcined version as well as their nanohybrid counterparts.

2.8.4 Nanotracking analysis (NTA)

To truly study a nanoparticle one not only has to look at aspects of surface morphology and aggregation properties of a nanoparticle thus another important aspect of our study was the colloidal characterization of our LDH nanoparticles and their respective Nanocomplexes (with 5-Fluorouracil). Being in the range of 35nm to 70nm the LDH exhibits the Brownian motion in suspension, governed by both gravity as well as sedimentation. LDHs are fairly stable nanoparticles in solution but they have been found to be highly sediment. To fully study the colloidal properties of LDHs we employed the use of the Malvern-NS500 Nanosight's technology (Choy et al., 2007, Del Hoyo, 2007).

The Malvern Nanosight NS500 utilizes technology the company termed Nanoparticle Tracking Analysis (NTA) which applies the Stokes-Einstein equation for nanoparticle tracking(Malvern, 2016). Light scattering as well as Brownian motion properties are used to acquire the nanoparticle's size distribution and concentration. Using a laser beam that is passed through the sample chamber containing the sample in suspension. As the light scatters the nanoparticle is visualized through a 20X magnification microscope. As the nanoparticle is bombarded with laser beams a camera records and captures a video(Malvern, 2016). To measure the Zeta potential of a nanoparticle, an electric field is applied (electrophoretic velocity). This field allows for the

movement of the nanoparticles as well as movement of the suspending solution. By measuring the total drift velocity composing of both the electrophoresis and electro-osmosis movements the zeta potential is measured for a single particle (Malvern, 2016).

2.8.5 Cytotoxicity Studies

2.8.5.1 MTT Assay

To determine the cytotoxic effect of the 5-Fluorouracil after treatment of cells with the drug at increased concentrations the MTT Assay was used. The MTT assay or 3-[4,5-dimethylthiazol-2-yl]-2,5 diphenyl tetrazolium bromide assay is based on the principle that the MTT reagent is converted into formazan crystals by cells which are proliferating, this action which determines mitochondrial activity is then used to quantify the amount of cells after treatment, (thus the total mitochondrial activity is related to the number of viable cells). The MTT assay is applied in the determination of the in vitro cytotoxic effects of drugs such as anticancer drugs on multiple cell lines or primary patient cells (van Meerloo et al., 2011). NAD(P)H-dependent cellular oxidoreductase is an enzyme that is capable of reducing the yellow tetrazolium dye or MTT (3-(4,5-dimethylthiazol-2-yl)-2,5-diphenyltetrazolium bromide) to insoluble purple formazan crystals , these formazan crystals are then solubilised with dimethyl sulfoxide (DMSO) which halts the reduction reaction (Senthilraja and Kathiresan, 2015).

2.8.5.2 Sulphorhodamine B Assay (SRB).

The Sulphorhodamine B (SRB) assay is a colorimetric assay originally developed by Skehan and colleagues to measure drug-induced cytotoxicity and cell proliferation for large-scale drug screening applications (Voigt, 2005). This assay is based on the principle that is based on the ability of the Sulphorhodamine B protein dye to bind electrostatically and pH dependently on protein basic amino acid residues of trichloroacetic acid–fixed cells. Under mild acidic conditions it binds to and under mild basic conditions it can be extracted from cells and solubilized for measurement (Vichai and Kirtikara, 2006). The Sulphorhodamine B dye or Kiton Red 620 is a water soluble fluorescent dye normally used for the quantification of cellular proteins of cultured

cells. Using a 96 well plate for this assay, cell monolayers are fixed with trichloroacetic acid (50%) and stained for 20 minutes with SRB dye, after which excess dye is washed with 1% acetic acid to remove all excess. The protein bound dye is dissolved in 10mM Tris-base and the readings are determined using a Microplate reader at 565nm and background absorbance measured at 690nm for greater accuracy (Vichai and Kirtikara, 2006) (Coppeta and Rogers, 1998)

2.9 Novelty of study

As history has often demonstrated, medicine is a dynamic sector with many improved processes being introduced daily. As times change so do the methods often used to combat diseases such as cancer. The application of various technologies is helping to provide, more efficient, less costly, timeous and non-invasive treatment routes. Nanotechnology is a relatively new approach to medicine. Thus, this project looks at the benefits that nanotechnology can provide in the search for a treatment for cancer, with the introduction of layered double hydroxides (LDHs) as potential nanoparticles for the delivery of chemotherapeutic agents to cancer cells in a safe and controlled drug delivery system. This work is cutting-edge and novel not only in a national context but also globally. Although previously used to deliver therapeutic nucleic acids such as nucleic acids, LDHs are proving to be unique to other nanoparticles, with its intricate design and yet simple structure.

2.9 References

- Abraham, L. M., Selva, D., Casson, R. & Leibovitch, I. 2007. The clinical applications of fluorouracil in ophthalmic practice. *Drugs*, 67, 237-255.
- Ahmad, I., Akhter, S., Ahmad, M. Z., Shamim, M., Rizvi, M. A., Khar, R. K. & Ahmad, F. J. 2014. Collagen loaded nano-sized surfactant based dispersion for topical application: formulation development, characterization and safety study. *Pharmaceutical development and technology*, 19, 460-467.
- Alcantara, A., Aranda, P., Darder, M. & Ruiz-Hitzky, E. 2010. Bionanocomposites based on alginate–zein/layered double hydroxide materials as drug delivery systems. *Journal of Materials Chemistry*, 20, 9495-9504.
- Alfarouk, K. O., Muddathir, A. K. & Shayoub, M. E. 2011. Tumor acidity as evolutionary spite. *Cancers*, 3, 408-414.
- Arruda, C., Cardoso, P., Dias, I. & Salomão, R. 2013. Hydrotalcite ($\text{Mg}_6\text{Al}_2(\text{OH})_{16}(\text{CO}_3)_4\cdot 4\text{H}_2\text{O}$): A Potentially Useful Raw Material for Refractories. *INTERCERAM*, 3, 202,623
- Balasubramanian, S. & Neidle, S. 2009. G-quadruplex nucleic acids as therapeutic targets. *Current opinion in chemical biology*, 13, 345-353.
- Balcomb, B., Singh, M. & Singh, S. 2015. Synthesis and characterization of layered double hydroxides and their potential as nonviral gene delivery vehicles. *ChemistryOpen*, 4, 137-145.
- Bao, H., Yang, J., Huang, Y., Xu, Z. P., Hao, N., Wu, Z., Lu, G. Q. M. & Zhao, D. 2011. Synthesis of well-dispersed layered double hydroxide core@ ordered mesoporous silica shell nanostructure (LDH@ m SiO₂) and its application in drug delivery. *Nanoscale*, 3, 4069-4073.

- Barahuie, F., Hussein, M. Z., Fakurazi, S. & Zainal, Z. 2014. Development of drug delivery systems based on layered hydroxides for nanomedicine. *International journal of molecular sciences*, 15, 7750-7786.
- Bhattacharyya, S., Kudgus, R. A., Bhattacharya, R. & Mukherjee, P. 2011. Inorganic nanoparticles in cancer therapy. *Pharmaceutical research*, 28, 237-259.
- Brunton, L. L., Chabner, B. & Knollmann, B. C. 2011. *Goodman & Gilman's the pharmacological basis of therapeutics*, McGraw-Hill Medical New York.
- Bullo Saifullah, M. Z. B. H. 2015. Inorganic nanolayers: structure, preparation, and biomedical applications. *International journal of nanomedicine*, 10, 5609.
- Cancer.Net. 2015. *The Genetics of Cancer* [Online]. :<http://www.cancer.net/navigating-cancer-care/cancer-basics/genetics/genetics-cancer> :<http://www.cancer.net/navigating-cancer-care/cancer-basics/genetics/genetics-cancer> Available: :<http://www.cancer.net/navigating-cancer-care/cancer-basics/genetics/genetics-cancer> [Accessed 06 June 2016 2016].
- Cardonick, E. & Iacobucci, A. 2004. Use of chemotherapy during human pregnancy. *The lancet oncology*, 5, 283-291.
- Cavalli, R., Leone, F., Minelli, R., Fantozzi, R. & Dianzani, C. 2014. New Chitosan Nanospheres for the Delivery of 5-Fluorouracil: Preparation, Characterization and in vitro Studies. *Current drug delivery*, 11, 270-278.
- Centers for diseases control and prevention, Casey research,DC. 2016. Available: <http://www.cdc.gov/cancer/international/statistics.htm>.
- Chemistry, P. O. 2016. 5-Fluorouracil. In: 5-FLUOROURACIL, D. (ed.) *Compound Summary for CID 3385*. PubChem.

- Chen, B. K. a. H. 2016. *Chemotherapy* [Online]. HealthLine. Available: <http://www.healthline.com/health/chemotherapy#Overview1> [Accessed 19 October 2016 2016].
- Cole, W. H. 1973. The mechanisms of spread of cancer. *Surgery, gynecology & obstetrics*, 137, 853-871.
- Colledge, W. & Evans, M. 1995. Cystic fibrosis gene therapy. *British medical bulletin*, 51, 82-90.
- De Jong, W. H. & Borm, P. J. 2008. Drug delivery and nanoparticles: applications and hazards. *International journal of nanomedicine*, 3, 133.
- de Mol, M., Visser, S., Den Oudsten, B., Van Walree, N., Belderbos, H. & Aerts, J. 2016. 187P: Patient's feelings about side-effects are predictive for (Health Related) Quality of Life in patients with advanced stage lung cancer treated with chemotherapy. *Journal of Thoracic Oncology*, 11, S138.
- Del Hoyo, C. 2007. Layered double hydroxides and human health: an overview. *Applied Clay Science*, 36, 103-121.
- Dianzani, C., Zara, G. P., Maina, G., Pettazzoni, P., Pizzimenti, S., Rossi, F., Gigliotti, C. L., Ciamporcero, E. S., Daga, M. & Barrera, G. 2014. Drug delivery nanoparticles in skin cancers. *BioMed research international*, 2014.
- dos Santos Guimarães, I., Daltoé, R. D., Herlinger, A. L., Madeira, K. P., Ladislau, T., Valadão, I. C., Junior, P. C. M. L., Teixeira, S. F., Amorim, G. M. & dos Santos, D. Z. 2013. Conventional Cancer Treatment. *Cancer Treatment-Conventional and Innovative approaches*.

- Fadaeian, G., Shojaosadati, S. A., Kouchakzadeh, H., Shokri, F. & Soleimani, M. 2015. Targeted Delivery of 5-fluorouracil with Monoclonal Antibody Modified Bovine Serum Albumin Nanoparticles. *Iranian journal of pharmaceutical research: IJPR*, 14, 395.
- Fitzakerley, D. J. 2015. Pharmacokinetics 5F-Fluorouracil. 5 May 2015 ed. University of Minnesota Medical School Duluth: 2015 Antineoplastics.
- Flotte, T. & Carter, B. 1995. Adeno-associated virus vectors for gene therapy. *Gene therapy*, 2, 357-362.
- Folprecht, G., Cunningham, D., Ross, P., Glimelius, B., Di Costanzo, F., Wils, J., Scheithauer, W., Rougier, P., Aranda, E. & Hecker, H. 2004. Efficacy of 5-fluorouracil-based chemotherapy in elderly patients with metastatic colorectal cancer: a pooled analysis of clinical trials. *Annals of Oncology*, 15, 1330-1338.
- Fu, H.-B. & Yao, J.-N. 2001. Size effects on the optical properties of organic nanoparticles. *Journal of the American Chemical Society*, 123, 1434-1439.
- Gatenby, R. A. & Gillies, R. J. 2004. Why do cancers have high aerobic glycolysis? *Nature Reviews Cancer*, 4, 891-899.
- Gill, P., Grothey, A. & Loprinzi, C. 2006. Nausea and vomiting in the cancer patient. *Oncology*. Springer.
- Griesenbach, U. & Alton, E. W. 2013. Moving forward: cystic fibrosis gene therapy. *Human molecular genetics*, 22, R52-R58.
- Gu, Z., Atherton, J. J. & Xu, Z. P. 2015. Hierarchical layered double hydroxide nanocomposites: structure, synthesis and applications. *Chemical Communications*, 51, 3024-3036.
- Gu, Z., Wu, A., Li, L. & Xu, Z. P. 2014. Influence of hydrothermal treatment on physicochemical properties and drug release of anti-inflammatory drugs of intercalated layered double hydroxide nanoparticles. *Pharmaceutics*, 6, 235-248.

- Hashida, M., Opanasopit, P. & Nishikawa, M. 2002. Factors affecting drug and gene delivery: effects of interaction with blood components. *Critical Reviews™ in Therapeutic Drug Carrier Systems*, 19.
- Hawkins, M. M., Wilson, L. M., Stovall, M. A., Marsden, H. B., Potok, M. H., Kingston, J. E. & Chessells, J. M. 1992. Epipodophyllotoxins, alkylating agents, and radiation and risk of secondary leukaemia after childhood cancer. *British Medical Journal*, 304, 951-958.
- Huang, X., Jain, P. K., El-Sayed, I. H. & El-Sayed, M. A. 2007. Gold nanoparticles: interesting optical properties and recent applications in cancer diagnostics and therapy.
- Kamb, A., Wee, S. & Lengauer, C. 2007. Why is cancer drug discovery so difficult? *Nature Reviews Drug Discovery*, 6, 115-120.
- Karpanen, T., Egeblad, M., Karkkainen, M. J., Kubo, H., Ylä-Herttuala, S., Jäättelä, M. & Alitalo, K. 2001. Vascular endothelial growth factor C promotes tumor lymphangiogenesis and intralymphatic tumor growth. *Cancer research*, 61, 1786-1790.
- Khan, A. I., Lei, L., Norquist, A. J. & O'Hare, D. 2001. Intercalation and controlled release of pharmaceutically active compounds from a layered double hydroxide. Electronic supplementary information (ESI) available: Fig. S1: X-ray diffraction patterns of (a) $[\text{LiAl}_2(\text{OH})_6]\text{Cl}\cdot\text{H}_2\text{O}$ and (b) LDH/Ibuprofen intercalate. See <http://www.rsc.org/suppdata/cc/b1/b106465g>. *Chemical Communications*, 2342-2343.
- Kim, J.-w. & Dang, C. V. 2006. Cancer's molecular sweet tooth and the Warburg effect. *Cancer research*, 66, 8927-8930.
- Kim, T.-H., Lee, G. J., Kang, J.-H., Kim, H.-J., Kim, T.-i. & Oh, J.-M. 2014. Anticancer drug-incorporated layered double hydroxide nanohybrids and their enhanced anticancer

- therapeutic efficacy in combination cancer treatment. *BioMed research international*, 2014.
- Kim, W. J., Christensen, L. V., Jo, S., Yockman, J. W., Jeong, J. H., Kim, Y.-H. & Kim, S. W. 2006. Cholesteryl oligoarginine delivering vascular endothelial growth factor siRNA effectively inhibits tumor growth in colon adenocarcinoma. *Molecular Therapy*, 14, 343-350.
- Kucia, M., Reza, R., Miekus, K., Wanzeck, J., Wojakowski, W., Janowska-Wieczorek, A., Ratajczak, J. & Ratajczak, M. Z. 2005. Trafficking of Normal Stem Cells and Metastasis of Cancer Stem Cells Involve Similar Mechanisms: Pivotal Role of the SDF-1–CXCR4 Axis. *Stem cells*, 23, 879-894.
- Kumari, A., Singla, R., Guliani, A. & Yadav, S. K. 2016. Biodegradable Nanoparticles and Their In Vivo Fate. In: YADAV, S. K. (ed.) *Nanoscale Materials in Targeted Drug Delivery, Theragnosis and Tissue Regeneration*. Singapore: Springer Singapore.
- Ladewig, K., Niebert, M., Xu, Z. P., Gray, P. P. & Lu, G. Q. M. 2010. Controlled preparation of layered double hydroxide nanoparticles and their application as gene delivery vehicles. *Applied Clay Science*, 48, 280-289.
- Li, B., He, J., Evans, D. G. & Duan, X. 2004. Enteric-coated layered double hydroxides as a controlled release drug delivery system. *International journal of pharmaceutics*, 287, 89-95.
- Li, T.-J., Huang, C.-C., Ruan, P.-W., Chuang, K.-Y., Huang, K.-J., Shieh, D.-B. & Yeh, C.-S. 2013. In vivo anti-cancer efficacy of magnetite nanocrystal-based system using locoregional hyperthermia combined with 5-fluorouracil chemotherapy. *Biomaterials*, 34, 7873-7883.

Li, X., Xu, Y., Chen, G., Wei, P. & Ping, Q. 2008. PLGA nanoparticles for the oral delivery of 5-Fluorouracil using high pressure homogenization-emulsification as the preparation method and in vitro/in vivo studies. *Drug development and industrial pharmacy*, 34, 107-115.

Lind, M. 2008. Principles of cytotoxic chemotherapy. *Medicine*, 36, 19-23.

Lindgren, M., Rosenthal-Aizman, K., Saar, K., Eiríksdóttir, E., Jiang, Y., Sassian, M., Östlund, P., Hällbrink, M. & Langel, Ü. 2006. Overcoming methotrexate resistance in breast cancer tumour cells by the use of a new cell-penetrating peptide. *Biochemical pharmacology*, 71, 416-425.

Liu, F.-S. 2009. Mechanisms of chemotherapeutic drug resistance in cancer therapy—a quick review. *Taiwanese Journal of Obstetrics and Gynecology*, 48, 239-244.

Lohse, S. E. & Murphy, C. J. 2012. Applications of colloidal inorganic nanoparticles: from medicine to energy. *Journal of the American Chemical Society*, 134, 15607-15620.

Longley, D. B., Allen, W. L. & Johnston, P. G. 2006. Drug resistance, predictive markers and pharmacogenomics in colorectal cancer. *Biochimica et Biophysica Acta (BBA)-Reviews on Cancer*, 1766, 184-196.

Longley, D. B., Harkin, D. P. & Johnston, P. G. 2003. 5-fluorouracil: mechanisms of action and clinical strategies. *Nature Reviews Cancer*, 3, 330-338.

Marwa, A., Omaima, S., Hanaa, E.-G. & Mohammed, A.-S. 2013. Preparation and in-vitro evaluation of diclofenac sodium niosomal formulations. *International Journal of Pharmaceutical Sciences and Research*, 4, 1757.

- Mascolo, G. & Mascolo, M. 2015. On the synthesis of layered double hydroxides (LDHs) by reconstruction method based on the “memory effect”. *Microporous and Mesoporous Materials*, 214, 246-248.
- Maxwell, P. J., Longley, D. B., Latif, T., Boyer, J., Allen, W., Lynch, M., McDermott, U., Harkin, D. P., Allegra, C. J. & Johnston, P. G. 2003. Identification of 5-fluorouracil-inducible target genes using cDNA microarray profiling. *Cancer research*, 63, 4602-4606.
- MedicineNet.com. 2016. *Cancer Risk Factors* [Online]. Available: <http://www.medicinenet.com/cancer_causes/article.htm> Viewed 05 May 2016 [Accessed 06 June 2016].
- Mittermeyer, G., Christine, C. W., Rosenbluth, K. H., Baker, S. L., Starr, P., Larson, P., Kaplan, P. L., Forsayeth, J., Aminoff, M. J. & Bankiewicz, K. S. 2012. Long-term evaluation of a phase 1 study of AADC gene therapy for Parkinson's disease. *Human gene therapy*, 23, 377-381.
- Monje, M. & Dietrich, J. 2012. Cognitive side effects of cancer therapy demonstrate a functional role for adult neurogenesis. *Behavioural brain research*, 227, 376-379.
- Na, H. B., Song, I. C. & Hyeon, T. 2009. Inorganic nanoparticles for MRI contrast agents. *Advanced materials*, 21, 2133-2148.
- Navigating Cancer, I. 2016. *List of Cancer Chemotherapy Drugs* [Online]. Patient Engagement Portal v.5.1. Available: https://www.navigatingcancer.com/library/all/chemotherapy_drugs [Accessed 15 May 2016].
- Niidome, T. & Huang, L. 2002. Gene therapy progress and prospects: nonviral vectors. *Gene therapy*, 9, 1647-1652.

- Novio, F., Simmchen, J., Vázquez-Mera, N., Amorín-Ferré, L. & Ruiz-Molina, D. 2013. Coordination polymer nanoparticles in medicine. *Coordination Chemistry Reviews*, 257, 2839-2847.
- Pabla, N. & Dong, Z. 2012. Curtailing side effects in chemotherapy: a tale of PKC β in cisplatin treatment.
- Palfi, S., Gurruchaga, J. M., Ralph, G. S., Lepetit, H., Lavisse, S., BATTERY, P. C., Watts, C., Miskin, J., Kelleher, M. & Deeley, S. 2014. Long-term safety and tolerability of ProSavin, a lentiviral vector-based gene therapy for Parkinson's disease: a dose escalation, open-label, phase 1/2 trial. *The Lancet*, 383, 1138-1146.
- Petrak, K. 2005. Essential properties of drug-targeting delivery systems. *Drug discovery today*, 10, 1667-1673.
- Pharmaceutics 2016. Anticancer drugs. In: FACTZ, A. D. P. (ed.). Pharmaceutics.com: Pharmaceutics.com.
- Prabhakar, U., Maeda, H., Jain, R. K., Sevick-Muraca, E. M., Zamboni, W., Farokhzad, O. C., Barry, S. T., Gabizon, A., Grodzinski, P. & Blakey, D. C. 2013. Challenges and key considerations of the enhanced permeability and retention effect for nanomedicine drug delivery in oncology. *Cancer research*, 73, 2412-2417.
- Prado, C. M., Baracos, V. E., McCargar, L. J., Mourtzakis, M., Mulder, K. E., Reiman, T., Butts, C. A., Scarfe, A. G. & Sawyer, M. B. 2007. Body composition as an independent determinant of 5-fluorouracil-based chemotherapy toxicity. *Clinical Cancer Research*, 13, 3264-3268.
- Praetorius, N. P. & Mandal, T. K. 2007. Engineered nanoparticles in cancer therapy. *Recent Patents on Drug Delivery & Formulation*, 1, 37-51.

- Rahman, A. & Al-Deyab, S. S. 2011. Structure, characterization and application of Ni hydrotalcite as solid base catalysts for organic transformations. *Journal of the Chilean Chemical Society*, 56, 598-600.
- Rang, H. P., Bloom, F. E., Stringer, J. L., Cuthbert, A. W., Thomas, J. A. & Scarne, J. 2016. TYPES OF DRUGS. Available: <https://global.britannica.com/science/drug-chemical-agent/Types-of-drugs> [Accessed 25 May 2016].
- Rives, V., del Arco, M. & Martín, C. 2014. Intercalation of drugs in layered double hydroxides and their controlled release: A review. *Applied clay science*, 88, 239-269.
- Rojas, R. 2014. Copper, lead and cadmium removal by Ca Al layered double hydroxides. *Applied Clay Science*, 87, 254-259.
- Russ, V. & Wagner, E. 2007. Cell and Tissue Targeting of Nucleic Acids for Cancer Gene Therapy. *Pharmaceutical Research*, 24, 1047-1057.
- , S. H. & Kim, S. 2014. Long dsRNA-mediated RNA interference and immunostimulation: a targeted delivery approach using polyethyleneimine based nano-carriers. *Molecular pharmaceuticals*, 11, 872-884.
- Salata, O. 2004. Applications of nanoparticles in biology and medicine. *Journal of Nanobiotechnology*, 2, 3.
- Sanofi-Aventis. 2002. Treatment for: Metastatic colon or rectum carcinomas that have recurred or progressed within six months following first-line treatment [Online]. Available: <http://www.medilexicon.com/drugs/eloxatin.php>
- Schwarzenbach, H., Hoon, D. S. & Pantel, K. 2011. Cell-free nucleic acids as biomarkers in cancer patients. *Nature Reviews Cancer*, 11, 426-437.

- Singh, R. & Lillard, J. W. 2009. Nanoparticle-based targeted drug delivery. *Experimental and molecular pathology*, 86, 215-223.
- Song, W., Tang, Z., Li, M., Lv, S., Sun, H., Deng, M., Liu, H. & Chen, X. 2014. Polypeptide-based combination of paclitaxel and cisplatin for enhanced chemotherapy efficacy and reduced side-effects. *Acta biomaterialia*, 10, 1392-1402.
- Soppimath, K. S., Aminabhavi, T. M., Kulkarni, A. R. & Rudzinski, W. E. 2001. Biodegradable polymeric nanoparticles as drug delivery devices. *Journal of controlled release*, 70, 1-20.
- Thorn, C. F., Oshiro, C., Marsh, S., Hernandez-Boussard, T., McLeod, H., Klein, T. E. & Altman, R. B. 2011. Doxorubicin pathways: pharmacodynamics and adverse effects. *Pharmacogenetics and genomics*, 21, 440.
- Tiwari, G., Tiwari, R., Sriwastawa, B., Bhati, L., Pandey, S., Pandey, P. & Bannerjee, S. K. 2012. Drug delivery systems: An updated review. *International journal of pharmaceutical investigation*, 2, 2.
- van Kuilenburg, A. B. & Maring, J. G. 2013. Evaluation of 5-fluorouracil pharmacokinetic models and therapeutic drug monitoring in cancer patients. *Pharmacogenomics*, 14, 799-811.
- Vander Heiden, M. G., Cantley, L. C. & Thompson, C. B. 2009. Understanding the Warburg effect: the metabolic requirements of cell proliferation. *science*, 324, 1029-1033.
- Wagner, E., Kircheis, R. & Walker, G. F. 2004. Targeted nucleic acid delivery into tumors: new avenues for cancer therapy. *Biomedicine & pharmacotherapy*, 58, 152-161.
- Wang, Z., Wang, E., Gao, L. & Xu, L. 2005a. Synthesis and properties of Mg₂Al layered double hydroxides containing 5-fluorouracil. *Journal of Solid State Chemistry*, 178, 736-741.

- Wang, Z., Wang, E., Gao, L. & Xu, L. 2005b. Synthesis and properties of Mg₂Al layered double hydroxides containing 5-fluorouracil. *Journal of Solid State Chemistry*, 178, 736-741.
- Weinreb, R. N. 1987. Adjusting the dose of 5-fluorouracil after filtration surgery to minimize side effects. *Ophthalmology*, 94, 564-570.
- Wong, Y., Markham, K., Xu, Z. P., Chen, M., Lu, G. Q. M., Bartlett, P. F. & Cooper, H. M. 2010. Efficient delivery of siRNA to cortical neurons using layered double hydroxide nanoparticles. *Biomaterials*, 31, 8770-8779.
- Zhang, K., Xu, Z. P., Lu, J., Tang, Z. Y., Zhao, H. J., Good, D. A. & Wei, M. Q. 2014. Potential for layered double hydroxides-based, innovative drug delivery systems. *International journal of molecular sciences*, 15, 7409-7428.
- Zhang, L., Gu, F., Chan, J., Wang, A., Langer, R. & Farokhzad, O. 2008a. Nanoparticles in medicine: therapeutic applications and developments. *Clinical pharmacology and therapeutics*, 83, 761-769.
- Zhang, N., Yin, Y., Xu, S.-J. & Chen, W.-S. 2008b. 5-Fluorouracil: mechanisms of resistance and reversal strategies. *Molecules*, 13, 1551-1569.

CHAPTER 3

THE APPLICATION OF MgAl-LDHs AS POTENTIAL ANTICANCER DRUG DELIVERY VEHICLES

Zoleka Mncwabe and Moganavelli Singh^{*}

¹Non-Viral Gene Delivery Laboratory, Discipline of Biochemistry, School of Life Sciences,
UKZN, Westville Campus

^{*}Corresponding author: Prof Moganavelli Singh, email:Singhm1@ukzn.ac.za

Abstract

To this end, more research is required for the development of efficient delivery systems for these drugs, with nanoparticles emerging as a potential strategy for the delivery for many therapeutic biomolecules. Thus, our study focuses on designing a drug delivery system capable of delivering the broad spectrum drug, 5-fluorouracil (5-Fu). Our study looks at the design and application of the MgAl Layered Double Hydroxide nanoparticles (MgAl-LDHs), for the delivery of the 5-Fu *in vitro*. We synthesized two MgAl-LDHs, namely MgAl 2:1 and MgAl 3:1, containing intercalated 5-Fu within the gallery, to create nanohybrids, namely, MgAl 2:1-5-Fu and MgAl 3:1-5-Fu. We characterized the uncalcined, calcined and nanohybridized MgAl LDHs using XRD, FTIR, ICP-OES, SEM, TEM, and NTA to confirm synthesis, structural properties, surface morphologies, size distribution, stability and zeta potential of these nanoparticles. The synthesis of a true LDH and the intercalation of 5-Fu within these nanoparticles was initially confirmed using UV-Vis. Percentage encapsulated drug was quantified using the encapsulation efficiency formula (%EE). A comparative assessment on the effects of the freely delivered 5-Fu versus the LDH delivered 5-Fu were studied using the MTT and SRB assays in four cell lines, namely human embryonic kidney (HEK293), colorectal adenocarcinoma (CaCo-2), breast adenocarcinoma (MCF-7), and the hepatocellular carcinoma (HepG2) cell lines, at varied drug concentrations of 12.5 µg/ mL, 25 µg/ mL, 50 µg/ mL and 100 µg/ mL. A significant cytotoxicity profile was observed across the four cell lines treated with free 5-Fu, with IC₅₀ values ranging between 65.25-92.25 µg/mL. The IC₅₀ value of the cells treated with LDH encapsulated 5-Fu was lower and ranged from 21.95-36.56 µg/mL. Nanohybrids were observed to be better tolerated than free 5-Fu in the all cell lines whilst eliciting the greatest cytotoxicity in the MCF-7 and CaCo-2 cell lines.

Key Words: Layered Double Hydroxides (LDHs), Chemotherapy, 5-Fluorouracil, cytotoxicity, nanohybrids

3.1 Introduction

Previously, drug delivery systems (DDS) have focused on the use of organic nanoparticles such as lipids and cationic polymers to deliver therapeutic drugs (Kumari *et al.*, 2010). However these systems have proven to be poor drug delivery vehicles, due to their inability to provide a stable encapsulating environment in which the drug is protected against physiological parameters in the body (Wilczewska *et al.*, 2012). Even when these organic DDSs were co-synthesized with other moieties to form ligand based delivery systems, they were still unstable leading to their disintegration and subsequent premature drug release (Hofheinz *et al.*, 2005). This has led to the introduction of inorganic nanoparticles which has the potential to overcome some of the shortfalls of previously employed nanoparticles. From the array of nanoparticles utilised in chemotherapeutics today, MgAl-LDHs are slowly showing the ability to be an efficient vehicle for delivery (Ladewig *et al.*, 2010, Xu *et al.*, 2006). The structurally simple and one of the most abundant LDHs available, MgAl-LDH, has been used for the delivery of anticancer drugs such as methotrexate (MTX) (Baldo and Pagani, 2014), 5-fluorouracil (5-Fu) (Choi *et al.*, 2008, Longley *et al.*, 2003), doxorubicin (DOX) among others (Gunawan and Xu, 2008).

This LDH has been used previously in the pharmaceutical industry as components in deodorant sprays, antacids (Newton *et al.*, 2008), antiseptic agents (Katheria *et al.*, 2016) and commercial products such as Talcid® and Bemolan® (Del Arco *et al.*, 2004). Their good adsorbent properties have also made them suitable for the adsorption of intestinal phosphates (Gunawan and Xu, 2008). Some of the advantages of using this LDH include low to negligible toxicity, ease and low cost of preparation, ability to customize their physicochemical properties, anion exchange capacity, and weathering reactions as observed at lowered pHs, which allow for targeting of cancer cells (Gatenby and Gillies, 2004). The lowered pH of cancerous cells is due to the high rate of aerobic glycolysis. This is advantageous for the LDH as it enables slow drug release in the cancerous cells without harming healthy and pH balanced cells (Gatenby and Gillies, 2004). These nanoparticles largely resemble the brucite structure with the chemical formula $Mg(OH)_2$, and were among the first LDHs to be used in drug delivery.

The most commonly known MgAl-LDHs have the chemical formula $\text{Mg}_6\text{Al}_2(\text{OH})_{16}\text{CO}_3 \cdot 0.4\text{H}_2\text{O}$ or general formula: $[\text{M}^{\text{II}}_{1-x}\text{M}^{\text{III}}_x(\text{OH})_2]^{x+}(\text{A}^{\text{m}-})_{x/m} \cdot n\text{H}_2\text{O}$ ($x = 0.2-0.4$; $n = 0.5-1$), where M^{II} represents magnesium (Mg^{2+}) and M^{III} represents aluminium (Al^{3+}), A^{m} would be the anionic species and although there is a wide range of x values to describe the MgAl-LDH structure, pure MgAl-LDHs are usually limited to the range of $0.2 \leq x \leq 0.3$. MgAl LDHs have also been applied in industrial settings as, absorbents for toxic chemicals, stable and recyclable heterogeneous catalysts, as well as in other essential industrial applications (Fan *et al.*, 2014). The successful delivery of MTX and 5-Fu to cancer cells using the MgAl-LDH has been reported (Choi *et al.*, 2008). Furthermore, their enhanced cellular uptake and improved drug efficacy compared to free MTX or 5-Fu have been confirmed (Kim *et al.*, 2014). The co-delivery of 5-Fu and MTX with MgAl-LDH, leading to effective cancer cell death was also reported (Choi and Choy, 2011, Choi *et al.*, 2008); (Kim *et al.*, 2014). MgAl-LDH loaded 5-Fu and PI3K/mTOR dual inhibitor (BEZ-235) was able to produce effective inhibition of colon cancer cells utilizing the apoptotic pathways, with reduced cytotoxic effects observed with the co-delivery of 5-fluorouracil in colon cancer, HCT-116 cell. BEZ-235 was also introduced as a potential inhibitor of the phosphoinositide 3-kinase (PI3K)/protein kinase B (Akt) pathway which is responsible for colon cancer development (Chen *et al.*, 2015)

3.2 Materials

Sodium carbonate (NaCO_3), sodium hydroxide (NaOH), HCl , MTT reagent, dimethylsulfoxide (DMSO), phosphate buffered saline (PBS) tablets, trichloroacetic acid (TCA), acetic acid and Tris EDTA were purchased from Merck, Darmstadt, Germany. Aluminium nitrate, $\text{Al}(\text{NO}_3)_3 \cdot 9\text{H}_2\text{O}$, was obtained from C.C. Imelmann, Southdale, South Africa, and magnesium nitrate, $\text{Mg}(\text{NO}_3)_2 \cdot 6\text{H}_2\text{O}$ from Holpro Analytic (PTY) LTD, Krugersdorp, South Africa. The anticancer drug, 5-fluorouracil (5-Fu) and sulphorhodamine B (SRB) were purchased from Sigma-Aldrich, St Louis, USA. Eagles Minimum Essential Medium (EMEM), Penicillin/ Streptomycin, and Trypsin-versene were all obtained from Lonza Biowhittaker, Walkersville, USA. Fetal bovine serum (FBS) was purchased from Hyclone, GE Healthcare, Utah, USA.

Human embryonic kidney cells were provided by the Anti-viral gene therapy unit, Medical School, University of the Witwatersrand, South Africa. Human hepatocellular carcinoma, breast adenocarcinoma and colorectal cancer cells were purchased from Highveld Biological (PTY) LTD., Lyndhurst, South Africa. All sterile tissue culture plasticware was obtained from Corning, NY, USA. All reagents were of analytical grade, and Milli-Q 18 M Ω water was used throughout.

3.3 Methods

3.3.1 Synthesis of the MgAl layered double hydroxides

LDHs were synthesized using the co-precipitation method. Approximately 25,6 g of 0.1 M Mg(NO₃)₂ · 6H₂O and 18.7g of 0.05M Al(NO₃)₃ · 9H₂O for (MgAl 2:1), and 25.6 g 0.1 M Mg(NO₃)₂ · 6H₂O and 12.8g of 0.05M Al(NO₃)₃ · 9H₂O for (MgAl3:1) were dissolved separately in 150 ml of distilled 18 M Ω water. Na₂CO₃ (53 g) was then dissolved in 600 ml of distilled water with stirring at 720 rpm at room temperature. This was then titrated to pH~11 with Al(NO₃)₃ · 9H₂O and Mg(NO₃)₂ · 6H₂O using NaOH for pH adjustments. The mixtures were aged overnight at 80 °C, and then washed again with 18 M Ω water. The slurries were first vacuum dried and placed overnight in an oven at 110 °C. The LDHs were then crushed to a talc-textured powder and stored at room temperature.

3.3.2 Calcination

The synthesis of the nanocomplexes composed of the MgAl LDHs and the anticancer drug, 5-Fu involved the calcination of the LDH to form mixed metal oxides before complexation. This phase transition assists in a smoother intercalation of 5-Fu into its host during the complexation process. Simultaneously, the LDH structure is completely recovered due to its “memory effect” with addition of the solution containing the 5-Fu. In a typical calcination procedure, 50 mg of the synthesized MgAl-LDH (MgAl- 2:1 and 3:1, respectively) were placed in a horizontal furnace (Labofern PUB002) set at 400 °C and maintained at this temperature for 8 hours under N₂. After calcination, each of the samples were labelled and stored in a glass bottle for later use.

3.3.3 MgAl-LDH: 5-Fu conjugate synthesis

To intercalate 5-Fu into both the MgAl-LDHs (2:1 and 3:1 respectively) the reconstruction method was used. Approximately, 11.1 mg of the calcined MgAl LDH powders were suspended in 20 mL (diluted with distilled water) of 5-Fu (0.0114 M in 18 M Ω water, pH 8.0) solution (5-Fu alkalized with 0.1M NaOH). The mixture was then vigorously stirred under N₂ atmosphere for 24 hours at room temperature to obtain the MgAl-LDH-5-Fu conjugates for both LDHs. The samples were stored at 4 °C until needed.

3.3.4 Drug encapsulation efficiency

The drug encapsulation efficiency study was conducted to determine how much of the drug was actually encapsulated or bound to the respective LDHs. The respective LDH-5-Fu suspensions were centrifuged at 12000 rpm for 5 minutes, and the supernatants assayed by UV-Vis spectroscopy (Biomate, Thermoscientific) for presence of free 5-Fu. The pellets were then resuspended and readings were taken again to measure absorbance of bound drug. Readings were taken at 266 nm and the results were calculated using the formula:

$$\% \text{Encapsulation Efficiency} = (\text{Total drug} - \text{Free "untrapped drug"}) / \text{Total drug} \times 100$$

3.3.5 Powder X-Ray diffraction

Powder X-Ray diffraction (XRD) was performed for the uncalcined (pure), calcined and drug conjugated MgAl LDHs. The analysis was carried out using a Bruker D8 Advanced XRD analyzer (CuK α radiation) equipped with Bruker analysis software. In each of the runs, 0.5 g of the sample was used and signals were recorded for 2 θ values between 5 and 90 ° at a scan rate of 0.5°/min.

3.3.6 Fourier Transform Infrared Spectroscopy (FTIR)

Infra-red (IR) spectra of the LDH and nanocomplexes were obtained with a Perkin Elmer FTIR Spectrometer equipped with a Universal ATR sampling accessory using a diamond crystal. Spectrum Analysis Software was used for analysis of the data.

3.3.7 Inductively Coupled Plasma Analysis-Optical Emission Spectroscopy (ICP-OES)

Elemental detection and quantification of metal content of the LDH and its complexes were obtained by inductively coupled plasma-optical emission spectroscopy (ICP-OES), performed on a Perkin Elmer Optima 5300 DV Optical Emission Spectrometer. Standard calibration curves were set up between 1 and 20 ppm, using 100 ppm standard stock solutions of the respective metal solutions purchased from Fluka.

3.3.8 Electron Microscopy

Electron microscopy (EM) was used to confirm the morphologies, structural orientation and the general surface anatomy of the pristine (i) MgAl-LDHs along with their calcined derivatives and (ii) MgAl-LDH-5-Fu conjugates (2:1 and 3:1). Scanning Electron Microscopy (SEM) using 0.1 mg samples was carried out using a ZEISS LEO 1450 scanning electron microscope. Transmission Electron Microscopy (TEM), using 1 μ l of each sample, was done in a JOEL1010 electron microscope fitted with Megaview 3 soft imaging system and images were viewed using the iTEM software.

3.3.9 Nanoparticle Tracking Analysis (NTA)

The nanosight NTA NS500 (Malvern Instruments Ltd, Worcestershire, United Kingdom) was used to visualize and analyse the pristine and drug conjugated samples. NTA analyses the sample's size and zeta potential by tracking the rate of the Brownian motion to the particle's size. The samples were diluted to approximately 0.1 mg/mL in deionized 18 M Ω water. All measurements were acquired at 25 °C. To eliminate the risk of indiscrepancies in the results, the instrument was routinely flushed with 18 M Ω water.

3.3.10 Drug release Studies

Drug release studies were performed by dialysis as described by (Maghsoudi *et al.*, 2008). Briefly, 1 mL of the MgAl-5-Fu solutions (2:1 and 3:1 respectively) were dialyzed (MWCO ~ 7000 KDa), against 20 mL of phosphate buffered saline PBS (pH 4 and pH 7) under constant stirring for 7 hours. Aliquots of 1 ml from the PBS solution were removed for UV-Vis analysis at 266 nm every hour. Fresh PBS (1 mL) at the same pH was replenished each time.

3.3.11 *In vitro* cell culture studies

All cell culture studies were conducted under sterile conditions. Cell growth and morphology were constantly monitored using an inverted microscope (Nikon TMS F 6V, Tokyo, Japan). Growth medium in cells were replenished when required, and cells were routinely split at or near confluency into sterile cell culture flasks to prevent overgrowth and keep the cells in the log phase. For cell culture assays, cells were counted using an haemocytometer and plated into either 96 or 48-well tissue culture plates

3.3.12 MTT Cytotoxicity assay

Cell toxicity of the free drug and LDH encapsulated drug was evaluated using the four mammalian cell lines: CaCo-2, HepG2, MCF-7 and HEK293. Cells were seeded into 96-well plates at a density of 1×10^4 cells/well in 100 μ L of complete medium (EMEM +10% FBS + antibiotics) and incubated overnight at 37 °C in a humidified CO₂ incubator. Following incubation, cells were treated with the drug alone and MgAl encapsulated drug at increased concentrations (12.5 μ g/ mL, 25 μ g/ mL, 50 μ g/ mL and 100 μ g/ mL), and incubated for 48 hours. Thereafter, the medium was removed and 100 μ L of MTT reagent and 100 μ L of medium was added to the cells, which were then incubated for a further 4 hours at 37 °C. The MTT infused medium was then removed and 100 μ L of DMSO was added to the cells to dissolve the formazan crystals produced.

The coloured solutions were then read using a MR-96A microplate reader (Vacutec, Hamburg, Germany) at wavelength of 570 nm, with 650 nm being used for reading.

The assay was conducted in triplicate (n=3), and percentage cell viability was calculated using the following formula:

$$\% \text{ cell survival} = (\text{A}_{570 \text{ nm}} \text{ treated cells}) / (\text{A}_{570 \text{ nm}} \text{ untreated cells}) \times 100$$

3.3.13 Sulphorhodamine B (SRB) Cytotoxicity assay

Cells were seeded and treated as in 3.3.12. After the 48-hour incubation at 37 °C, cells were fixed by gently layering with ¼ volume of cold 50% TCA on top of the growth medium and incubated for an hour at 4 °C. Cells were then rinsed with deionized water to remove the TCA and other serum proteins. After air-drying, 50 µL of 0.4 % SRB solution was added to the cells for 20 minutes. Thereafter, the cells were washed with a 1% acetic acid solution.

To solubilize the dye, 100 µL of a 10 mM Tris-EDTA solution was added and the plate rocked gently on a platform shaker (Stuart Scientific, STR 6) for 5 minutes. Absorbance was then read in a microplate reader at 565 nm with 690 nm used for background reading.

3.3.14 Apoptosis

Apoptosis studies were carried out using the dual-staining acridine orange and ethidium bromide (AO/EB) method to compare the effects of exposure of the cells to “free” 5-Fu and MgAl-LDH-5-Fu. Approximately, 100 mg/mL of both dyes (1:1 ratio) were prepared in sterile PBS. Cells at confluency were plated into 24 well plates at a seeding density of 1.2×10^5 cells/well, incubated for 24 hours at 37 °C, and then treated with free and MgAl encapsulated drug (20 µL) for 48 hours. Thereafter, cells were washed with 100 µL PBS, and 15 µl of the dual stain was added and cells kept at room temperature for 5 minutes. These cells were then visualized using an Olympus fluorescent microscope at X200 magnification, following which apoptotic indexes were calculated using the described formula:

$$\text{Apoptotic Index} = \frac{\text{Number of apoptotic cells}}{\text{Number of total cells}}$$

3.3.15 Statistical analyses

All statistical analyses were performed using Graph pad prism 5.0 (GraphPad Software, Inc., San Diego, CA), one-way analysis of variance (ANOVA). Differences between groups were considered to be significant at a P value of $* < 0.05$. (* represents degree of statistical significance)

3.4 Results and Discussion

3.4.1 Syntheses of LDHs

We successfully synthesised MgAl-LDHs (2:1 and 3:1) through the co-precipitation method, yielding 1.18 g and 1.33 g, respectively. The talcum textured LDH powders were pristinely white and had no visible contaminants (Figure 3.1). There was a measureable loss in the mass of the LDHs after calcination, so that 0.56 g and 0.60 g of the MgAl 2:1 and MgAl 3:1 LDHs respectively. This is due to the processes of dehydration, dihydroxylation, and decarbonation that the LDHs undergo during calcination (Yamashita *et al.*, 1998).

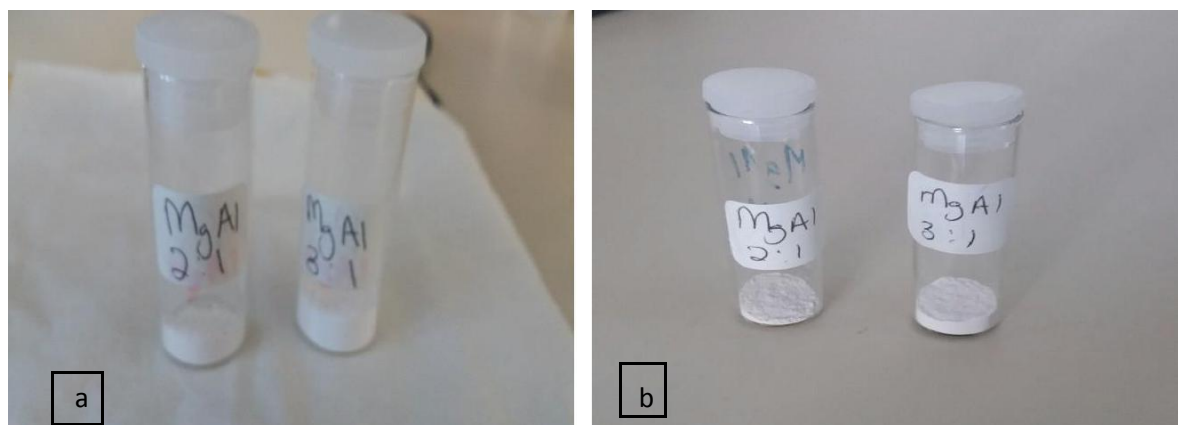


Figure 3.1: (a) Pristine MgAl 2:1 and MgAl 3:1 (b) Calcined MgAl 2:1 and MgAl 3:1

3.4.2 UV-Vis spectroscopy.

UV-Vis spectroscopy was employed to determine the binding or encapsulation efficiency percentages of the drug-loaded LDHs (Figure 3.2, Table 3.1). The calcination method incorporates the drug as the LDH is being resynthesized after exposure to drug solution, however the structure may be compromised, thus affecting the encapsulation efficiency of the LDH (Zhang *et al.*, 2006). Overall the encapsulation efficiency of 5-Fu was above 40 %, with 58.94 % and 42.85 % obtained for MgAl LDHs 2:1 and 3:1 respectively.

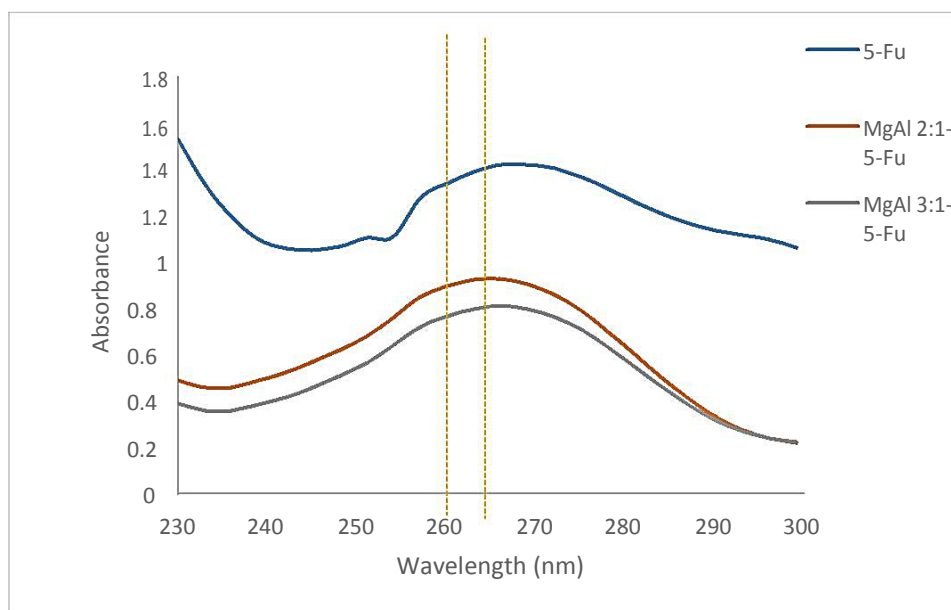


Figure 3.2 UV-Vis spectroscopy of 5-Fu, MgAl 2:1-5-Fu and MgAl 3:1 5-Fu

Table 3.1: MgAl-LDHs Encapsulation Efficiencies (% EE)

LDH	Nanohybrid formula	Encapsulation Efficiency (%EE)
MgAl 2:1	MgAl 2:1-5-Fu	58.94
MgAl 3:1	MgAl 3:1-5-Fu	42.85

3.4.3 Powder X-ray Diffraction Spectroscopy.

We further confirmed the synthesis, calcination, as well as reconstitution of the structure of the LDHs utilizing XRD spectroscopy (Appendix A.1). The synthesized LDHs, showed the characteristic (003) peak approximately around 2-theta 14.50 ° for pristine MgAl 2:1 and at approximately 2-theta 13.00 ° for pristine MgAl 3:1. These peaks may correspond to the *d*-spacing of 0.75 nm due to the carbonate within this gallery space, which were both lost after calcination of the respective MgAl-LDHs, as a result of decarboxylation and dehydration reactions. Our findings confirm thinning of the gallery space as well as loss of the 'house-of cards' lattice of the LDHs. A shift was observed in the peaks for both MgAl 2:1-5-Fu and MgAl 3:1-5-Fu. These clear shift indicate the possible change in the dimension of the gallery space due to an intercalation of an anionic molecule, which in this case is the 5-Fu. The reconstituted structure, although shows good intercalation of 5-Fu, also indicates structural compromise. This could be due to the partial decomposition of the original LDHs.

3.4.4 Fourier Transform Infrared Spectroscopy

Fourier Transform Infrared spectroscopies were performed and also confirmed the presence of the 5-Fu molecules in the respective MgAl-LDHs (Appendix A.2). Comparative IR readings of the pristine MgAl 2:1 LDH and the MgAl 3:1 indicated characteristic hydroxyl groups around 3000cm⁻¹ for both LDHs. The strong absorption bands within the range of 1500cm⁻¹ can be attributed to the multi-substituted 5-fluorouracil in both the LDHs. For both LDHs, bands were also observed at the lower-frequency region, due to the vibration of M-O and M-O-M (M=Mg, Al) at their various atomic ratios. These lattice vibrations were observed around 500 cm⁻¹ to 700 cm⁻¹.

3.4.5 Inductively coupled plasma-optical emission spectroscopy (ICP-OES)

Inductively coupled plasma-optical emission spectroscopy (ICP-OES) was performed on the MgAl-LDHs (2:1 and 3:1) and their nanohybrids confirmed the presence of magnesium and aluminium in their appropriate ratios. The nanohybrids also confirmed presence of 5-Fu within the respective MgAl LDHs (2:1 and 3:1) (Appendix C.)

3.4.6 Electron Microscopy (TEM and SEM)

TEM and SEM microscopies were performed for the characterisation of the respective MgAl-LDHs (MgAl 2:1 and 3:1), their calcined derivatives as well as the resulting nanohybrids after reconstruction. Significant differences were noted between the two MgAl-LDHs. Pristine MgAl-LDH 2:1 (Figure 3.3) showed a more defined structure with more defined edges and a clearly anisotropic shape compared to the MgAl-LDH 3:1 under TEM (Figure 3.4). This observation was further clarified with SEM imaging (Figure 3.5). This was also the case for MgAl 2:1. It has been previously reported that the difference in surface structure of LDHs of the same type (however differing elemental compositions) is due to active surface atoms, with LDHs generally aggregating during storage and application (Kuang *et al.*, 2010). The lateral size and thickness of MgAl 3:1, nanohybrid before and after calcination as well as after reconstruction was observed again with SEM (Figure 3.6).

MgAl 2:1 changed in lateral size and thickness after calcination, from an average of $\sim 70 \text{ nm} \pm 15$ before calcination to $\sim 58 \text{ nm} \pm 12$ after calcination, while MgAl 3:1 changed from $\sim 60 \text{ nm} \pm 16$ to $\sim 55 \text{ nm} \pm 14$, respectively. Calcination topochemically decomposes the LDH due to water loss in the gallery space, resulting in a decrease of the gallery space (d value). However, it was discovered that after exposure to the drug solution, the LDH recovered its characteristic hexagonal shape, as seen with the increase in lateral size and thickness to an average size of $\sim 68 \text{ nm} \pm 14$. Overall, electron microscopy confirmed the intricate “house-of-cards” structure characteristic of the LDHs, due to the enhanced particle-edge interaction, which was recovered after reconstruction. Interestingly, the respective MgAl-LDHs displayed a tendency of “sitting on their edge”, a feature

that reveals that aggregation and distribution characteristics vary to a great degree, due to the method of synthesis.

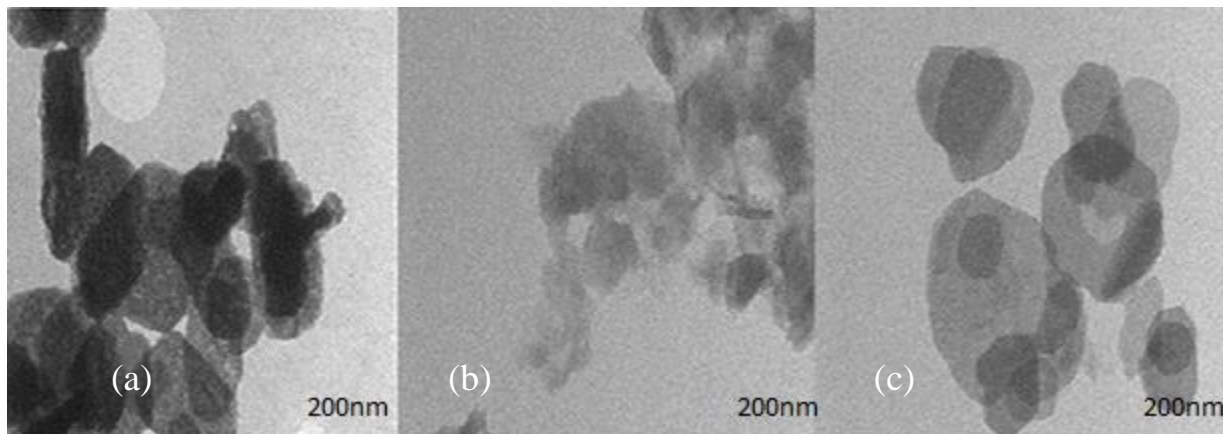
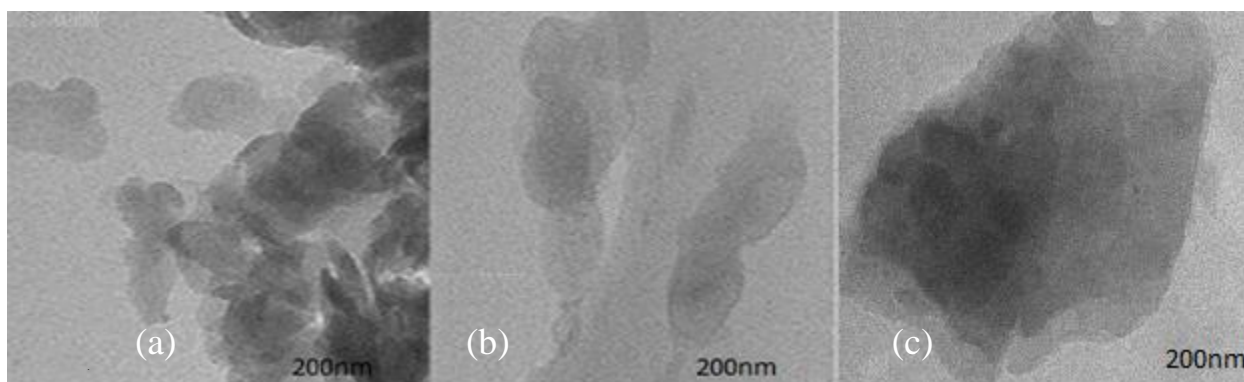


Figure 3.3 TEM images of (a) MgAl 2:1, (b) Calcined MgAl 2:1 (c) and MgAl 2:1-5-Fu (Bar =200 nm).



3.4 TEM images of (a) MgAl 3:1, (b) Calcined MgAl 3:1 and (c) MgAl 3:1-5-Fu (Bar = 200 nm).

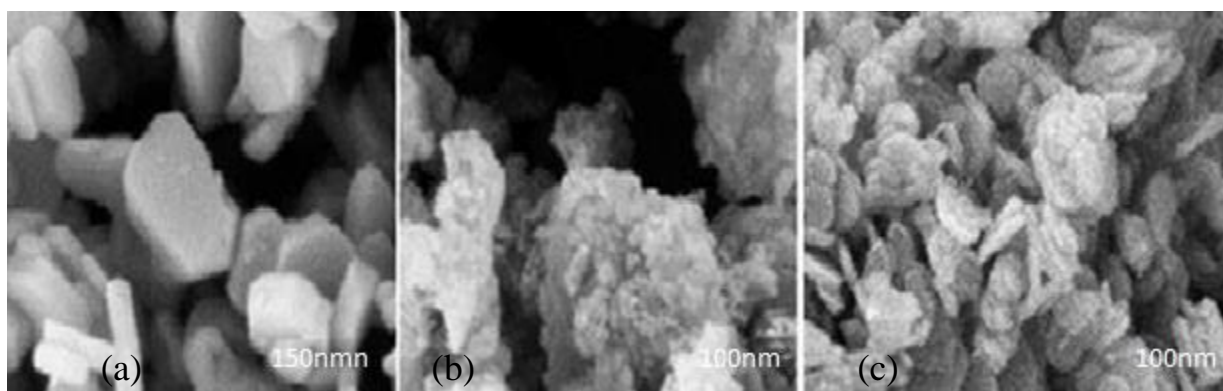


Figure 3.5 SEM micrographs of (a) MgAl 2:1 pure (b) calcined MgAl 2:1 (c) MgAl 2:1-5-Fu (scale bar \leq 100nm).

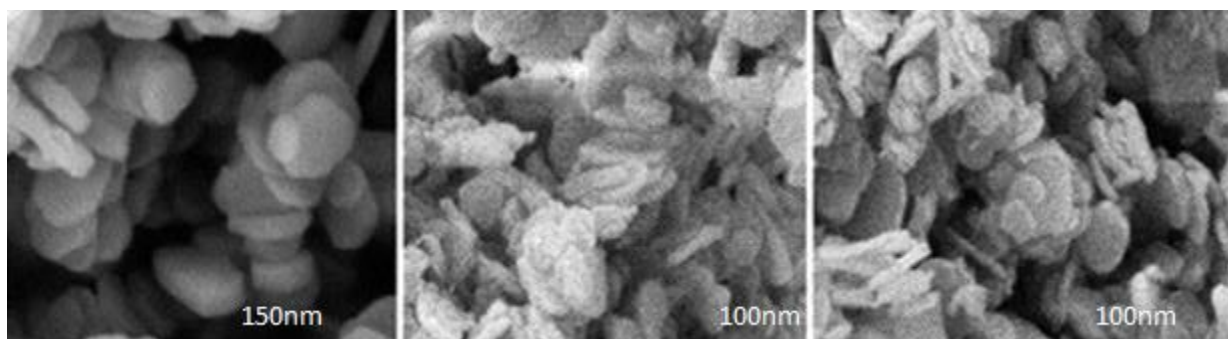


Figure 3.6 SEM micrographs of (a) MgAl 3:1 pure (b) calcined MgAl 3:1 (c) MgAl 3:1-5-Fu (Bar ≤ 150 nm).

3.4.6 Nanoparticle Tracking Analysis (NTA)

NTA was performed to accurately determine nanoparticle size distribution and zeta potential (Table 3.2, Appendix A.3). It was observed that the pristine LDHs had a tendency to aggregate much further in solution. However, we noted very slight changes in the size of the nanohybrids (138 -140 nm for MgAl 2:1 and MgAl 2:1-5-Fu; and 179.9 to 178 nm for MgAl 3:1 and MgAl 3:1-5-Fu respectively). This could possibly be due to the effects of calcination and reconstruction with 5-Fu. Importantly, all sizes were below 200 nm, an important cut off for *in vitro* cellular uptake. Zeta potential values observed were in accordance with previous reported research (Choi and Choy, 2011). The LDH nanoparticle are composed of the cationic layers that dominate the outer space of the nanoparticle (Kim *et al.*, 2014). The interesting twist we observed was that the nanohybrid MgAl 2:1-5-Fu displayed a slightly negative zeta potential (-37.3 mV), this could largely be influenced by the effects of the nanoparticles calcination and subsequent encapsulation of 5-Fu rendering an ion exchange within the gallery space. Overall the MgAl 3:1 (31 mV) and MgAl 3:1-5-Fu (32 mV) nanoparticles retained their net positive charges.

Table 3.2: Size and zeta potential of MgAl 2:1, MgA 2:1-5-Fu, MgAl 3:1 and MgAl 3:1-5-Fu

PROPERTY	LDH SAMPLE			
	MgAl 2:1	MgAl 2:1-5-Fu	MgAl 3:1	MgAl 3:1-5-Fu
Sample name	MgAl 2:1	MgAl 2:1-5-Fu	MgAl 3:1	MgAl 3:1-5-Fu
Size (nm)	138 ±2.1	140 ±2.1	179.9 ±2.1	178.1 ± 0.2
Zeta Potential (mV)	108 ±8.8	-37.3 ± 0.22	31.0±0.2	32.2 ±0.1

Importantly, the higher the zeta potential values (irrespective whether they are positive or negative), the greater the mobility of the nanoparticles, and the better the colloidal stability, which favours cellular uptake and internalisation, and reduces aggregation effects. This also bodes well for systemic delivery. Based on this the MgAl 3:1-5-Fu (32.2±0.1 mV), seem to have the most favourable zeta potential.

3.4.7 Drug release studies

It has been previously reported that 5-Fu released from various LDHs retained its pharmacological activity. Thus, we hypothesise that due to LDH's disintegration pattern at lower pHs, 5-Fu could also be easily and controllably released from the LDHs. Hence, pH dependent drug release studies somewhat confirmed the MgAl-LDHs' a pattern of drug release at the different pHs. MgAl 2:1-5-Fu showed release of the drug, but rather very slowly in comparison to the drug release at pH 4 at pH~ 7, over the 7-hour period after an initial burst release from t=0 to t=1. At pH~ 4, the drug was initially released quicker than at the neutral pH (Figure 3.7a). At pH=4, 80 % of the drug had been released from the MgAl 2:1-LDH over the time period tested. A similar profile was observed for MgAl 3:1-5-Fu (Figure 3.7b) from t=0 to t=6. However the release was slower and could be due to better structural recovery after reconstitution. Approximately, 60 % of the drug had been released at t=7. These results however show that due to the lowered pH of cancerous cells the drug could be released gradually within cells offering maximum effect of the drug.

Furthermore, the endosomal compartments which generally pose a barrier in intracellular trafficking, have an acidic pH, which will be favourable for drug release using these LDH constructs.

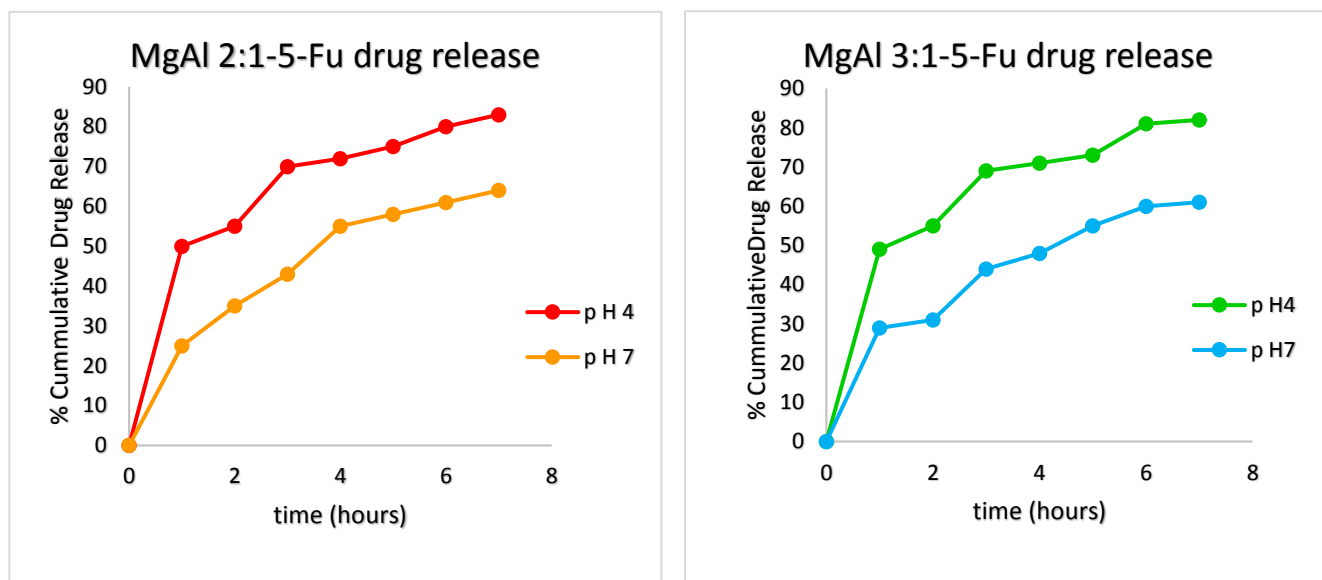


Figure 3.7: Drug release profiles of MgAl 2:1-5-Fu (a) and MgAl 3:1-5-Fu (b) at pH ~4 and pH ~7 respectively.

3.4.8 Cytotoxicity studies.

3.4.8.1 MTT assay

The MTT (3-[4,5-dimethylthiazol-2-yl]-2,5 diphenyl tetrazolium bromide) assay was used to determine the cytotoxic effect of the 5-Fu after treatment of cells with the drug at increased concentrations on the four cell lines, HEK293, MCF-7, Hep-G-2 and CaCo-2 cell lines. This assay is based on the principle that the MTT reagent is converted into formazan crystals by mitochondrial reductases in viable cells. It hence determines mitochondrial activity and can be used to quantify the amount of viable cells after treatment. From Figures 3.8-3.9, it is evident that the unbound /free 5-Fu resulted in a greater cell death of all cell lines, which is further confirmed by the IC_{50} values calculated (Table 3.3). The IC_{50} values ranged from 22.18-36.56 $\mu\text{g}/\text{mL}$ for the cells exposed to free 5-Fu, but were slightly higher for the MgAl 2:1-5-Fu (82.25-92.25 $\mu\text{g}/\text{mL}$) (Figure 3.6) at the same drug concentration. A similar pattern was observed for the cells exposed to MgAl-3:1-5-Fu and free 5-Fu again (Figure 3.9), with IC_{50} values ranging from 65.25 -72.25 $\mu\text{g}/\text{mL}$ and 21.25-28.57 $\mu\text{g}/\text{mL}$ respectively, at the same concentrations. This high cell death with free 5-Fu could be due to the rapid uptake of the drug into the cell at its full dose, leading to immediate cytotoxicity effects within

the cell. However, a gradual cell death profile correlating with increased LDH-5-Fu concentrations in all cell lines was observed, which could be due to the slow controlled release of the drug from the LDHs leading to gradual uptake by the cells. Hence, there is gradual but significant cytotoxicity effect in the cells as the drug is released in smaller doses over a period of time.

The MgAl-LDH-5-Fu nanohybrids did not show any particular cell specificity, but an overall lower level of cytotoxicity in the HEK293 cells was noted for the MgAl 2:1-5-Fu complexes only. The HEK293 cell line has an intracellular pH of 7.3 (Stoop *et al.*, 1997), which could offer slight protection to this cell line. LDHs will only release the encapsulated contents at low pHs and preferably in acidic environments, as the case is for almost all cancerous cell lines. Although a degree of cytotoxicity was seen across all cell lines, it is worth noting that MgAl-LDH elicited a greater cytotoxic effect on the HepG2 cell line followed by the CaCo-2 cell line (Figure 3.9, where the rate of cell death is indicated across all cell lines against the controls, i.e untreated cells (cntrl cell) and cells treated only with LDH (cntrl LDH)).

The increased cell death for the CaCo-2 cell line may also be attributed to their slightly higher sensitivity to 5-Fu line in particular to 5-Fu.

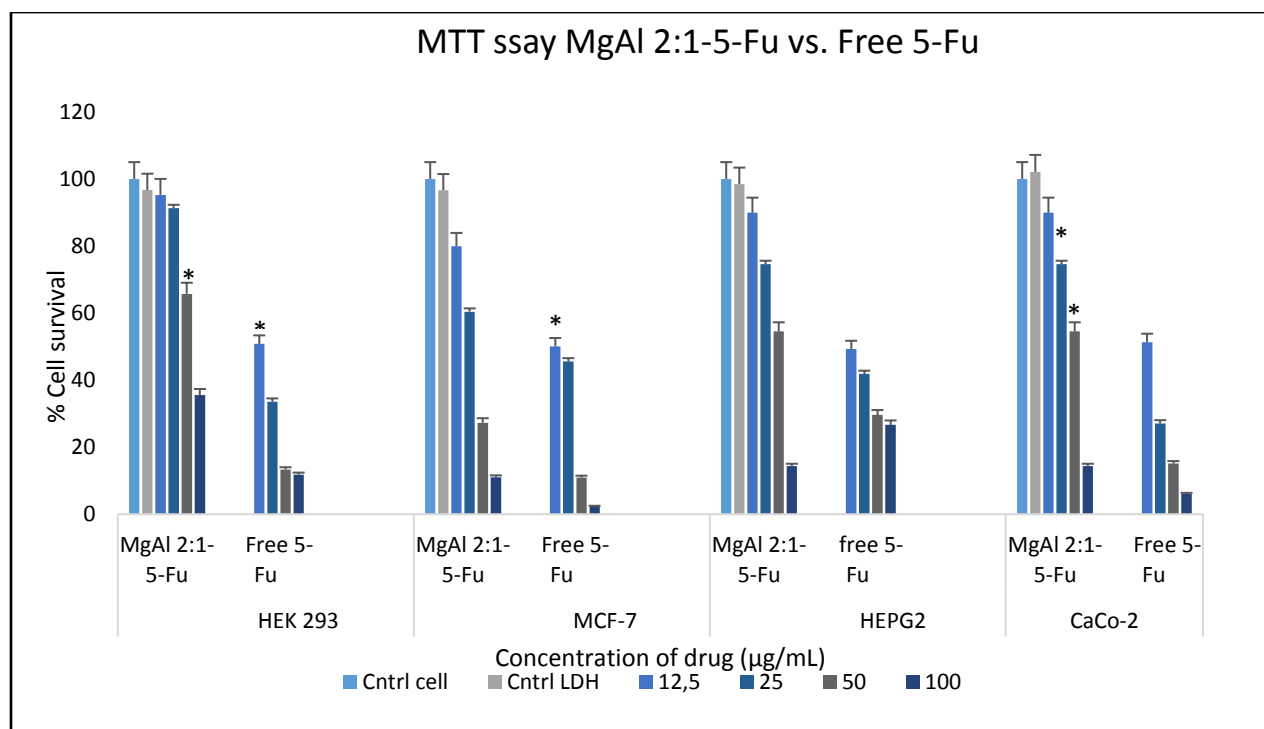


Figure 3.9: MTT Assay with MgAl-2:1-5-Fu and free 5-Fu at concentrations 12.5 µg/mL, 25 µg/mL, 50 µg/mL and 100µg/ mL on HEK293, MCF-7, HepG2 and CaCo-2 cell lines [data presented as means SD±(n=3) (*p<0.05).

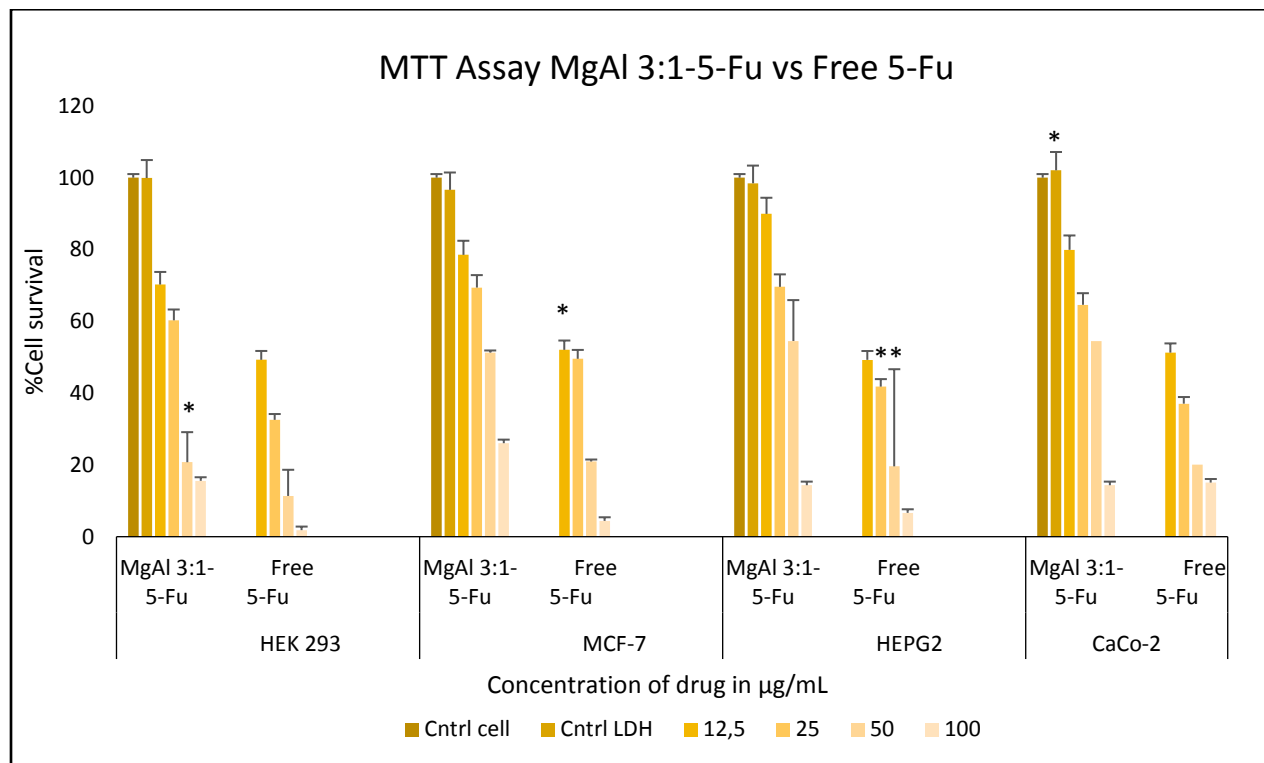


Figure 3.10: MTT assay with MgAl-3:1-5-Fu and free 5-Fu at concentrations 12.5 µg/mL, 25 µg/mL, 50 µg/mL and 100 µg/mL, in HEK293, MCF-7, HepG2 and CaCo-2 cell lines against [data presented as means SD± (n=3) (*p<0.05; **p<0.01).

Table 3.3: IC₅₀ (µg/mL) values for MgAl 2:1-5-Fu, MgAl 3:1-5-Fu versus free 5-Fu (respectively).

Cell line	MgAl 2:1-5-Fu	Free 5-Fu	MgAl 3:1-5-Fu	Free 5-Fu
HEK293	92.25	22.18	65.25	21.95
MCF-7	90	35.25	73.95	35.25
HepG2	82.25	36.00	79.75	30.69
CaCo-2	82.25	36.56	72.25	28.57

3.4.8.2 Sulphorhodamine B (SRB) assay

The Sulphorhodamine B (SRB) assay is a colorimetric assay used to measure drug-induced cytotoxicity and cell proliferation for large-scale drug screening applications (Voigt, 2005). This assay is based on the ability of the Sulphorhodamine B protein dye to bind electrostatically and pH dependently basic amino acid residues in TCA-fixed cells. It binds to cells under mild acidic conditions can be extracted from cells under mild basic conditions, and solubilized for measurement (Vichai and Kirtikara, 2006). The SRB assay cytotoxicity findings correlated with those of the MTT assay results. A similar cytotoxicity profile was observed in all cells with free 5-Fu and LDH-loaded nanohybrids (Figures 3.11-3.12). Herein, we also noticed no significant cell specificity, but this assay also confirmed the controlled release properties of the drug loaded LDHs.

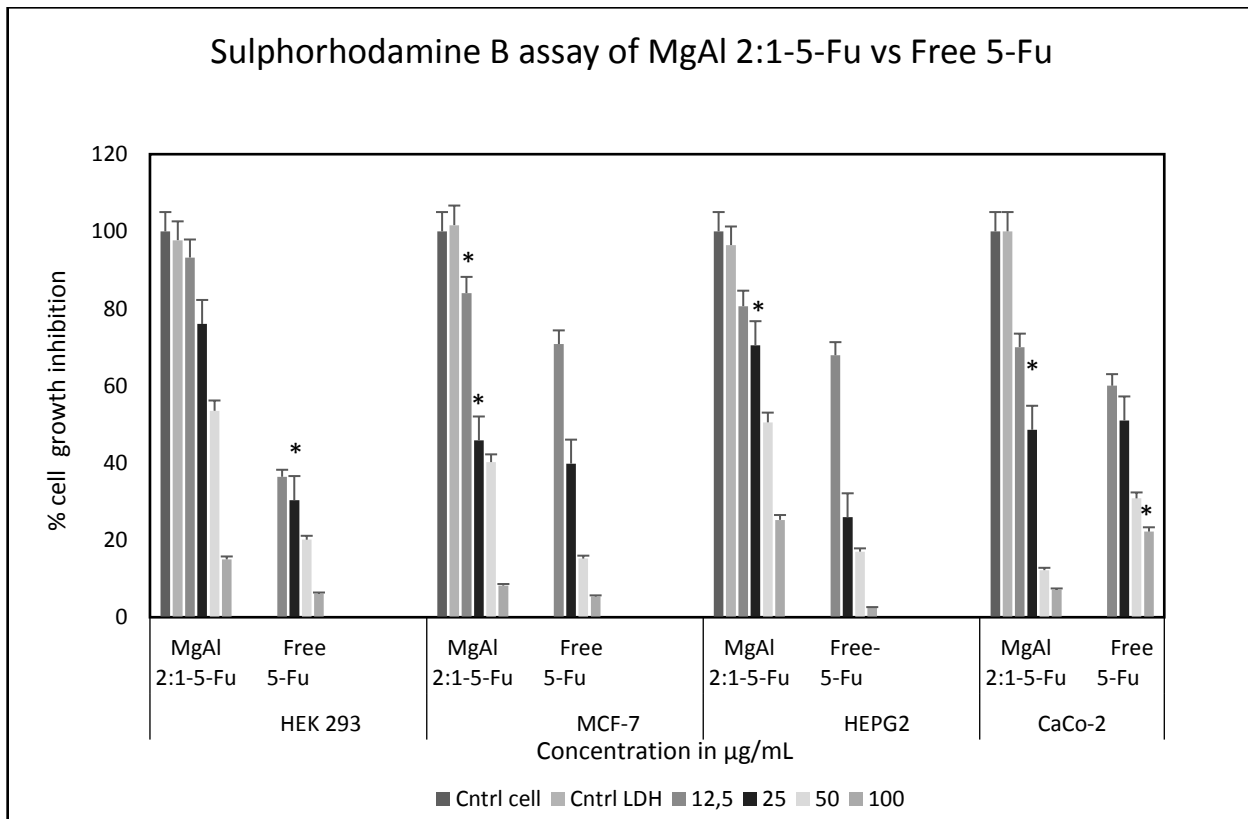


Figure 3.11: SRB assay for MgAl-2:1-5-Fu and free 5-Fu at 12.5 µg/mL, 25µg/mL, 50µg/ mL and 100 µg/ mL in HEK293, MCF-7, HepG2 and CaCo-2 cell lines [data presented as means SD± (n=3) (*p<0.05)]

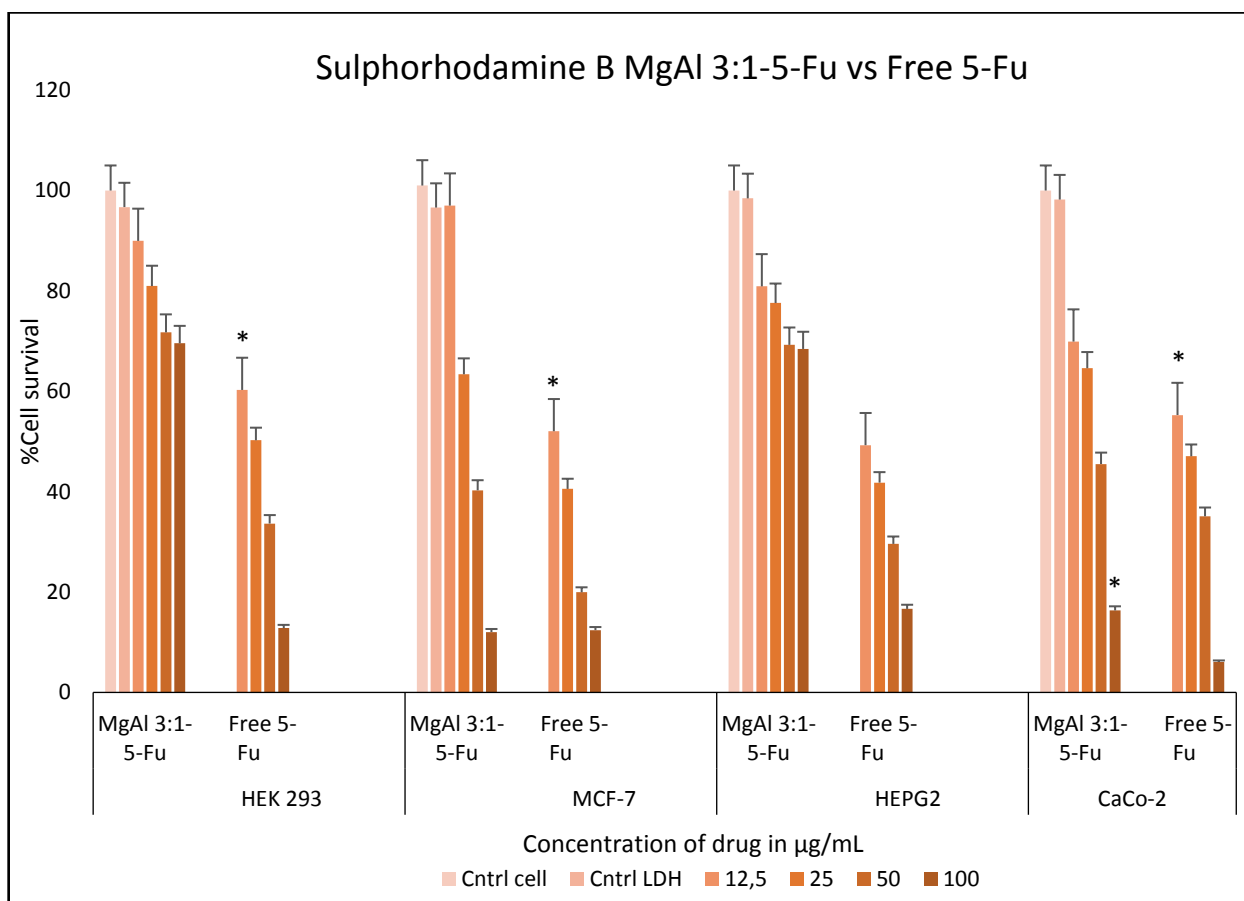


Figure 3.12: SRB assay of MgAl-3:1-5-Fu and free 5-Fu at 12, 5 µg/mL, 25 µg/mL, 50 µg/mL and 100 µg/mL in HEK293, MCF-7, HepG2 and CaCo-2 cell lines [data presented as means SD± (n=3) (*p<0.05)]

Table 3.4: IC₅₀ (µg/mL) values for MgAl 2:1-5-Fu, MgAl 3:1-5-Fu versus Free 5-Fu respectively.

Cell line	MgAl 2:1-5-Fu	Free 5-Fu	MgAl 3:1-5-Fu	Free 5-Fu
	IC ₅₀ values in µg/mL			
HEK293	67.25	22.95	77.25	18.25
MCF-7	63.69	30.25	76.69	20.75
HepG2	77.25	31.19	80.25	28.19
CaCo-2	72.25	21.87	82.19	41.07

3.4.9 Apoptosis studies

Apoptosis studies were performed using the dual staining acridine orange and ethidium bromide (AO/EB) method. Following from their low cytotoxicity in the MTT and SRB assays, the apoptosis

studies showed a more controlled apoptotic pattern (Figure 3.13 and 3.14). Apoptotic indexes were calculated to determine the impact of the LDH delivered drug against the freely delivered drug and these are tabulated in Table 3.5.

Overall, the drug loaded LDHs produced lower apoptotic indices compared to the free drug. The apoptotic cells appear red, with live cells appearing green. From the images it can be seen that there was greater apoptotic induction by the 5-Fu in all cell lines, with drug loaded LDHs produced high apoptosis in the HepG2 and CaCo-2 cell line. Using the dual staining method, live cells (L) usually appear green, early apoptotic cells appear yellow (EA), late apoptotic cells are orange and apoptotic cells are (red).

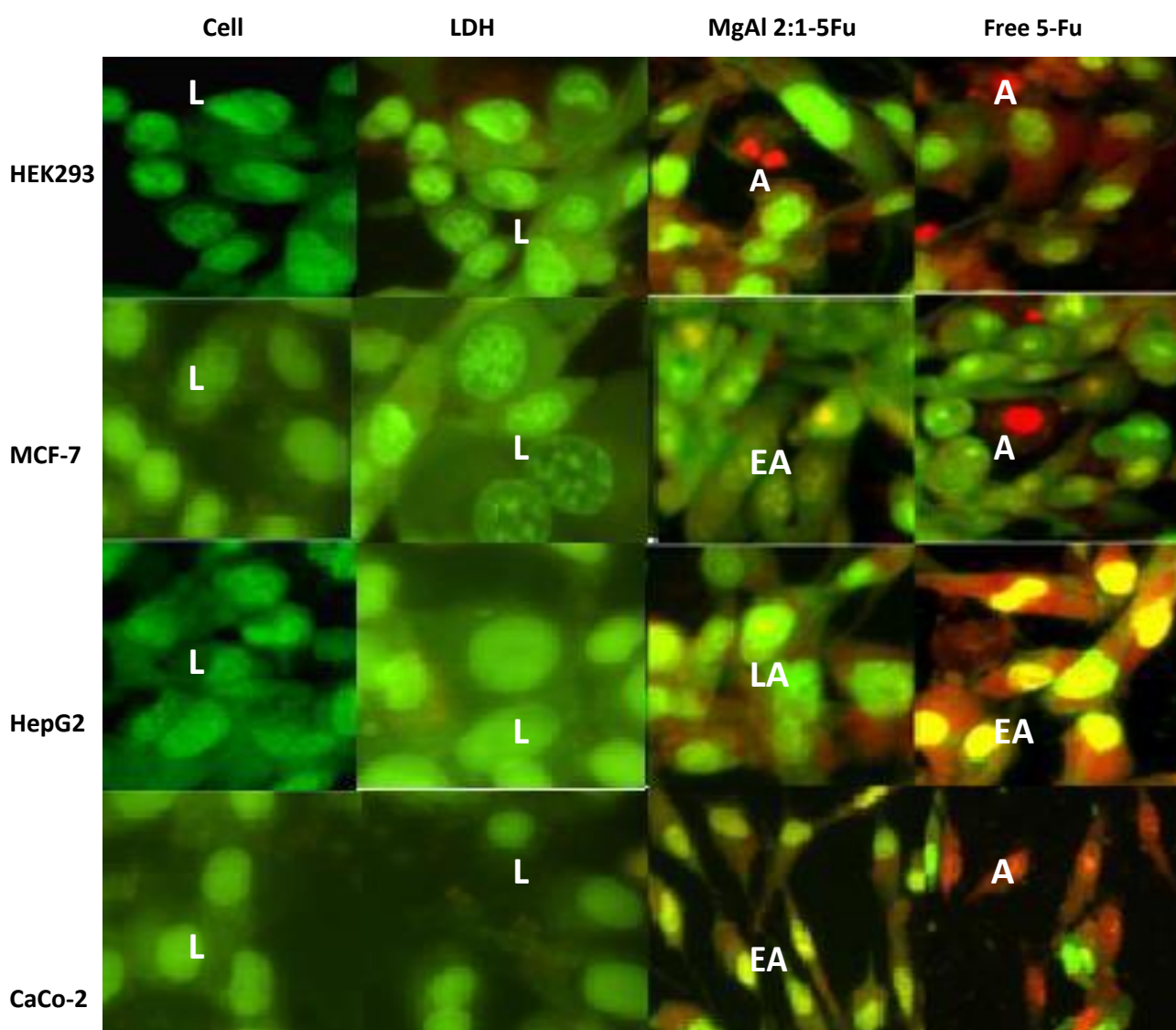


Figure 3.13: Fluorescent images of apoptosis induced by (A) MgAl 2:1-5-Fu and free 5-Fu, in HEK293, MCF-7, HepG2 and CaCo-2 cell lines (L=Live cells, A=Apoptotic cells, LA= Late Apoptotic cells and EA= Early Apoptotic cells).

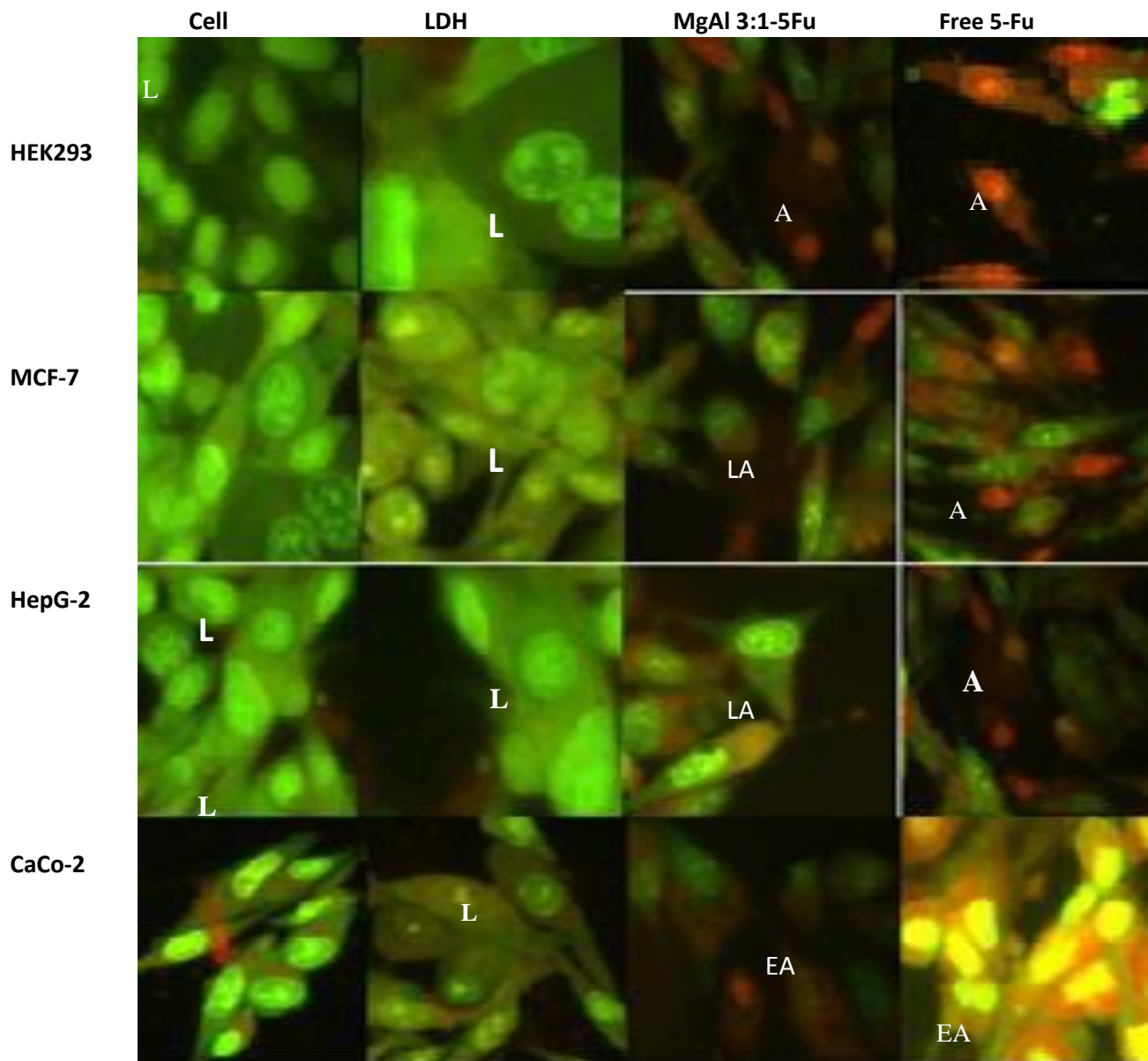


Figure 3.14: Fluorescent images of apoptosis induced by (A) MgAl 3:1-5-Fu and free 5-Fu, in HEK293, MCF-7, HepG2 and CaCo-2 cell lines (L=Live cells, A=Apoptotic cells, LA= Late Apoptotic cells and EA= Early Apoptotic cells).

Table 3.5: Apoptotic Index (AI) of cells exposed to MgAl-2:1-5-Fu, MgAl 3:1-5-Fu and free 5-Fu

Cell lines	APOPTOTIC INDEX (AI)					
	Control Cell	Control LDH	MgAl 2:1-5-Fu	Free 5-Fu	MgAl 3:1-5-Fu	Free 5-Fu
HEK293	0.00	0.00	0.1	0.25	0.02	0.05
MCF-7	0.00	0.00	0.15	0.111	0.09	0.210
HepG2	0.00	0.00	0.1	1	0.1	1.15
CaCo-2	0.00	0.00	1	0.2	0.1	1

3.5 Conclusion

Layered double hydroxides are perhaps the most intricate, sophisticated yet simple nanoparticles, and their ability to intercalate and protect biomolecules comes as a huge scientific advantage. MgAl LDHs can prove to be potentially beneficial nanoparticles in the challenging process of chemotherapy. In this study we have discovered that the structure of the LDH plays a vital role in the encapsulation of 5-Fu. The intercalation property of LDHs offers a degree of control over the amount of drug encapsulated and released. Drug encapsulation efficiency was above 40 %, with a maximum drug release of 80 % occurring in a controlled manner over a 7-hour period. Cytotoxicity studies showed that these LDHs had a dose-dependent profile in the four cell lines tested. However, it is interesting to note that the level of cytotoxicity was higher for cells treated with free 5-Fu, which was further confirmed by the fluorescent apoptosis assay, which showed that greater apoptosis was induced by the drug alone than the LDH bound drug as evidenced by its' higher apoptotic index.

The LDHs furthermore did not show significant cell specificity, although they had a dose dependent reaction with gradual cell death. This profile added to the notion that these LDHs were able to slowly release the drug over time, bodes well for their *in vivo* use. The ability of LDHs to disintegrate at acidic pH, is another advantageous feature, which ensures that the acidic environment of cancerous cells will be favourable for the release of therapeutic contents. Although the intercalation of species within the LDHs is a rapid process, their deintercalation is

not. Very low pH levels are required for the nanoparticle to fully disintegrate as observed in the pH-dependent drug release studies. 5-Fu is an anticancer drug predominantly used to treat colon-cancers, and 5-Fu loaded LDHs may be suitable for the oral administration of 5-Fu with further optimizations. The LDH property of drug release at a lower pH would be beneficial in this case, where pH is below 6. Overall, this study has shown the potential of MgAl-LDHs as promising drug delivery systems. Future studies and recommendations include testing the release profile over a longer time period, increasing the steric stability of the LDHs, using a polymer such as polyethylene glycol to increase systemic circulation and evaluation of the LDHs in a suitable *in vivo* model.

3.6 References

- Allen, T. M. & Cullis, P. R. 2004. Drug delivery systems: entering the mainstream. *Science*, 303, 1818-1822.
- Baldo, B. A. & Pagani, M. 2014. Adverse events to nontargeted and targeted chemotherapeutic agents: emphasis on hypersensitivity responses. *Immunology and allergy clinics of North America*, 34, 565-596.
- Chen, J., Shao, R., Li, L., Xu, Z. P. & Gu, W. 2014b. Effective inhibition of colon cancer cell growth with MgAl-layered double hydroxide (LDH) loaded 5-Fu and PI3K/mTOR dual inhibitor BEZ-235 through apoptotic pathways. *International Journal of Nanomedicine*, 9, 3403-3411.
- Cho, K., Wang, X., Nie, S., Chen, Z. & Shin, D. M. 2008. Therapeutic Nanoparticles for Drug Delivery in Cancer. *Clinical Cancer Research*, 14, 1310-1316.
- Choi, S.-J. & Choy, J.-H. 2011. Layered double hydroxide nanoparticles as target-specific delivery carriers: uptake mechanism and toxicity. *Nanomedicine*, 6, 803-814.
- Choy, J.-H., Choi, S.-J., Oh, J.-M. & Park, T. 2007. Clay minerals and layered double hydroxides for novel biological applications. *Applied Clay Science*, 36, 122-132.
- Del Arco, M., Cebadera, E., Gutierrez, S., Martin, C., Montero, M., Rives, V., Rocha, J. & Sevilla, M. 2004. Mg, Al layered double hydroxides with intercalated indomethacin: synthesis, characterization, and pharmacological study. *Journal of pharmaceutical sciences*, 93, 1649-1658.
- Del Hoyo, C. 2007. Layered double hydroxides and human health: an overview. *Applied Clay Science*, 36, 103-121.

- Fan, G., Li, F., Evans, D. G. & Duan, X. 2014. Catalytic applications of layered double hydroxides: recent advances and perspectives. *Chemical Society Reviews*, 43, 7040-7066.
- Gatenby, R. A. & Gillies, R. J. 2004. Why do cancers have high aerobic glycolysis? *Nature Reviews Cancer*, 4, 891-899.
- Huang, X., Jain, P. K., El-Sayed, I. H. & El-Sayed, M. A. 2007. Gold nanoparticles: interesting optical properties and recent applications in cancer diagnostics and therapy.
- Katheria, S., Gupta, A., Deo, G. & Kunzru, D. 2016. Effect of calcination temperature on stability and activity of Ni/MgAl₂O₄ catalyst for steam reforming of methane at high pressure condition. *International Journal of Hydrogen Energy*.
- Khan, A. I., Lei, L., Norquist, A. J. & O'Hare, D. 2001. Intercalation and controlled release
- Kim, T.-H., Lee, G. J., Kang, J.-H., Kim, H.-J., Kim, T.-i. & Oh, J.-M. 2014. Anticancer drug-incorporated layered double hydroxide nanohybrids and their enhanced anticancer therapeutic efficacy in combination cancer treatment. *BioMed research international*, 2014.
- Kim, W. J., Christensen, L. V., Jo, S., Yockman, J. W., Jeong, J. H., Kim, Y.-H. & Kim, S. W. 2006. Cholesteryl oligoarginine delivering vascular endothelial growth factor siRNA effectively inhibits tumor growth in colon adenocarcinoma. *Molecular Therapy*, 14, 343-350.
- Kompella, U. B. 2013. Nanotechnology and Drug Delivery. *Journal of Ocular Pharmacology and Therapeutics*, 29, 89-89.

- Kuang, Y., Zhao, L., Zhang, S., Zhang, F., Dong, M. & Xu, S. 2010. Morphologies, preparations and applications of layered double hydroxide micro-/nanostructures. *Materials*, 3, 5220-5235.
- Kumari, A., Yadav, S. K. & Yadav, S. C. 2010. Biodegradable polymeric nanoparticles based drug delivery systems. *Colloids and Surfaces B: Biointerfaces*, 75, 1-18.
- Ladewig, K., Niebert, M., Xu, Z. P., Gray, P. P. & Lu, G. Q. M. 2010. Controlled preparation of layered double hydroxide nanoparticles and their application as gene delivery vehicles. *Applied Clay Science*, 48, 280-289.
- Maghsoudi, A., Shojaosadati, S. A. & Farahani, E. V. 2008. 5-Fluorouracil-loaded BSA nanoparticles: formulation optimization and in vitro release study. *Aaps Pharmscitech*, 9, 1092-1096.
- Newton, M. S., Morrison, J. D., Pennell, R. D., Phodes, N. P. & Toft, A. J. 2008. Mixed metal compounds used as antacids. Google Patents.
- Stoop, R., Surprenant, A. & North, R. A. 1997. Different sensitivities to pH of ATP-induced currents at four cloned P2X receptors. *Journal of Neurophysiology*, 78, 1837-1840.
- Wilczewska, A. Z., Niemirowicz, K., Markiewicz, K. H. & Car, H. 2012. Nanoparticles as drug delivery systems. *Pharmacological reports*, 64, 1020-1037.
- Xu, Z. P., Zeng, Q. H., Lu, G. Q. & Yu, A. B. 2006. Inorganic nanoparticles as carriers for efficient cellular delivery. *Chemical Engineering Science*, 61, 1027-1040.

Yamashita, H., Honda, M., Harada, M., Ichihashi, Y., Anpo, M., Hirao, T., Itoh, N. & Iwamoto, N. 1998. Preparation of titanium oxide photocatalysts anchored on porous silica glass by a metal ion-implantation method and their photocatalytic reactivities for the degradation of 2-propanol diluted in water. *The Journal of Physical Chemistry B*, 102, 10707-10711.

Zhang, H., Zou, K., Guo, S. & Duan, X. 2006. Nanostructural drug-inorganic clay composites: structure, thermal property and in vitro release of captopril-intercalated Mg–Al-layered double hydroxides. *Journal of Solid State Chemistry*, 179, 1792-1801.

CHAPTER 4

THE APPLICATION OF ZnAl-LDHs AS POTENTIAL ANTICANCER DRUG DELIVERY VEHICLES

Zoleka Mncwabe¹ and Moganavelli Singh^{*}

¹Non-Viral Gene Delivery Laboratory, Discipline of Biochemistry, School of Life Sciences,
UKZN, Westville Campus

^{*}Corresponding author: Prof Moganavelli Singh, email:Singhm1@ukzn.ac.za

Abstract

Inorganic-based delivery systems have attracted attention especially due to their relative inertness, allowing for safe and stable delivery of macromolecules in biological systems, and their ability to be easily manipulated. ZnAl-LDH layered double hydroxides (LDHs) have long been utilized to deliver anti-inflammatory drugs as well as antibiotics. In this study we successfully synthesized two 5-Fluorouracil (5-Fu) delivery systems, namely, ZnAl 2:1-5-Fu and ZnAl 3:1-5-Fu, from the pristine LDHs ZnAl 2:1 and ZnAl 3:1 using a reconstruction technique. All LDHs and conjugates were characterized using SEM, TEM, XRD, FTIR, ICP-OES and NTA. Encapsulation efficiencies (%EE) of the nanoparticles were above 50 % for both ZnAl 2:1-5-Fu (64.92 %) and the ZnAl 3:1-5-Fu (56.56 %) nanohybrids. Drug release profiles revealed a steady and gradual release of 5-Fu from the gallery space of the respective ZnAl-LDH the ZnAl 3:1-5-Fu nanohybrid 89 % of drug after 7 hours. *In vitro* studies were carried out to determine the cytotoxicity conferred by the LDH-encapsulated and the free drug at the same concentrations on four human cell lines, embryonic kidney (HEK293), breast adenocarcinoma (MCF-7), hepatocellular carcinoma (HepG2) and colorectal adenocarcinoma (CaCo-2). The MTT 3-(4,5-dimethylthiazol-2-yl)-2,5-diphenyltetrazolium bromide (MTT) and sulphorhodamine B assays (SRB) cytotoxicity assays, demonstrated higher cell death for free 5-Fu treated cells. The HEK293 cells through the virtue of their neutral intracellular pH were affected to a lesser degree. The ZnAl-LDHs were most effective at conferring controlled cell death on the MCF-7 and CaCo-2 cell lines, although a considerable cell death was observed. The LDHs offered a more controlled system of drug delivery than the freely delivered 5-Fu as was seen with IC_{50} ranging from 41-54 (free 5-Fu) and high IC_{50} s at 65.50-77.05 (ZnAl-LDH) encapsulated 5-Fu. Apoptosis studies conducted, confirmed that much of the cell death was due to apoptosis.

Key Words: Layered double hydroxides LDHs, 5-Fluorouracil, cytotoxicity

4.1 Introduction

Cancer is a global chronic disease and is fast becoming a lead cause of mortality, despite the vast array of cancer therapeutics available. Chemotherapy is the common technique for cancer therapy, but comes with significant side-effects, and the need for repeated treatments which does not guarantee the remediation of the cancer. Most conventional drug delivery systems (DDS) have shortfalls such as poor oral bioavailability, low therapeutic indices, lack of water solubility, nonspecific biodistribution and targeting (Allen and Cullis, 2004, Cho *et al.*, 2008, O'hare, 2014). It is for these reasons, the field of nanomedicine has evolved, using nanotechnology for the designing of new methods for cancer therapy. Thus researchers are currently looking into the application of nanotechnology in solving the problem of the lack of effective and inexpensive DDS (Cho *et al.*, 2008). Nanotechnology is on the verge of becoming one of the breakthroughs, presenting the potential for the development of nanoparticles that could be used as delivery vehicles for these therapeutic drugs (Kompella, 2013, Liu *et al.*, 2012). Among the nanoparticles currently being researched, LDHs, are proving to be promising due to their structural uniqueness and versatile surface topography (Choy *et al.*, 2007, Rives *et al.*, 2014, Wang *et al.*, 2015). LDHs are composed of a two dimensional structural network composed of different hydroxy layers of divalent and trivalent metal ions in determined ratios (Mandal and Mayadevi, 2008, Manzi-Nshuti *et al.*, 2009). Isomorphic substitution of some divalent metal ions of LDHs with trivalent ions, gives rise to a positive residual charge in the structure, which is counterbalanced with anions and water molecules located interstitially (Mandal and Mayadevi, 2008). LDHs are defined by the general formula $[M_{1-x}^{II}M^x^{III}(\text{OH})_2]x^+[X_{x/mm}^-] \cdot n\text{H}_2\text{O}x^-$, abbreviated as $[M^{II}M^{III} - X]$, where $M^{II} = \text{Mg}^{2+}, \text{Mn}^{2+}, \text{Zn}^{2+} \dots$ $M^{III} = \text{Al}^{3+}, \text{Fe}^{3+}, \text{Cr}^{3+}$ and $X^- = \text{CO}_3^{2-}, \text{Cl}^{2-}, \text{NO}^{3+}$ (Chen *et al.*, 2014a, He *et al.*, 2006, Pérez *et al.*, 2006, Perioli *et al.*, 2011), with a molar ratio in the range of 0.2 to 0.4. The ordering of the cations affects the charge density of the LDH sheets, which is the main reason why LDHs have a tendency to have a high positive charge (Ma *et al.*, 2006). This factor has consequences for a variety of physicochemical parameters, such as bonding, reactivity, orientation, and mobility of the chemical species in the interlayer gallery and on the surface (Bi *et al.*, 2014b). Previously LDHs have been used in ceramic development (Evans and Duan, 2006), water purification (Goh *et al.*, 2008), toxic waste removal (Choy *et al.*, 2007).

In this study, we present ZnAl-LDHs as potential anticancer drug delivery vehicles. This type of LDH is no stranger to chemotherapy as it has been previously employed in the delivery of also drugs such as 5-Fu (Bi *et al.*, 2014a, Li *et al.*, 2014), and methotrexate (Chakraborty *et al.*, 2011,

Oh *et al.*, 2009). ZnAl have been intercalated with drugs such as diclofenac (DIK), a non-steroidal anti-inflammatory drug (Perioli *et al.*, 2011). The application of LDHs as novel antibacterial drug delivery systems, with intercalated cefazolin have also been reported. LDHs are suitable nanoparticles to be used in drug delivery as they are (i) conveniently synthesized, (ii) offer structural manipulation, (iii) morphological tenability, (iv) low in toxicity and (v) biocompatible (Bi *et al.*, 2014b).

4.2 Materials

Zinc nitrate [$\text{Zn}(\text{NO}_3)_2 \cdot 6\text{H}_2\text{O}$ (0.1 M)], trichloroacetic acid (TCA), sodium hydroxide (NaOH), sodium anticancer drug 5-fluorouracil (5-Fu) and sulphorhodamine B (SRB) were purchased from Sigma-Aldrich, St Louis, MO, USA. Fetal carbonate (NaCO_3), HCl, MTT reagent, dimethylsulfoxide (DMSO), phosphate buffered saline (PBS) tablets, acetic acid and Tris EDTA were purchased from Merck, Darmstadt, Germany. Aluminium nitrate, $\text{Al}(\text{NO}_3)_3 \cdot 9\text{H}_2\text{O}$, was obtained from C.C. Imelmann, Southdale, South Africa. The bovine serum (FBS) was purchased from Hyclone, GE Healthcare, Utah, USA. Eagles Minimum Essential Medium (EMEM), Penicillin/ Streptomycin, trypsin-versene were all obtained from Lonza Biowhittaker, Walkersville, USA. Human embryonic kidney (HEK 293) cells were provided by the Anti-viral gene therapy unit, Medical School, University of the Witwatersrand, South Africa. Human hepatocellular carcinoma (HepG2), breast adenocarcinoma (MCF-7) and colorectal cancer (CaCo-2) cells were purchased from Highveld Biological (PTY) LTD., Lyndhurst, South Africa. All sterile tissue culture plastic ware was obtained from Corning, NY, USA. All reagents were of analytical grade, and Milli-Q 18 M Ω water was used throughout the experimentation.

4.3 Methods

4.3.1 Synthesis

All the ZnAl-LDH samples were synthesized using the co-precipitation. Briefly, 25.6 g of $\text{Zn}(\text{NO}_3)_2 \cdot 6\text{H}_2\text{O}$ (0.1M) and 18.75 g of $\text{Al}(\text{NO}_3)_3 \cdot 9\text{H}_2\text{O}$ (0.05M) for (ZnAl 2:1-LDH) and 25.6 g of $\text{Zn}(\text{NO}_3)_2 \cdot 6\text{H}_2\text{O}$ (0.1M) and 12.8 g of $\text{Al}(\text{NO}_3)_3 \cdot 9\text{H}_2\text{O}$ (0.05M) for (ZnAl 3:1-LDH) were added into 150 ml of distilled 18 M Ω water, and mixed. Thereafter 53g of Na_2CO_3 was put in a beaker containing 600mL of water. This was stirred and the pH was adjusted to 11 using 0.1M NaOH. $\text{Al}(\text{NO}_3)_3 \cdot 9\text{H}_2\text{O}$ and $\text{Zn}(\text{NO}_3)_2 \cdot 6\text{H}_2\text{O}$ were subsequently added into the solution. The mixture was then aged overnight at 80 °C, after which the LDHs were washed with 18 M Ω water repeatedly until pH was neutralised. The slurries were first vacuum dried and then dried further overnight in an oven at 110 °C. The dried samples were ground to a talc-like texture.

4.3.3 ZnAl-LDH: 5-Fu synthesis

The intercalation of 5-Fu into both the ZnAl-LDHs (2:1 and 3:1 respectively) was achieved using the reconstruction route. The procedure first involved the calcination of the respective LDHs in a horizontal furnace (Labofurn PUB002) set at 400 °C for 8 hours under N_2 atmosphere. Briefly, 11.1 mg of the calcined ZnAl LDH powders, suspended in 20 mL of 5-Fu (0.0114 M in 18 M Ω water, pH 8.0) solution, were vigorously stirred under N_2 atmosphere for 24 hours to obtain the respective ZnAl-LDH-5-Fu conjugates. Samples were stored at 4 °C until needed.

4.3.4 UV-Vis Spectroscopy.

The encapsulation efficiencies (%EE) of the respective ZnAl nanoparticles was determined by centrifugation and UV-Vis spectroscopy. The respective ZnAl-5-Fu suspensions were centrifuged at 12000 rpm for 5 minutes, and supernatants containing any free 5-Fu were assayed by UV-Vis spectroscopy (Biomate, Thermoscientific). The pellets were resuspended in 18 M Ω water and readings taken to measure absorbance of LDH bound 5-Fu. Absorbance readings were obtained at 266 nm and the results calculated using the formula:

% Encapsulation Efficiency = (total drug– free “untrapped drug”) / total drug X 100

4.3.5 Powder X-Ray diffraction

Powder X-Ray diffraction (XRD) was performed for the uncalcined (pure), calcined and drug conjugated ZnAl, using a Bruker D8 Advanced XRD analyzer (CuK α radiation) equipped with Bruker analysis software. In each of the runs, 0.5 g of the sample was used and signals were recorded for 2 θ values between 5 and 90° at a scan rate of 0.5 °/min.

4.3.6 Fourier Transform Infrared Spectroscopy (FTIR)

Infra-red (IR) spectra of the LDH and nanohybrids were obtained using a Perkin Elmer FTIR Spectrometer equipped with a Universal ATR sampling accessory using a diamond crystal. For analysis, Spectrum Analysis Software was used.

4.3.7 Inductively Coupled Plasma Analysis-Optical Emission Spectroscopy (ICP-OES)

Elemental detection and quantification of the metal content of the LDH and its complexes were obtained by inductively coupled plasma-optical emission spectroscopy (ICP-OES), performed on a Perkin Elmer Optima 5300 DV Optical Emission Spectrometer. Standard calibration curves were set up between 1 and 20 ppm using 100 ppm standard stock solutions of the respective metal solutions.

4.3.8 Electron Microscopy

The ultrastructural morphology of the calcined ZnAl LDHs and their nanohybrids were examined under scanning electron microscopy (SEM) and transmission electron microscopy (TEM). For SEM, 0.1 mg samples were examined using a ZEISS LEO 1450 scanning electron microscope, while for TEM, 1 μ l of each sample, was viewed in a Joel 1010 electron microscope (Tokyo, Japan) fitted with Megaview 3 soft imaging system and iTEM software for analysis.

4.3.9 Nanoparticle Tracking Analysis (NTA)

NTA studies were performed using nanoparticle tracking analysis (NTA) using a Nanosight NS500 (Malvern Instruments, Worcestershire, UK). NTA analyses the sample by tracking the rate of the Brownian motion to the particle's size and zeta potential. The pristine nanoparticle as well as their respective nanohybrids were diluted to approximately 0.1 mg/mL in 18 M Ω water for analysis at 25 °C.

4.3.10 Drug release Studies

Approximately, 1 mL of the ZnAl-5-Fu solutions (2:1 and 3:1 respectively) were dialyzed (MWCO of 7000 KDa), against 20 ml of PBS at pH 4 and pH 7, with stirring for 7 hours, as described previously (Maghsoudi *et al.*, 2008). Samples (1 mL) were removed every hour for UV-Vis analysis at 266 nm. PBS (1 mL) at the same pH was replaced each time.

4.3.11. *In vitro* Cell Culture studies

All cell culture studies were conducted under sterile conditions. Cells were routinely maintained in complete medium (EMEM containing 10% FBS, penicillin 100 μ g/mL and streptomycin 100 μ g/mL), and visualized under an inverted microscope (Nikon TMS F 6V, Tokyo, Japan). Upon confluency, cells were trypsinized and split as desired into sterile cell culture flasks or counted using a haemocytometer and plated into either 96 or 48-well tissue culture plates for cell based assays.

4.3.12 MTT Cytotoxicity Assay

The MTT assay or 3-[4,5-dimethylthiazol-2-yl]-2,5 diphenyl tetrazolium bromide assay is based on the principle that the MTT reagent (yellow) is converted into (purple) formazan crystals in actively metabolizing cells, by mitochondrial reductases. The MTT assay is a popular assay for

the determination of the *in vitro* cytotoxic effects of anticancer drugs on multiple cell lines or primary patient cells (van Meerloo *et al.*, 2011).

Cytotoxicity was evaluated in four human cell lines: CaCo-2, HepG2, MCF-7 and HEK293. Cells were seeded at a density of 1×10^4 cells/well in 100 μ L in 24 well plates and incubated overnight at 37°C. Thereafter, cells were treated with free 5-Fu and ZnAl-LDH-5-Fu (concentrations 12, 5 μ g/ mL, 25 μ g/ mL, 50 μ g/ mL and 100 μ g/ mL), and incubated for 48 hours at 37 °C. Assay was done in triplicate (n=3). Positive control cells containing no LDH or drugs were included. Medium was then removed and 100 μ L of MTT reagent and 100 μ L of medium was added and cells incubated at 37°C for 4 hours. The MTT/medium mixture was removed and 100 μ L of DMSO was added to dissolve the formazan crystals formed. Absorbance readings were taken using a MR-96A microplate reader (Vacutec, Hamburg, Germany) at wavelength 570 nm, with 650 nm for background reading. The cell viability was calculated using the following formula:

$$\% \text{ cell survival} = (A_{570 \text{ nm}} \text{ treated cells}) / (A_{570 \text{ nm}} \text{ untreated cells}) \times 100$$

4.2.13 Sulphorhodamine B (SRB) assay

SRB is a protein dye that binds electrostatically and pH dependently to basic amino acids of cells. Mild acidic and mild basic conditions it can be extracted from cells and solubilized respectively, and hence determined spectrophotometrically (Vichai and Kirtikara, 2006). Cells were plated and treated with the free drug and LDH-Fu as for 4.2.12. After 48 hours, cells were fixed by overlaying the growth medium with ¼ volume of cold 50% TCA, and incubated for 1 hour at 4 °C. Cells were then rinsed with deionized water, air dried, and covered with 50 μ L of 0.4% SRB solution for 20 minutes. Thereafter cells were washed with 1% acetic acid, and air dried, followed by the addition of 100 μ L of 10 mM Tris-EDTA solution to solubilize the dye. The plate was then shaken (Stuart Scientific, platform shaker STR 6) for 5 minutes, and absorbance read at 565 nm, with 690 nm for background.

4.3.14 Apoptosis Study

The dual-staining method for apoptosis using acridine orange and ethidium bromide (AO/EB) was employed. Mechanism of cell death from exposure to free 5-Fu and LDH-5-Fu was determined using 100 mg/mL of both dyes (1:1 ratio in PBS). Cells were plated in a 24 well plate at a seeding density of 1.2×10^5 cells/well, and incubated as in 4.3.12. Free and LDH bound 5-Fu (20 μ L each) were then added to cells and cells incubated for 48 hours at 37 °C. Thereafter, cells were washed (PBS, 100 μ L) and then covered with 15 μ L of the dual stain for 5 minutes. Cells were visualized using an Olympus inverted fluorescent microscope with a CC12 fluorescent camera (Olympus Co., Tokyo, Japan) at X200 magnification, and apoptotic indexes (AI) were calculated using the following formula;

$$\text{Apoptotic Index} = \frac{\text{Number of apoptotic cells}}{\text{Number of total cells}}$$

4.3.15 Statistical Analyses

All statistical analyses were performed using Graph pad prism 5.0 (GraphPad Software, Inc., San Diego, CA), one-way analysis of variance (ANOVA). Differences between groups were considered to be significant at a P value of <0.05.

4.4 Results and Discussion

4.4.1 Synthesis of ZnAl-LDH

ZnAl 2:1-LDH and ZnAl 3:1-LDH were successfully synthesized. Both LDHs had the characteristic pristine white appearance, but upon calcination changed to a light grey color (Figure 4.1). This was probably due to the decomposition and decarboxylation of the LDHs (Starukh *et al.*, 2016). Decomposition of the LDHs essentially leads to loss of its structural integrity, which is then converted to a mixture of oxides (zinc and aluminum). Thus the particle loses some of its original mass (Starukh *et al.*, 2016), as seen with a loss of 1 g for ZnAl 2:1-LDH and 0.5 g for ZnAl 3:1.

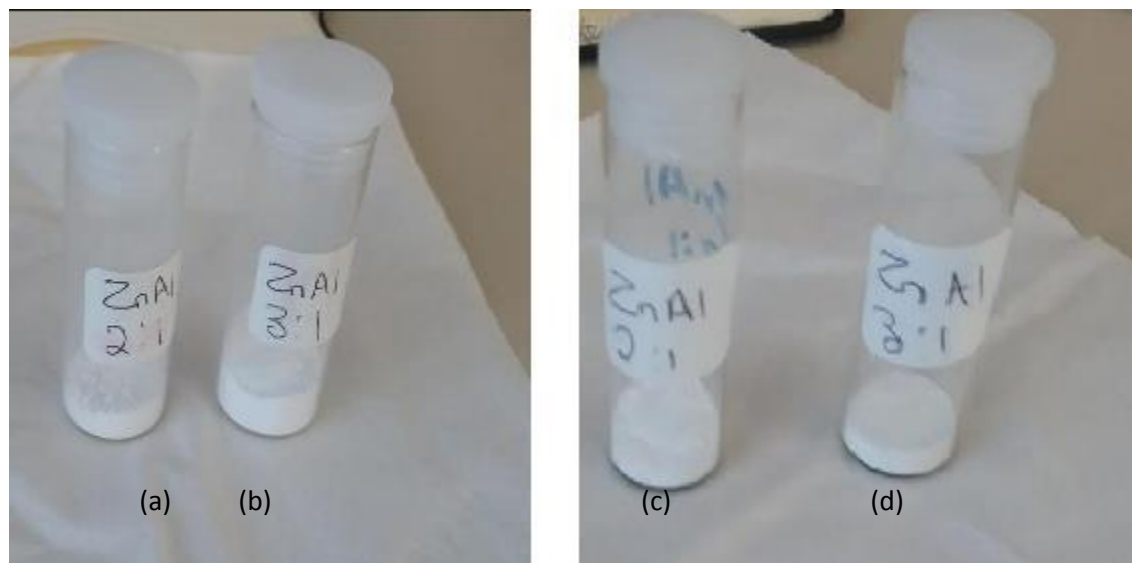


Figure 4.1: Synthesized LDHs (a) ZnAl 2:1 pristine (b) ZnAl 3:1 pristine (c) ZnAl 3:1-5-Fu calcined (d) ZnAl 3:1 calcined

4.4.2 UV-Vis spectroscopy

As 5-Fu is intercalated within the ZnAl LDHs, it is held together by electrostatic forces within the cationic layer of the LDHs. Thus to ascertain this, UV-Vis spectroscopy was conducted. UV-Vis spectroscopy confirmed the actual binding of 5-Fu within the LDH (Figure 4.2). This was observed as a shift in the wavelength from 266 nm (5-Fu) to 265 nm respectively for the nanohybrids. Drug encapsulation efficiencies were then calculated for both nanohybrids to quantitate the amount of bound drug (Table 4.1). These results displayed a much higher binding efficiency for ZnAl 3:1-5-Fu than ZnAl 2:1, which indicates a slightly higher electrostatic interaction of the drug with the second nanohybrid. This could be an advantage for the drug, as it will be protected from harsh physiological reactions, but may also be a disadvantage in a sense that the drug might be released too slowly from this nanohybrid.

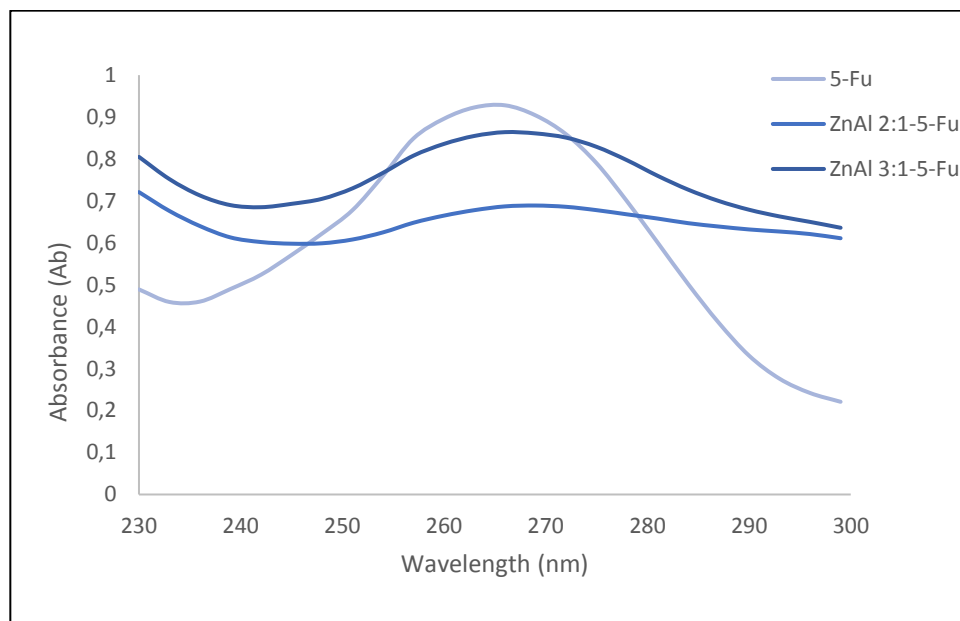


Figure 4.2 : UV-Vis spectroscopy of 5-Fu, ZnAl 2:1-5-Fu and ZnAl 3:1-5-Fu

Table 4.1 Al-LDHs Encapsulation Efficiencies (% EE)

Nanoparticle name	Nanohybrid formula	Encapsulation efficiency (%EE)
ZnAl 2:1	ZnAl 2:1-5-Fu	64.92
ZnAl 3:1	ZnAl 3:1-5-Fu	56.56

4.4.3 XRD Analysis.

XRD analyses (Appendix B.1), revealed the typical well crystallized hydrotalcite structure for ZnAl LDHs (2:1 and 3:1), both exhibiting fairly sharp and symmetric $00l$ reflections, (003) (006) and (009) which are characteristic of a lamellar material. Calcined ZnAl 2:1 And 3:1 LDH displayed loss of structural integrity as seen with the indistinguishable peak patterns around 2 theta 19° and 18° respectively. All ZnAl-LDHs and nanohybrids displayed a (110) reflection, however there was a slight shift in the peaks in then nanohybrids due to the intercalation of 5-Fu within the gallery space of the respective LDHs (Jin *et al.*, 2010).

4.4.4 Fourier Transform Infrared Spectroscopy

For all the LDHs, the bands near 3000 cm^{-1} corresponded to the vibration bands of hydroxyls (O-H). A shift of the O-H vibrational band to a higher wavelength with the increase in Zn/Al ratio was observed. Such a change is due to the smaller ionic radius of Al^{3+} in comparison to the larger radius of Zn^{2+} (Tong *et al.*, 2011). Thus this leads to a higher electrostatic interaction between Al^{3+} and OH versus the Zn^{2+} and OH interaction with the increased Zn/Al ratio. IR-spectra of 5-Fu exhibited characteristic peaks around 1600 cm^{-1} attributed to vibration stretching of C=O in amide, and C-N stretching. These characteristic peaks were also observed on the two respective nanohybrids, ZnAl 2:1-5-Fu and ZnAl 3:1-5-Fu. Hybridization, peaks corresponding to C=O in imide disappeared, and a broad band corresponding to C=C, C=N, and C=O stretching vibration appeared, which was in good agreement with the previous report on 5-Fu-incorporated LDH. Interestingly the peaks at 1636.18 cm^{-1} (ZnAl 2:1-5-Fu) and 1636.79 cm^{-1} (ZnAl 3:1-5-Fu) confirmed interaction of 5-Fu with a cationic substance, further verifying intercalation of 5-Fu within the respective ZnAl-LDHs.

4.4.5 Inductively coupled plasma-optical emission spectroscopy (ICP-OES)

Inductively coupled plasma-optical emission spectroscopy (ICP-OES) was performed on the ZnAl-LDHs (2:1 and 3:1) and their nanohybrids confirmed the presence of magnesium and aluminium in their appropriate ratios (Appendix C.)

4.4.6 Electron Microscopy (SEM and TEM)

Under SEM, both ZnAl 2:1-LDH and ZnAl 3:1, displayed the characteristic hexagonal shape, a distinguishing feature of these nanoparticles (Figures 4.3-4.4). Their sizes as assessed under EM ranged from 35 nm for the LDHs to 60 nm for the nanohybrids. Since this provides a limited view, a more accurate size distribution was obtained from NTA studies (4.3.7). Agglomeration of the nanoparticles was observed and indicated quite a unique dispersity property of the LDHs (both ZnAl 2:1-LDH and ZnAl 3:1). Lateral sizing and thickness of the nanoparticles was significantly reduced by calcination. Calcined nanoparticles appeared to have lost their

characteristic LDH structure, possibly due to the calcination process essentially decomposing the distinct house of cards structure and the subsequent loss of interlayer species (thus the loss in thickness) (Figures 4.3b-4.5b) (Patzkó *et al.*, 2005). Their structure was reformed after 5-Fu intercalation. This phenomenon of reconstruction after calcination of the LDHs allows for the intercalation of the drug safely into the interlayer space whilst also reconstructing the vertices of the respective LDHs. TEM further confirmed the formation of true LDHs (both ZnAl 2:1-LDH and ZnAl 3:1). The lateral sizes all LDHs were in the same range as that observed with SEM and the dispersity of the LDH discs was also visualized. The aggregation of these nanoparticles seemed a common feature. TEM of the calcined LDHs further confirmed a loss in the original hexagonal shape of the LDHs (Figures 4.4.-4.5), due to their exposure to high temperatures (400 °C) for a prolonged period of time (He *et al.*, 2010).

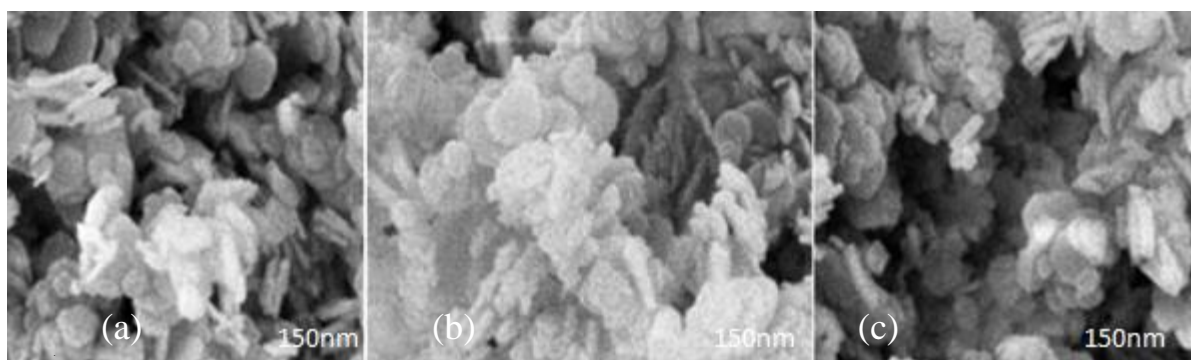


Figure 4.3 SEM micrographs of (a) ZnAl 3:1, (b) Calcined ZnAl 3:1 and (c) ZnAl 3:1-5-Fu (Bar $\leq 150\text{nm}$ nm).

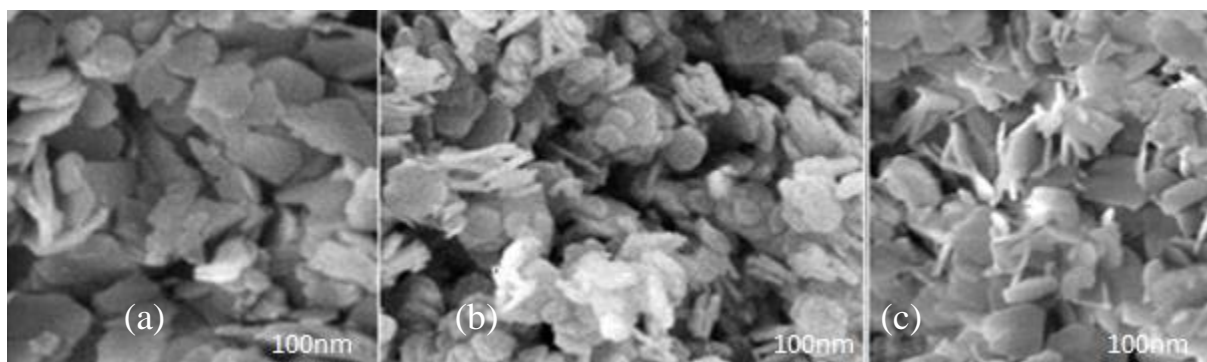


Figure 4.4 SEM micrographs of (a) ZnAl 3:1, (b) Calcined ZnAl 3:1 and (c) ZnAl 3:1-5-Fu (Bar $\leq 150\text{nm}$ nm).

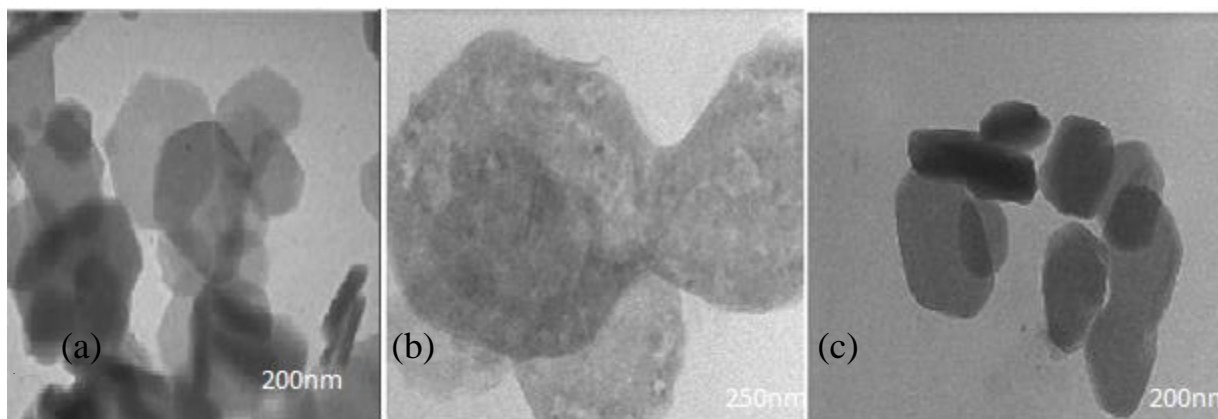


Figure 4.5 TEM images of (a) ZnAl 2:1, (b) Calcined ZnAl 2:1 and (c) ZnAl 2:1-5-Fu (Scale bar \leq 250nm).

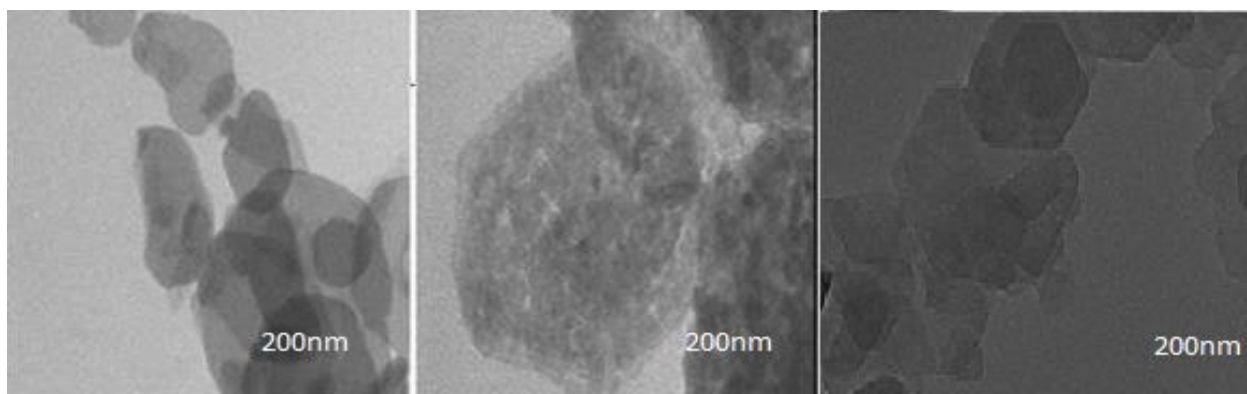


Figure 4.6 TEM images of (a) ZnAl 3:1, (b) Calcined ZnAl 3:1 and (c) ZnAl 3:1-5-Fu (Bar = 200 nm).

4.4.7 Nanoparticle tracking analysis (NTA)

Previous research has highlighted the importance of positively charged nanomaterials with regards to their favorable interaction with cellular membranes, stating that a net positive charge leads to their enhanced cellular uptake of, and subsequently the uptake of intercalated species (Kim *et al.*, 2014). However, net surface charge of ZnAl-LDHs, like most other LDHs, is largely affected by the surface coating of the molecules, the concentration of electrolytes, and the type or concentration of solutes in the suspending medium (Kim *et al.*, 2014). NTA served to establish the zeta potentials in addition to the sizes of the ZnAl-LDHs and their respective nanohybrids (Table 4.1, Appendix B.3). The net zeta potentials observed for ZnAl 2:1 was \sim above 50 mV and for ZnAl 2:1-5-Fu it was \sim 37.3 mV. The same trend was observed for ZnAl 3:1 (52.34 mV) and its nanohybrids ZnAl 3:1-5-Fu (23.24 mV). These readings confirm the colloidal stability of these LDHs and the reduced risk of systemic

aggregation. Another important factor to consider is that the anionic 5-Fu plays a part in the inhibition of the hydroxide layer growth, thus resulting in a slight decrease in the net zeta charge. It has also been reported that the intercalation of 5-Fu plays an important role in the hydrodynamic size distribution of the nanohybrids (Chen *et al.*, 2014b). The two LDHs had average sizes of 100 nm (ZnAl 2:1) and 150 nm (ZnAl 3:1) with correspond nanohybrids appearing slightly smaller (99 and 110 nm respectively). These reports do not necessarily reflect the percentage uptake of the anionic 5-Fu but the observed changes in zeta potential do reflect an intercalation of an anionic species.

Table 4.1: Net Zeta potentials of ZnAl 2:1, ZnAl 2:1-5-Fu, ZnAl 3:1 and ZnAl 3:1-5-Fu

PROPERTY	LDH SAMPLE			
	ZnAl 2:1	ZnAl 2:1-5-Fu	ZnAl 3:1	ZnAl 3:1-5-Fu
Sample name				
Size (nm)	100 ± 2.1	99±2.1	150 ± 0.1	110 ± 0.2
Zeta Potential (mV)	45.34 ±0.1	37.3 ±0.1	52.34 ±0.2	23.24 ±0.1

4.3.8 Drug release studies

The drug release profile of the ZnAl-LDH with corresponding nanohybrids was studied for both nanohybrids (2:1 and 3:1) (Figure 4.7). At pH~4 it was observed that both nanohybrids had a burst of drug release by t=1. This is due to the LDH being exposed to a low pH leading to its rapid disintegration and subsequent drug release. This property leads to a controlled release of 5-Fu once the cationic layers separate. At t=1, 25 % of 5-Fu had been released for the first nanohybrid and 29 % had been released for the second nanohybrid. Cancerous cells generally have a lower pH due to their high often intracellular anaerobic processes (Gerweck and Seetharaman, 1996). This could prove to be the advantage for the LDHs, as they will only fully disintegrate at a low pH, whilst protecting cells at neutral or higher pH (healthy cells).

This trend continued on until $t=7$, where for ZnAl 2:1-5-Fu 70% of the drug was released and for ZnAl 3:1-5-Fu, 60 % of the drug had been released.

Hence this slow release allows for a prolonged effect of the drug until 100 % of the drug is released, which is expected to occur after 7 hour, and needs to be further investigated. It has been previously reported that LDHs offer a system of controlled release for drugs (Kim *et al.*, 2014).

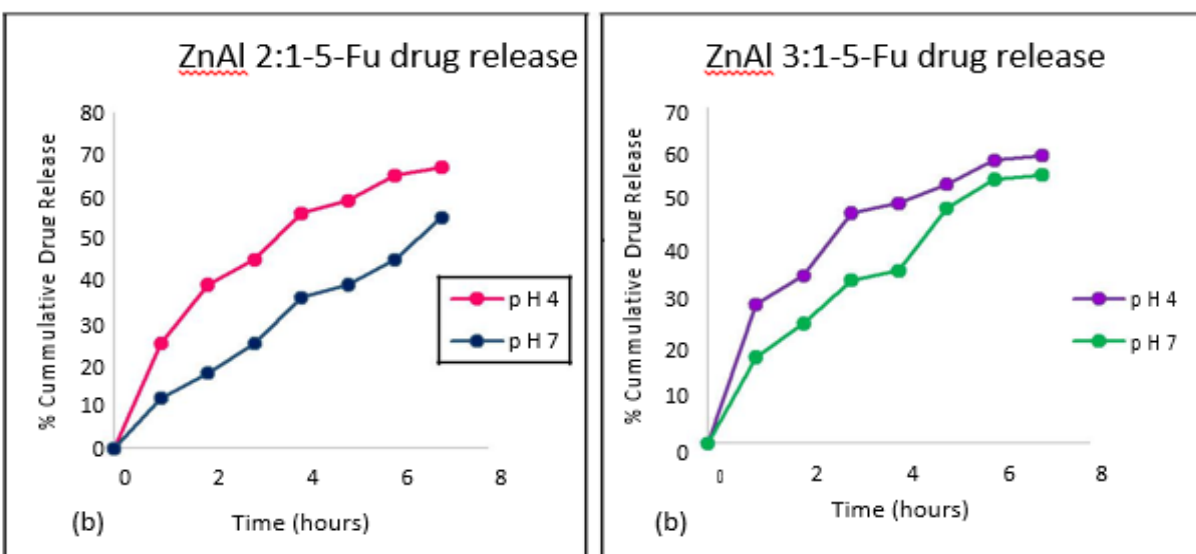


Figure 4.7: (a) Drug release profiles of ZnAl 2:1-5-Fu and (b) ZnAl 3:1-5-Fu at pH ~4 and pH ~7 respectively.

4.4.9 MTT Cytotoxicity Assay

To determine the cytotoxicity effects of the free 5-Fu and 5-Fu loaded LDHs in the four human cell lines (HEK293, MCF-7, Hep-G-2 and CaCo-2), the MTT cell viability assay was carried out. From the results it can be noted that the LDH encapsulated 5-Fu offered a gradual drug release which led to a steady decline in cell survival as the concentration of the drug increased, whilst at the same concentration significant cell death was observed for cells assaulted with free 5-Fu (Figures 4.8-4.9).

This rapid cell death for cells treated with pure 5-Fu indicates a less controllable and less predictable mode of delivery for the drug, providing immediate but probably not a sustained effect. Hence, the 5-Fu loaded LDHs provide a more prolonged effect of the drug. The significant difference in cell survival between ZnAl-5-Fu treated cells and those treated with free 5-Fu was further evident with the IC₅₀ values (Table 4.2).

ZnAl-5-Fu treated cells had a significantly higher IC₅₀ values, ranging between 49.55 -77.05 µg/mL, while lower IC₅₀ values ranging from 22.12 -54 µg/mL were observed for the cells treated with free 5-Fu. All cells showed similar cytotoxicity profiles but no significant cell specificity was observed.

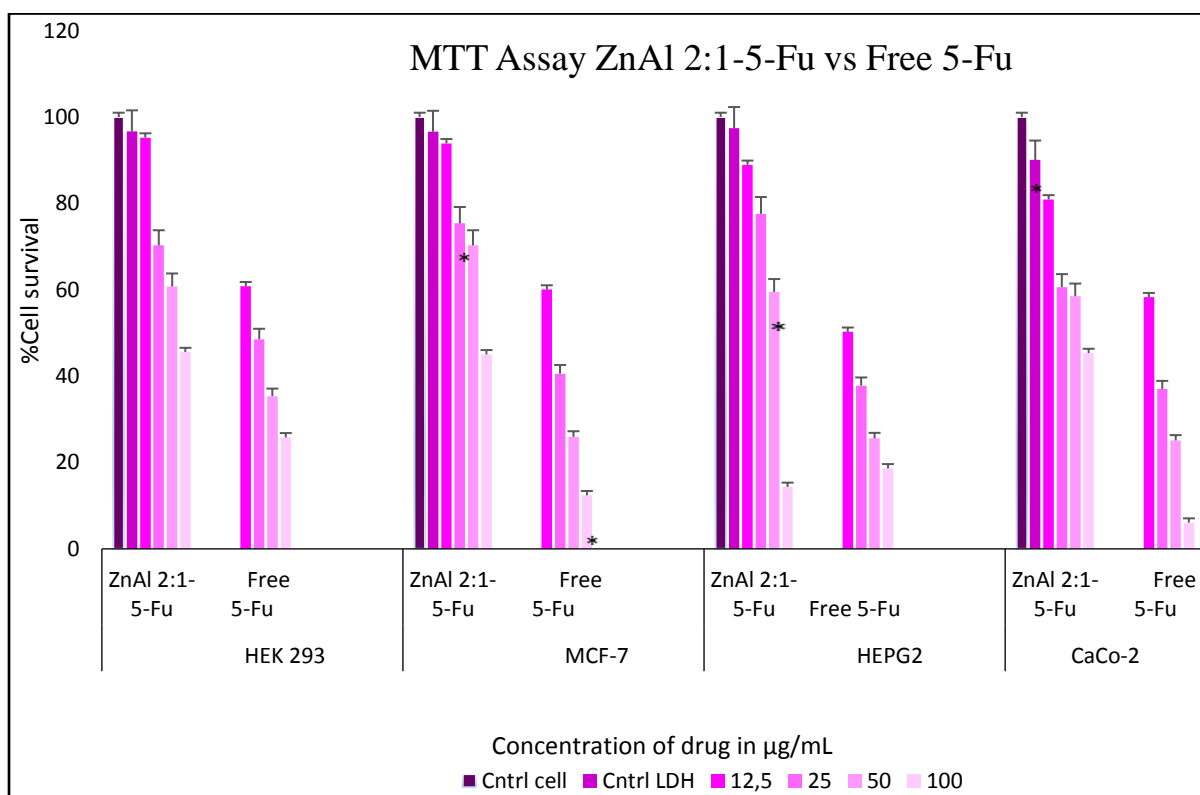


Figure 4.8 : MTT assay of ZnAl-3:1-5-Fu and free 5-Fu at concentrations 12.5 µg/mL, 25 µg/mL, 50 µg/mL and 100 µg/mL in HEK293, MCF-7, HepG2 and CaCo-2 cell lines [data presented as means SD ±(n=3) (*p < 0.05)].

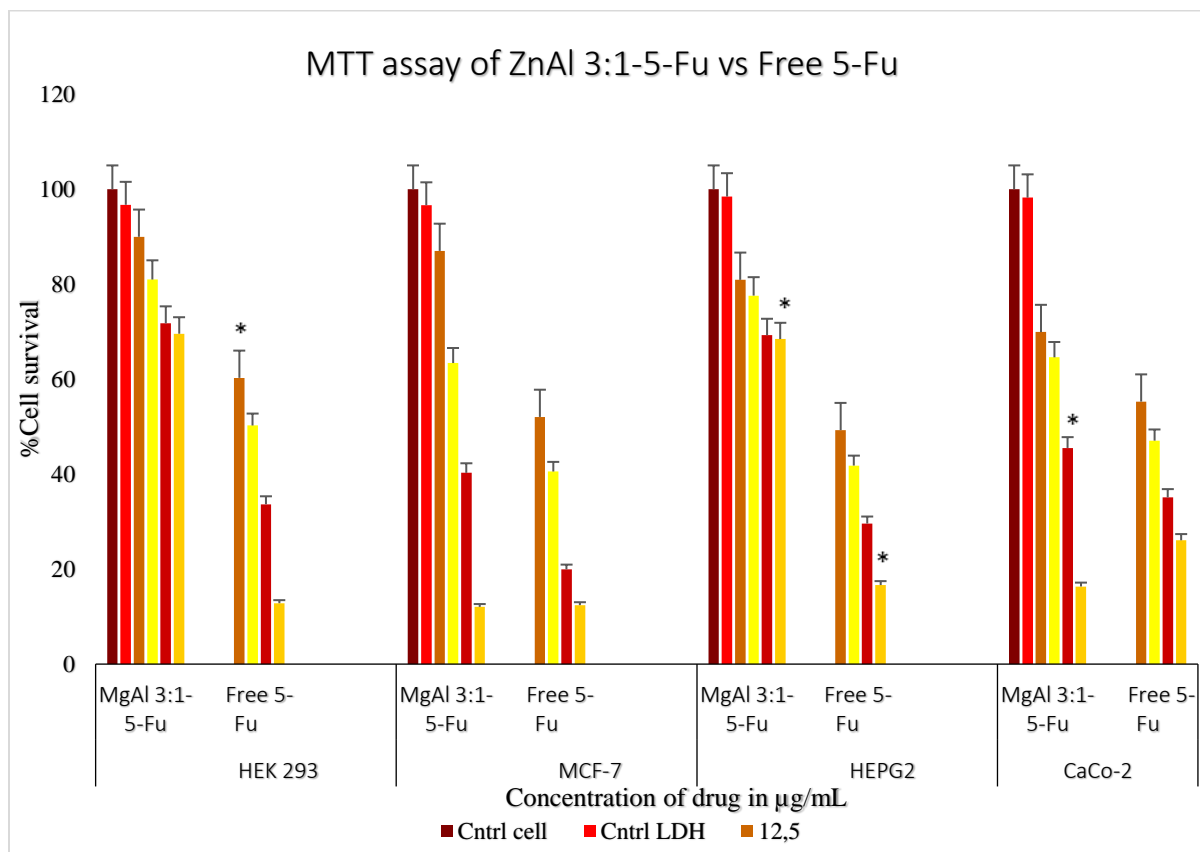


Figure 4.9: MTT assay of ZnAl-3:1-5-Fu and free 5-Fu at concentrations 12.5 µg/mL, 25 µg/mL, 50 µg/mL and 100 µg/mL) in HEK293, MCF-7, HepG2 and CaCo-2 cell lines [data presented as means $SD \pm$ (n=3) ($p^* < 0.05$)].

Table 4.2: IC₅₀ (µg/mL) values for ZnAl 2:1-5-Fu, ZnAl 3:1-5-Fu and free 5-Fu.

Cell line	ZnAl 2:1-5-Fu	Free 5-Fu	ZnAl 3:1-5-Fu	Free 5-Fu
	IC ₅₀ values in µg/mL			
HEK293	65.50	41.94	69.39	22.95
MCF-7	72.83	33.25	70.33	25.25
HepG2	68.55	31.69	77.05	64.84
CaCo-2	59.55	31.07	49.55	21.07

4.4.10 Sulphorhodamine B (SRB) assay

The SRB assay has been routinely used to evaluate drug-induced cytotoxicity especially in anticancer drug screening (Voigt, 2005). The principle behind this assay is based on the pH dependent electrostatic binding of the SRB protein dye to basic amino acid residues of cells. The SRB assay conducted across four the cell lines (HEK293, MCF-7, HepG2 and CaCo-2 cell lines), further confirmed that treatment with the LDH encapsulated 5-Fu offered a steady release of the drug to the cells, in comparison to the cells treated with free 5-Fu (Figures 4.10-4.11). Due to the LDHs being disintegrated at lowered pH this allows for the release of the LDH contents to the cancerous cell lines in a selective fashion as these cells have a lowered pH. Interestingly, in this assay both nanohybrids were least tolerated in the MCF-7 and CaCo-2 cell lines with cell death as much at 90 % at the highest concentration. Hence, some degree of cell specificity was observed, but this cannot be considered significant without further optimization studies. The cytotoxicity profiles were further confirmed by the IC₅₀ values calculated (Table 4.3). Although cell specificity was not clear, the dose dependent activity of both LDHs were evident. The SRB assay further corroborated the results from the MTT assay.

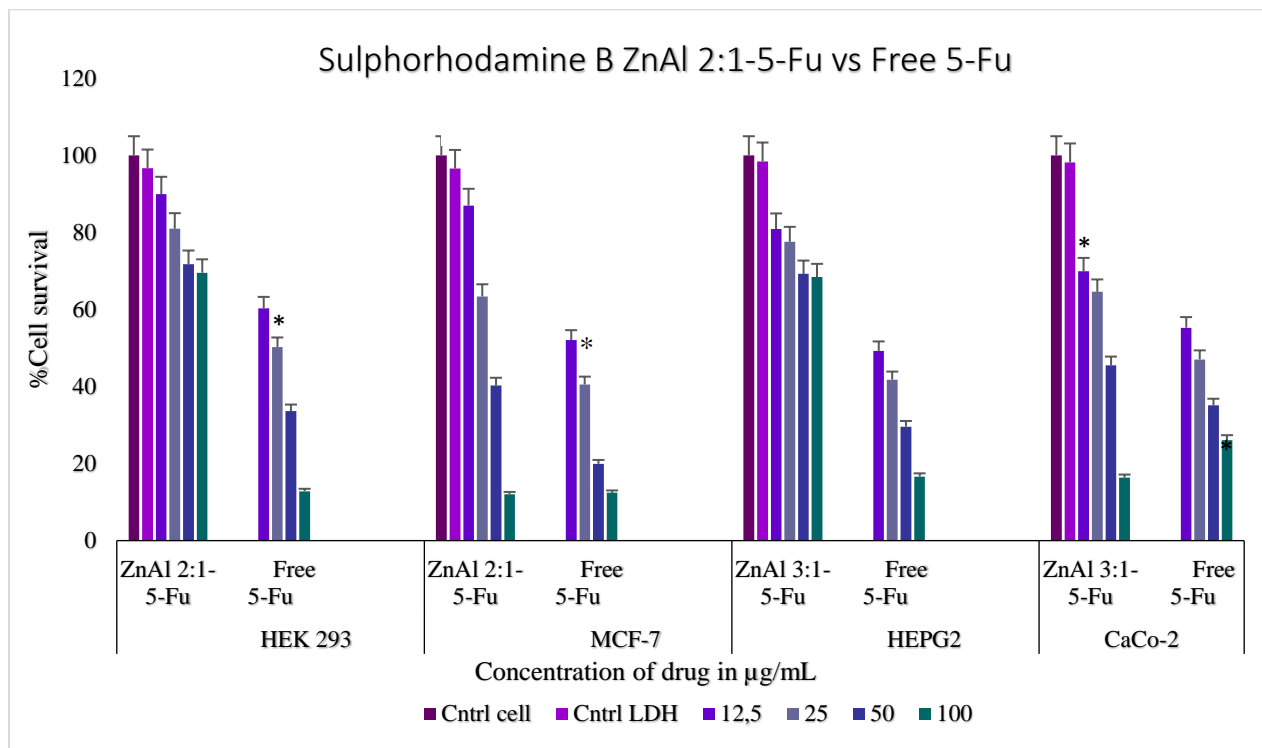


Figure 4.10: SRB assay of ZnAl-2:1-5-Fu and free 5-Fu at concentrations 12.5 µg/mL, 25 µg/mL, 50 µg/mL and 100 µg/mL in HEK293, MCF-7, HepG2 and Caco-2 cell lines [data presented as means SD± (n=3) (*p<0.05)].

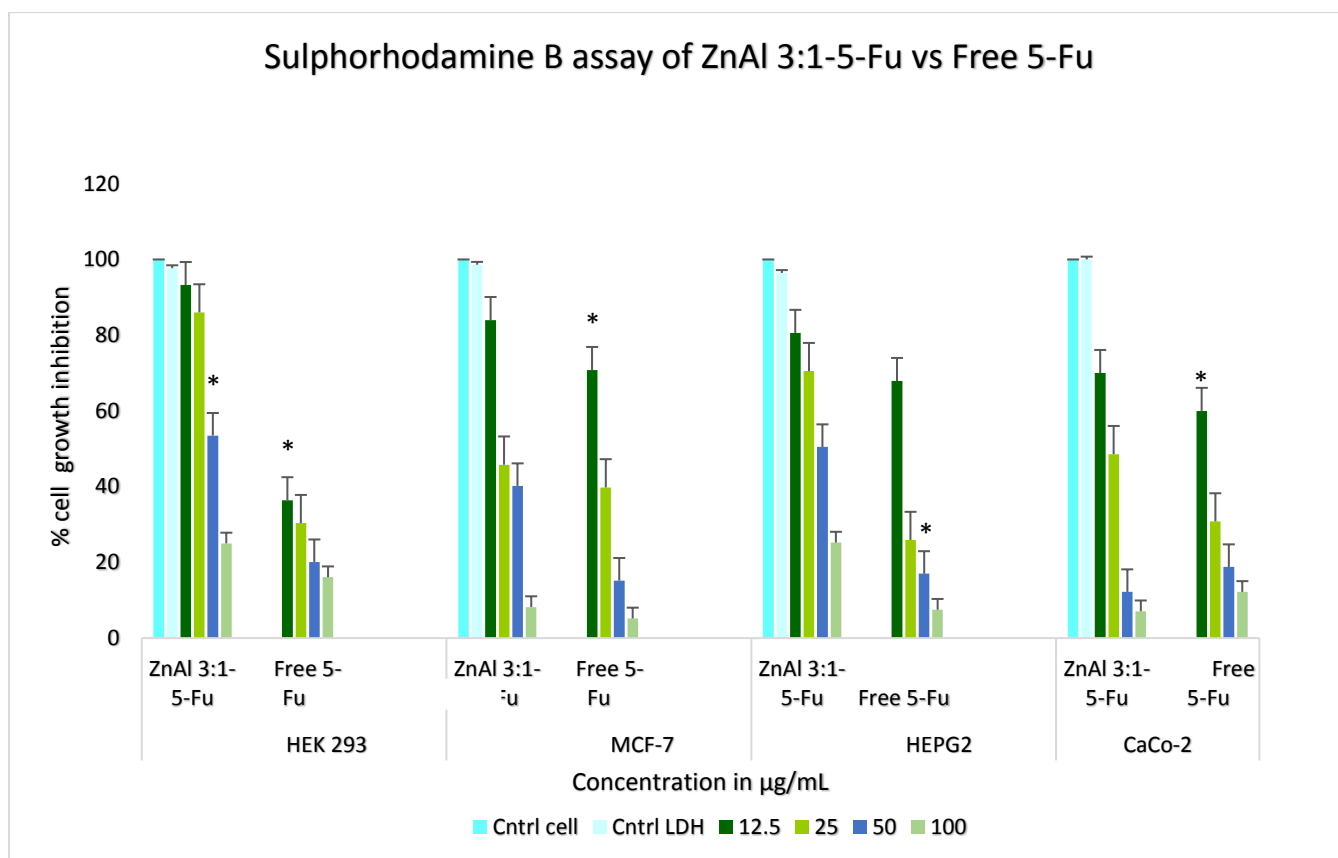


Figure 4.11: SRB assay of ZnAl-3:1-5-Fu and free 5-Fu at concentrations 12.5 µg/mL, 25 µg/mL, 50 µg/mL and 100 µg/mL in HEK293, MCF-7, HepG2 and CaCo-2 cell lines [data presented means SD± (n=3) (*p<0.05)]

Table 4.3: IC₅₀ (µg/mL) values for ZnAl 2:1-5-Fu, ZnAl 3:1-5-Fu and free 5-Fu.

Cell line	ZnAl 2:1-5-Fu	Free 5-Fu	ZnAl 3:1-5-Fu	Free 5-Fu
	IC ₅₀ values in µg/mL			
HEK293	76.35	41.94	69.75	22.25
MCF-7	51.38	30.25	43	27.5
HepG2	72.42	35.69	60.05	22.12
CaCo-2	55.05	41.07	32.84	24.8

4.4.11 Apoptosis studies

Free 5-Fu and ZnAl-LDH encapsulated 5-Fu were further investigated after cytotoxicity determinations, to determine their ability to induce apoptosis. This dual fluorescent staining with

acridine orange and ethidium bromide (AO/EB) can be used to visualize and identify apoptotic-associated changes in cells (Liu *et al.*, 2015). Some of these morphological changes that can be easily identified are (i) rounding off cells (ii) shrinkage (iii) condensing of chromatin and, (iv) fragmentation of the nucleus. Acridine orange is a vital dye that stains both live and dead cells (Liu *et al.*, 2015). Ethidium bromide stains cells that have lost membrane integrity only. Live cells will appear uniformly green. Early apoptotic cells stain green and have green dots in the nuclei due to chromatin condensation and nuclear fragmentation. Late apoptotic cells incorporate ethidium bromide and therefore stain orange, however in contrast to necrotic cells, the late apoptotic cells will show condensed and often fragmented nuclei. Necrotic cells stain orange, but have a nuclear morphology resembling that of viable cells, with no condensed chromatin (Kasibhatla *et al.*, 2006). The apoptosis induction was visualised under a fluorescent microscope. Cells treated with free 5-Fu displayed an increased apoptotic pattern when compared to cells treated with ZnAl-5-Fu (2:1 and 3:1). The results also almost no apoptotic induction in cells treated only with ZnAl LDH. This confirmed that the LDH's toxicity is almost negligible. The overall trend shows that free 5-Fu significantly increases apoptosis in all cell lines while LDH bound 5-Fu show lower apoptotic events (Figures 4.12 -4.13). Apoptosis indexes calculated also confirm this trend (Table 4.4). Using the dual staining method, live cells (L) usually appear green, early apoptotic cells appear yellow (EA), late apoptotic cells are orange and apoptotic cells are (red).

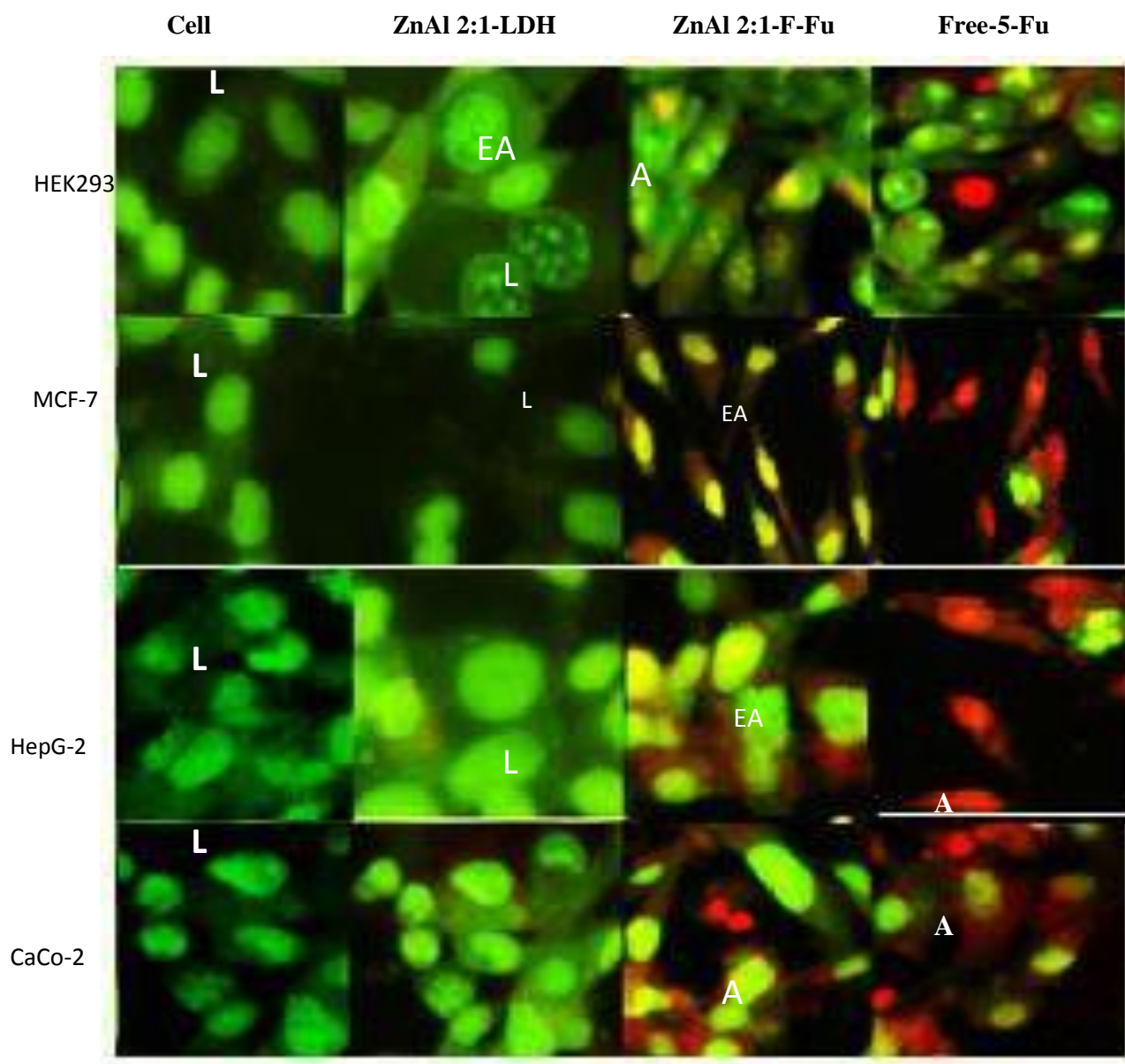


Figure 4.12: Fluorescent images of apoptosis induced by ZnAl 2:1-5-Fu and Free 5-Fu on HEK293, MCF-7, HepG2 and CaCo-2 cell lines (L=Live cells, A=Apoptotic cells, LA= Late Apoptotic cells and EA= Early Apoptotic cells)

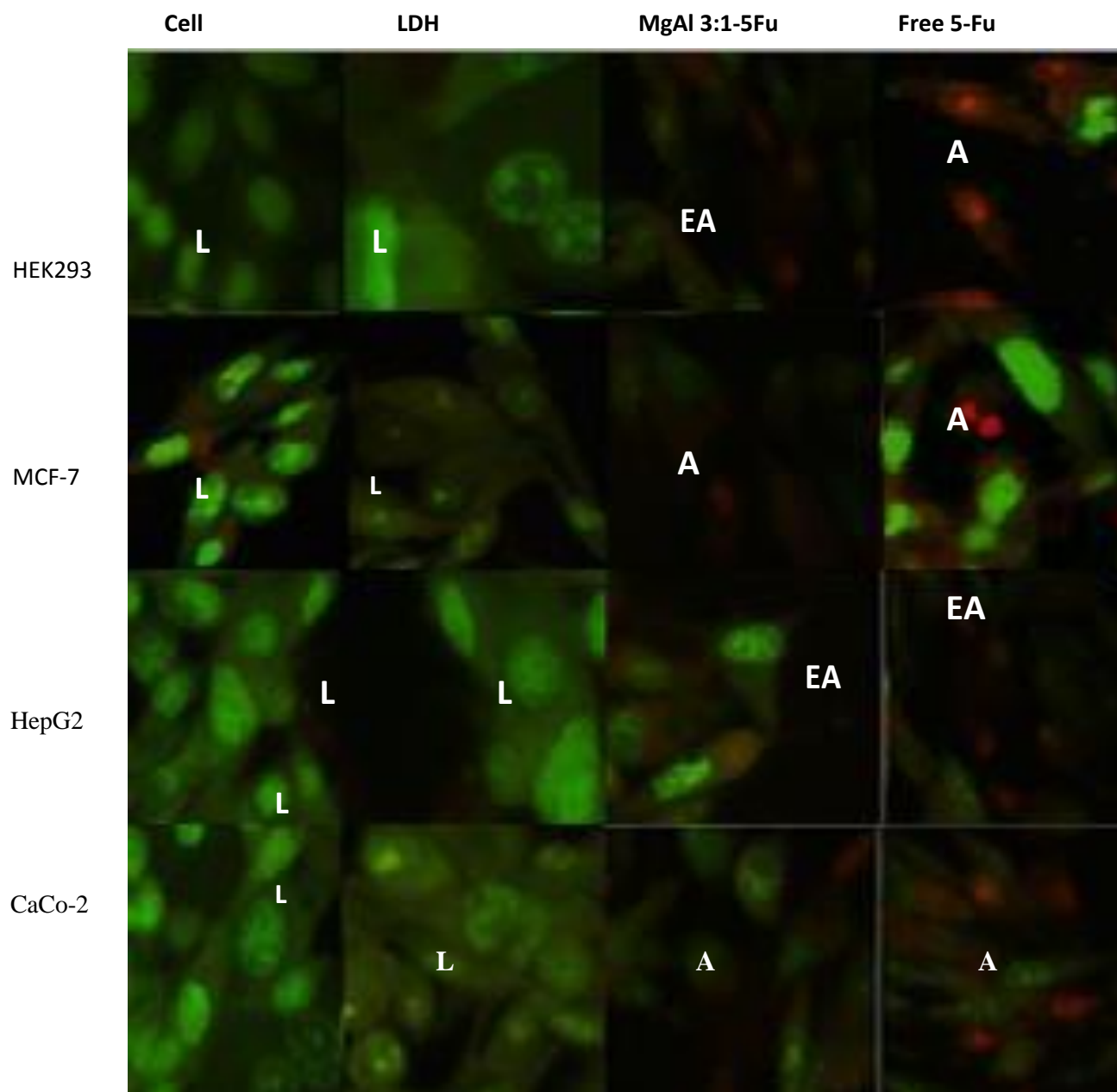


Figure 4.13: Fluorescent images of apoptosis induced by ZnAl 3:1-5-Fu and free 5-Fu on HEK293, MCF-7, HepG2 and CaCo-2 cell lines (L=Live cells, A=Apoptotic cells, LA= Late Apoptotic cells and EA= Early Apoptotic cells).

Table 4.4: Apoptotic Index (AI) of cells exposed to ZnAl-2:1-5-Fu, ZnAl 3:1-5-Fu and free 5-Fu

Cell lines	APOPTOTIC INDEX (AI)					
	Control Cell	Control LDH	ZnAl 2:1-5-Fu	Free 5-Fu	ZnAl 3:1-5-Fu	Free 5-Fu
HEK293	0.00	0.00	0.2	0.2	0.1	0.25
MCF-7	0.00	0.00	0.121	0.21	0.12	0.21
HepG2	0.00	0.00	0.21	0.35	0.2	1.06
CaCo-2	0.00	0.00	1.2	0.2	0.3	1.01

4.4 Conclusion

The ZnAl-LDH system evaluated, has shown potential to be utilized as a drug delivery system. This system is of suitable size, with high zeta potentials that favour colloidal stability and cellular uptake. Furthermore, this system offers a dose dependent cytotoxicity, coupled with a controlled system of drug release over a period of time. The disintegration of these LDHs at low pH, furthermore, allows for the selective release of its contents into cells with a lowered pH such as the cancerous cells, thereby offering selective protection and limited collateral damage to normal cells. Overall, these ZnAl LDH based drug delivery systems, are easy to synthesize, are cost effective, have favourable size distributions, are relatively stable, and importantly display controlled drug release. All these properties bode well for future use of these LDHs in nanomedicine.

Future studies and recommendations include the optimization of the systems with polymers such as polyethyleneglycol for steric stabilization, addition of a targeting ligand for cell/cancer specific drug delivery, and the testing of a wider array of cell lines to evaluate a broad spectrum of LDH activity.

4.6 References

- Allen, T. M. & Cullis, P. R. 2004. Drug delivery systems: entering the mainstream. *Science*, 303, 1818-1822.
- Bi, X., Zhang, H. & Dou, L. 2014a. Layered double hydroxide-based nanocarriers for drug delivery. *Pharmaceutics*, 6, 298-332.
- Bi, X., Zhang, H. & Dou, L. 2014b. Layered Double Hydroxide-Based Nanocarriers for Drug Delivery. *Pharmaceutics*, 6, 298.
- Chakraborty, M., Dasgupta, S., Soundrapandian, C., Chakraborty, J., Ghosh, S., Mitra, M. K. & Basu, D. 2011. Methotrexate intercalated ZnAl-layered double hydroxide. *Journal of Solid State Chemistry*, 184, 2439-2445.
- Chen, H., Hu, L., Chen, M., Yan, Y. & Wu, L. 2014. Nickel–Cobalt Layered Double Hydroxide Nanosheets for High- performance Supercapacitor Electrode Materials. *Advanced Functional Materials*, 24, 934-942.
- Chen, J., Shao, R., Li, L., Xu, Z. P. & Gu, W. 2014. Effective inhibition of colon cancer cell growth with MgAl-layered double hydroxide (LDH) loaded 5-Fu and PI3K/mTOR dual inhibitor BEZ-235 through apoptotic pathways. *International Journal of Nanomedicine*, 9, 3403-3411.
- Cho, K., Wang, X., Nie, S., Chen, Z. & Shin, D. M. 2008. Therapeutic Nanoparticles for Drug Delivery in Cancer. *Clinical Cancer Research*, 14, 1310-1316.
- Choy, J.-H., Choi, S.-J., Oh, J.-M. & Park, T. 2007. Clay minerals and layered double hydroxides for novel biological applications. *Applied Clay Science*, 36, 122-132.

- Evans, D. G. & Duan, X. 2006. Preparation of layered double hydroxides and their applications as additives in polymers, as precursors to magnetic materials and in biology and medicine. *Chemical Communications*, 485-496.
- Gerweck, L. E. & Seetharaman, K. 1996. Cellular pH gradient in tumor versus normal tissue: potential exploitation for the treatment of cancer. *Cancer research*, 56, 1194-1198.
- Goh, K.-H., Lim, T.-T. & Dong, Z. 2008. Application of Layered Double Hydroxides for removal of oxyanions: a review. *Water research*, 42, 1343-1368.
- He, H., Kang, H., Ma, S., Bai, Y. & Yang, X. 2010. High adsorption selectivity of ZnAl layered double hydroxides and the calcined materials toward phosphate. *Journal of colloid and interface science*, 343, 225-231.
- He, J., Wei, M., Li, B., Kang, Y., Evans, D. G. & Duan, X. 2006. Preparation of layered double hydroxides. *Layered double hydroxides*. Springer.
- Jin, L., Liu, Q., Sun, Z., Ni, X. & Wei, M. 2010. Preparation of 5-fluorouracil/ β -cyclodextrin complex intercalated in layered double hydroxide and the controlled drug release properties. *Industrial & Engineering Chemistry Research*, 49, 11176-11181.
- Kasibhatla, S., Amarante-Mendes, G. P., Finucane, D., Brunner, T., Bossy-Wetzler, E. & Green, D. R. 2006. Acridine orange/ethidium bromide (AO/EB) staining to detect apoptosis. *CSH Protoc*, 2006.
- Kim, T.-H., Lee, G. J., Kang, J.-H., Kim, H.-J., Kim, T.-i. & Oh, J.-M. 2014. Anticancer drug-incorporated layered double hydroxide nanohybrids and their enhanced anticancer therapeutic efficacy in combination cancer treatment. *BioMed research international*, 2014.
- Kompella, U. B. 2013. Nanotechnology and Drug Delivery. *Journal of Ocular Pharmacology and Therapeutics*, 29, 89-89.

- Li, L., Gu, W., Chen, J., Chen, W. & Xu, Z. P. 2014. Co-delivery of siRNAs and anti-cancer drugs using layered double hydroxide nanoparticles. *Biomaterials*, 35, 3331-3339.
- Liu, K., Liu, P.-c., Liu, R. & Wu, X. 2015. Dual AO/EB staining to detect apoptosis in osteosarcoma cells compared with flow cytometry. *Medical science monitor basic research*, 21, 15.
- Liu, Y., Tan, J., Thomas, A., Ou-Yang, D. & Muzykantov, V. R. 2012. The shape of things to come: importance of design in nanotechnology for drug delivery. *Therapeutic delivery*, 3, 181-194.
- Ma, R., Liu, Z., Li, L., Iyi, N. & Sasaki, T. 2006. Exfoliating layered double hydroxides in formamide: a method to obtain positively charged nanosheets. *Journal of Materials Chemistry*, 16, 3809-3813.
- Maghsoudi, A., Shojaosadati, S. A. & Farahani, E. V. 2008. 5-Fluorouracil-loaded BSA nanoparticles: formulation optimization and in vitro release study. *Aaps Pharmscitech*, 9, 1092-1096.
- Mandal, S. & Mayadevi, S. 2008. Adsorption of fluoride ions by Zn–Al layered double hydroxides. *Applied Clay Science*, 40, 54-62.
- Manzi-Nshuti, C., Wang, D., Hossenlopp, J. M. & Wilkie, C. A. 2009. The role of the trivalent metal in an LDH: synthesis, characterization and fire properties of thermally stable PMMA/LDH systems. *Polymer Degradation and Stability*, 94, 705-711.
- O'hare, D. M. 2014. Drug delivery system. Google Patents.
- Oh, J. M., Choi, S. J., Lee, G. E., Kim, J. E. & Choy, J. H. 2009. Inorganic Metal Hydroxide Nanoparticles for Targeted Cellular Uptake Through Clathrin- Mediated Endocytosis. *Chemistry–An Asian Journal*, 4, 67-73.

- Patzkó, Á., Kun, R., Hornok, V., Dékány, I., Engelhardt, T. & Schall, N. 2005. ZnAl-layer double hydroxides as photocatalysts for oxidation of phenol in aqueous solution. *Colloids and Surfaces A: Physicochemical and Engineering Aspects*, 265, 64-72.
- Pérez, M., Pavlovic, I., Barriga, C., Cornejo, J., Hermosin, M. & Ulibarri, M. 2006. Uptake of Cu 2+, Cd 2+ and Pb 2+ on Zn–Al layered double hydroxide intercalated with edta. *Applied Clay Science*, 32, 245-251.
- Perioli, L., Posati, T., Nocchetti, M., Bellezza, F., Costantino, U. & Cipiciani, A. 2011. Intercalation and release of antiinflammatory drug diclofenac into nanosized ZnAl hydrotalcite-like compound. *Applied Clay Science*, 53, 374-378.
- Rives, V., del Arco, M. & Martín, C. 2014. Intercalation of drugs in layered double hydroxides and their controlled release: A review. *Applied clay science*, 88, 239-269.
- Starukh, G., Rozovik, O. & Oranska, O. 2016. Organo/Zn-Al LDH Nanocomposites for Cationic Dye Removal from Aqueous Media. *Nanoscale Research Letters*, 11, 228.
- Tong, M., Chen, H., Yang, Z. & Wen, R. 2011. The effect of Zn-Al-Hydrotalcites composited with calcium stearate and β -diketone on the thermal stability of PVC. *International journal of molecular sciences*, 12, 1756-1766.
- van Meerloo, J., Kaspers, G. J. & Cloos, J. 2011. Cell sensitivity assays: the MTT assay. *Cancer cell culture: methods and protocols*, 237-245.
- Velu, S., Ramkumar, V., Narayana, A. & Swamy, C. S. 1997. Effect of interlayer anions on the physicochemical properties of zinc–aluminium hydrotalcite-like compounds. *Journal of Materials Science*, 32, 957-964.

Vichai, V. & Kirtikara, K. 2006. Sulforhodamine B colorimetric assay for cytotoxicity screening. *Nature protocols*, 1, 1112-1116.

Voigt, W. 2005. *Sulforhodamine B assay and chemosensitivity*, Springer.

Wang, Z., Ma, R., Yan, L., Chen, X. & Zhu, G. 2015. Combined chemotherapy and photodynamic therapy using a nanohybrid based on layered double hydroxides to conquer cisplatin resistance. *Chemical Communications*, 51, 11587-11590.

CHAPTER 5

5.1 Conclusion

Overall results from chapters 3 and 4, confirm that these LDHs are capable of being drug delivery vehicles for anionic drugs. The two MgAl-LDHs synthesized differed in many aspects, not only is their ability to deliver 5-Fu, but in their unique release of the nanoparticle's contents. We found that although these drug delivery systems are very well capable of delivering 5-Fu in particular, a few improvements can be made to increase these nanoparticles' encapsulation efficiencies to well over 70% encapsulation. LDH encapsulated 5-Fu may be effective against the certain forms of cancer as its mechanism of action was gradual and more controlled. The two MgAl-LDHs (2:1 and 3:1) were found to embody a very crucial aspect that is much needed in drug delivery, i.e. the ability to selectively release contents in a lowered pH, which favours cancer cells, and in turn offering partial protection to normal cells (pH 7.4) Experimental analyses revealed that true MgAl-LDH nanoparticles were synthesized and that reconstruction allowed for the successful incorporation of the anticancer drug 5-Fu to form the nanohybrids MgAl 2:1-5-Fu and MgAl 3:1-5-Fu. Finally, free 5-Fu caused greater cell death than LDH bound 5-Fu, enforcing the LDH slow release properties. The ZnAl-LDHs (2:1 and 3:1) have also been found to be an effective drug delivery system for the delivery of 5-Fu. This nanoparticle allowed for a much more stable nanohybrid system inside which the anticancer drug can be encapsulated and delivered to be affected cells. Furthermore, it allowed for the steady release of 5-Fu to the cells under investigation. This property of ZnAl LDH, is similar to previously reported LDH delivery systems and hence require future focused studies. High IC_{50} values observed for the nanohybrid against the cells treated with pure 5-Fu, further revealed that the gradual release offered by this nanoparticle allows for the calming of 5-Fu's aggressive chemotherapeutic effects.

The simplistic and cost effective development of the LDHs (both MgAl and ZnAl) nanoparticles presents an opportunity for the development of DDSs that are inexpensive as well as quick to manufacture. These nanoparticles can also help to alleviate the cost of chemotherapy to millions of people affected by cancer. The unique properties of these nanoparticles mean a more targeted, yet simplistic mode of drug delivery. The challenge to cancer researchers today is not the

discovery of new anticancer drugs, but rather the development of more effective and less costly drug delivery systems.

5.2 Future improvements and prospects.

1. A more targeted mode of delivery with LDHs can be achieved by the incorporation of coating targeting moieties onto the surface of this nanoparticle.
2. The incorporation of other drugs in these LDHs is also an important aspect to look at, either as individual drug formulations or combination-type of drug delivery.
3. The unique chemistry of the intercalation of substances in LDHs is another aspect worth looking at, in terms of bond chemistry and electrostatic interaction of incorporated substances
4. Further studies using more cell lines *in vitro* for a broader spectrum of cytotoxicity profile can be conducted, and later extended to an *in vivo* animal model.

APPENDIX

Appendix A.1

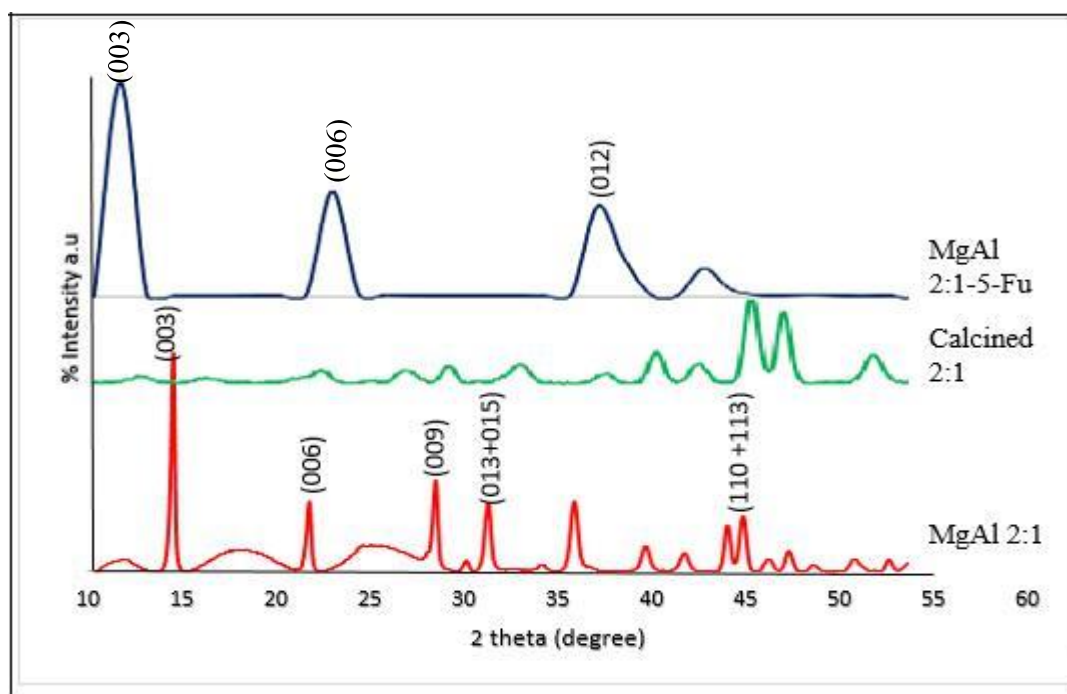


Figure 1: Xrd-spectra (MgAl 2:1, C alcined MgAl 2:1 and MgAl 2:1-5-Fu)

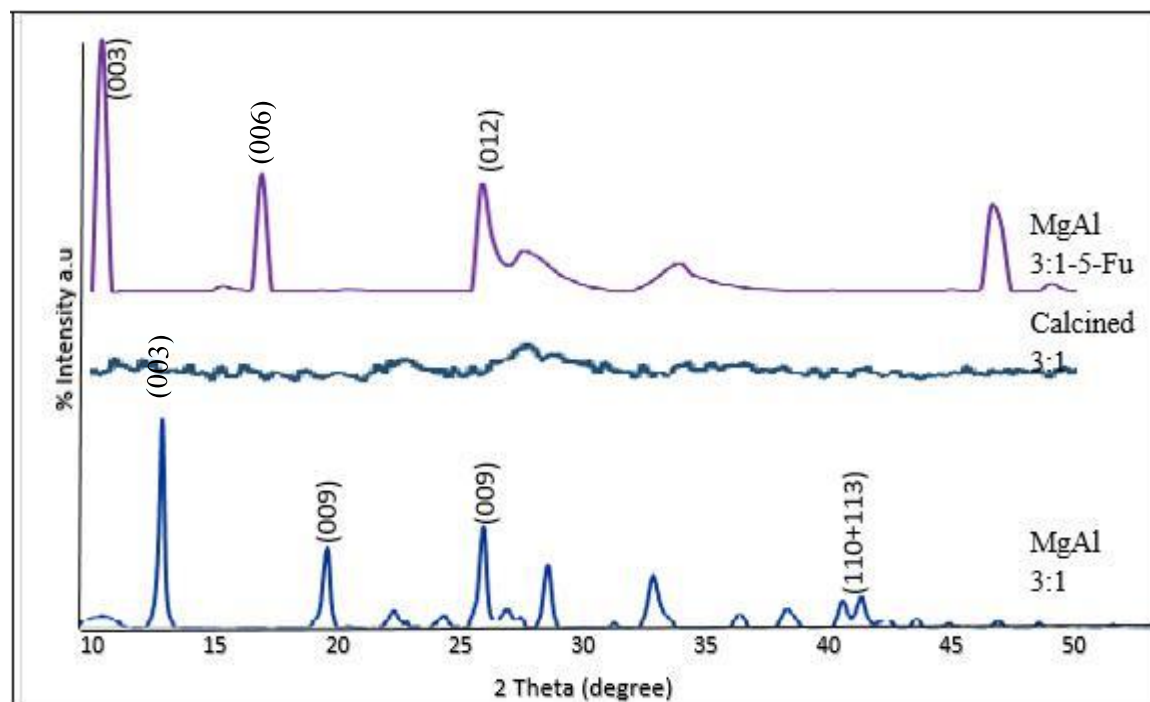


Figure 2: Xrd-spectra (MgAl 2:1, C alcined MgAl 2:1 and MgAl 2:1-5-Fu)

APPENDIX A.2

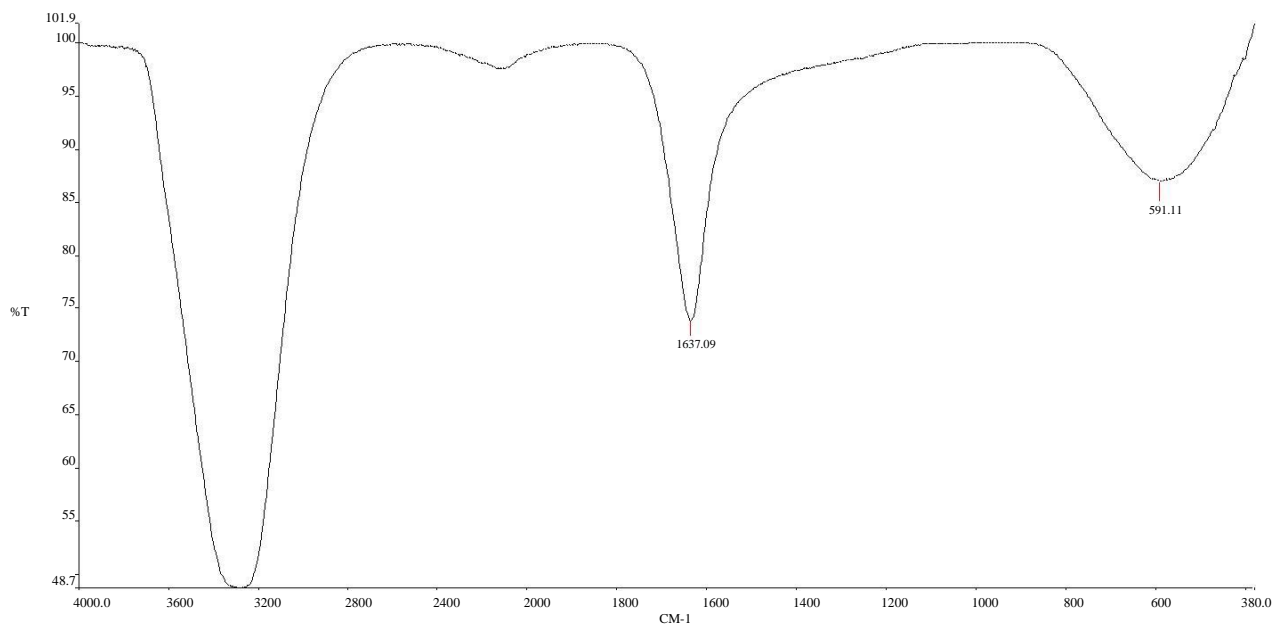


Figure 3 :FTIR Spectrum of 5-Fu

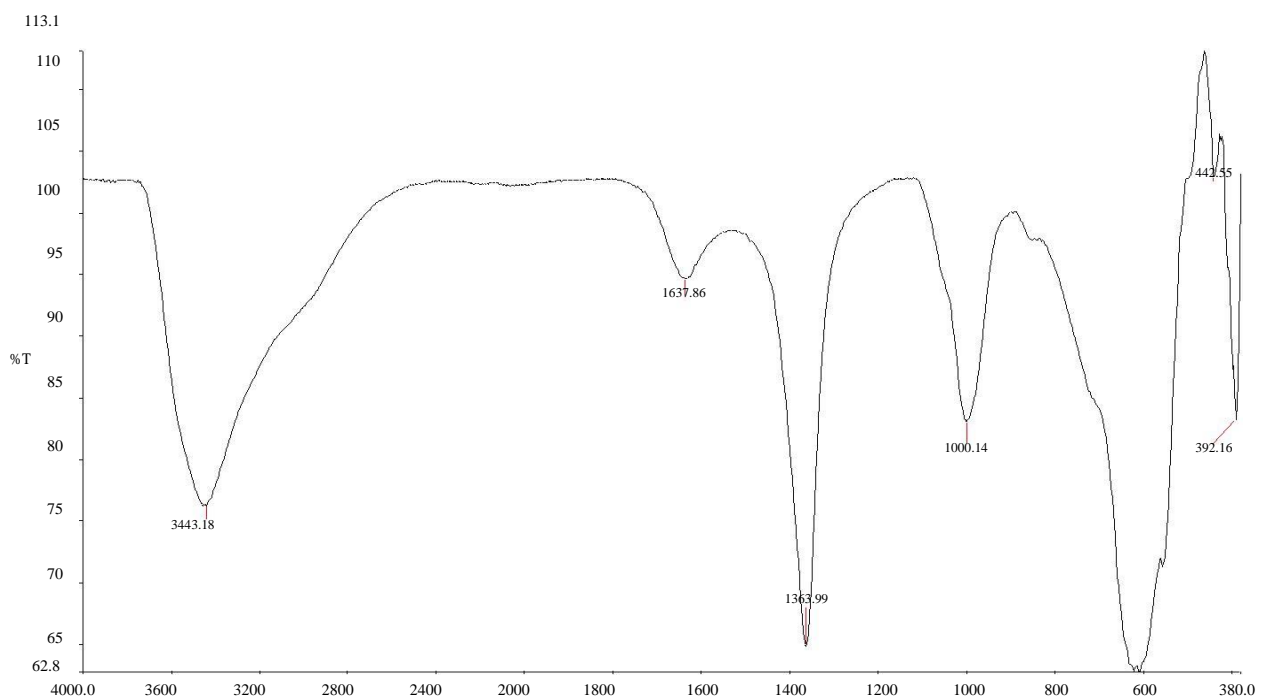


Figure 4 :FTIR spectrum of 5-Fu

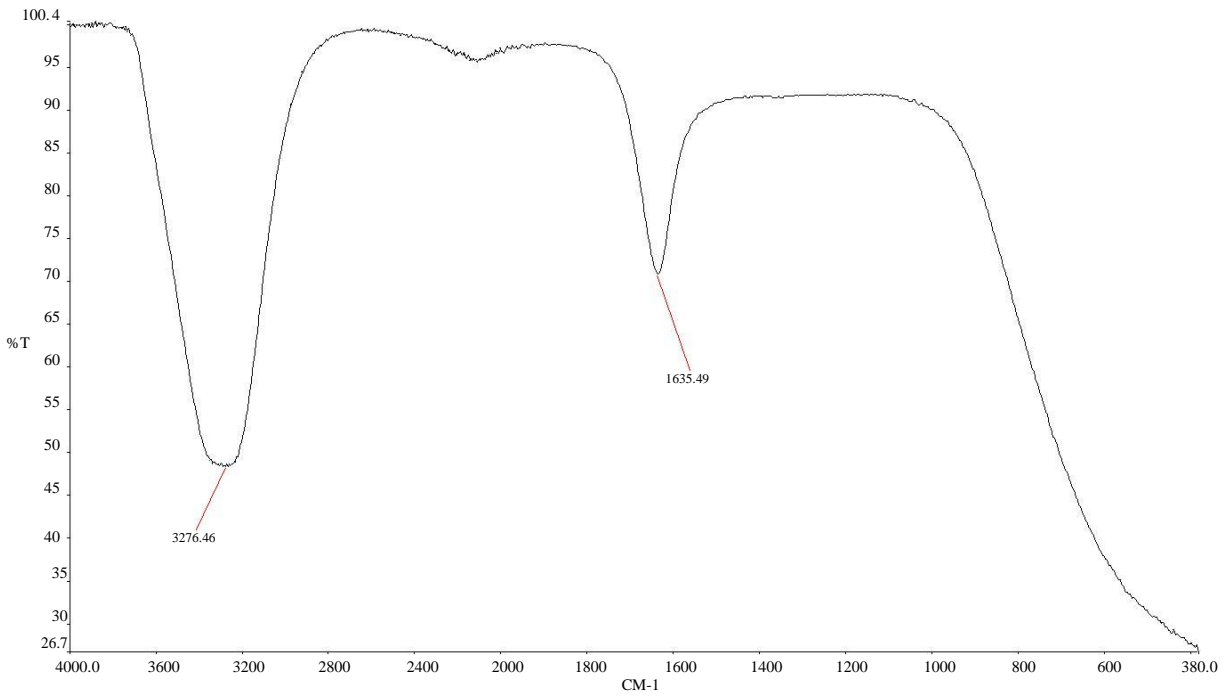


Figure 5 :FTIR spectratrum of MgAl 2:1-5-Fu

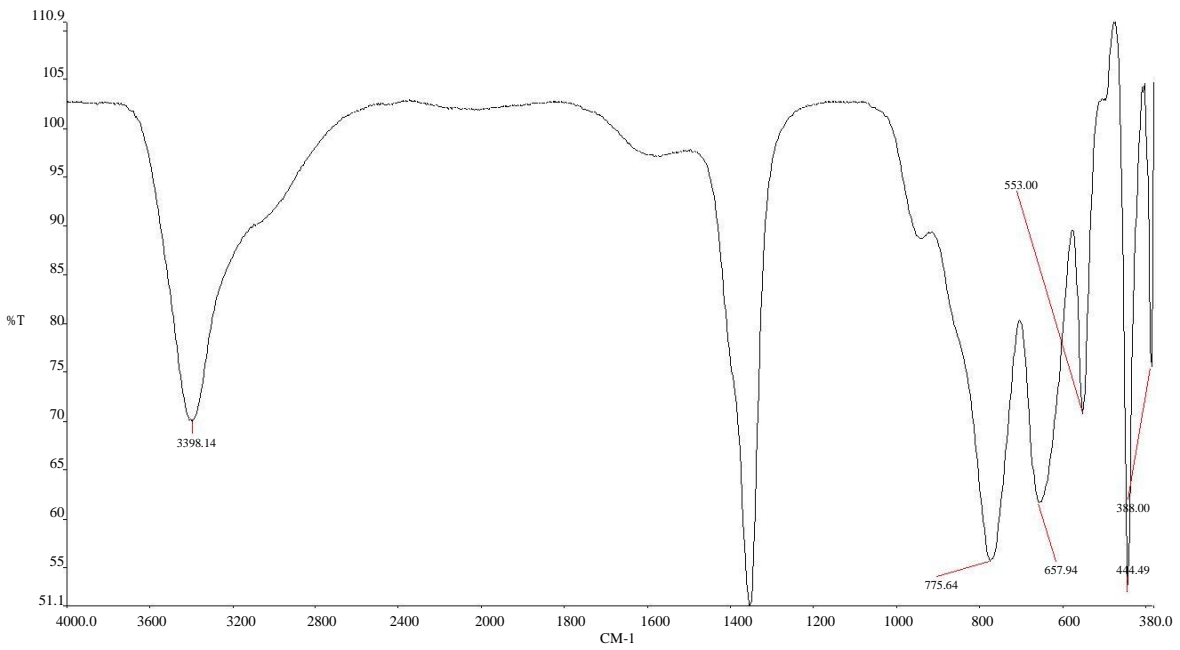


Figure 6 :FTIR spectra of MgA 3:1

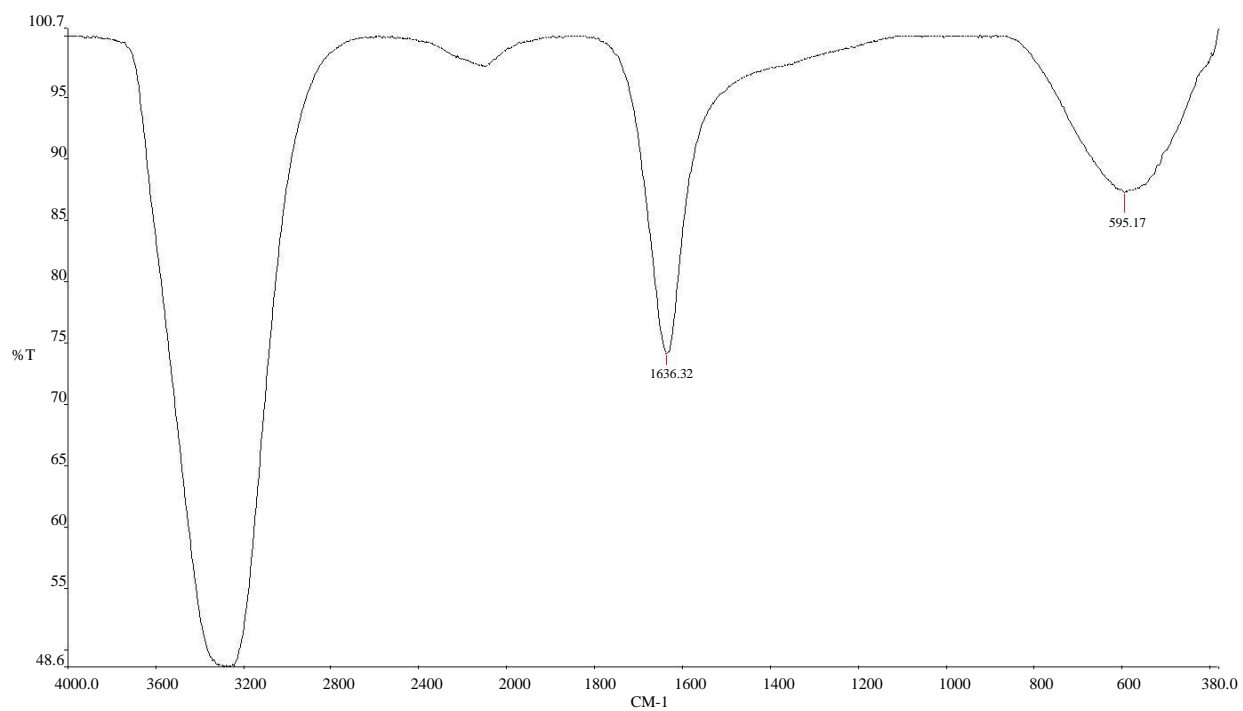


Figure 7 :FTIR spectrum of MgAl 3:1-5-Fu

FTIR Bond absorption frequencies recorded for MgAl 2:1, MgAl 2:1-5-Fu, MgAl 3:1MgAl 3:1-5-Fu and 5-Fu

APPENDIX A.3

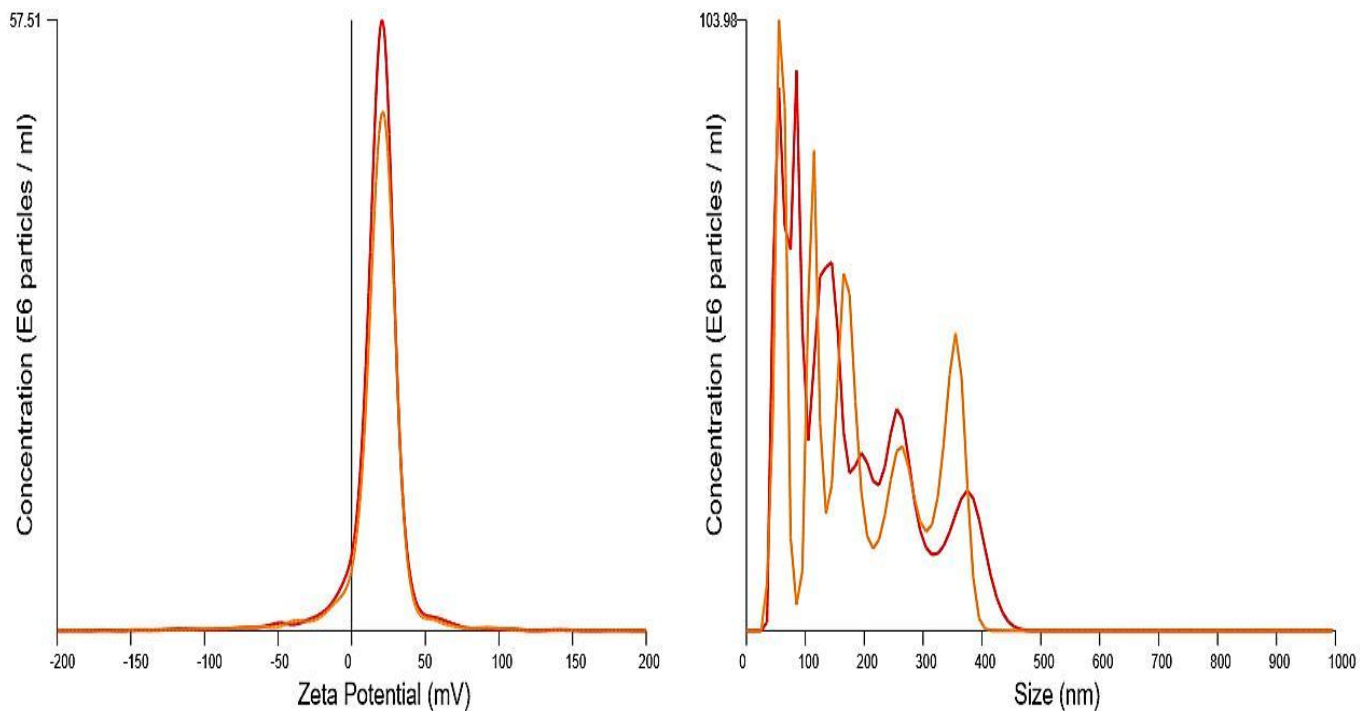


Figure 8: (a) Zeta potential (mV) of MgAl 2:1 (pristine) (b) Size(nm) of MgAl 2:1 (Pristine).

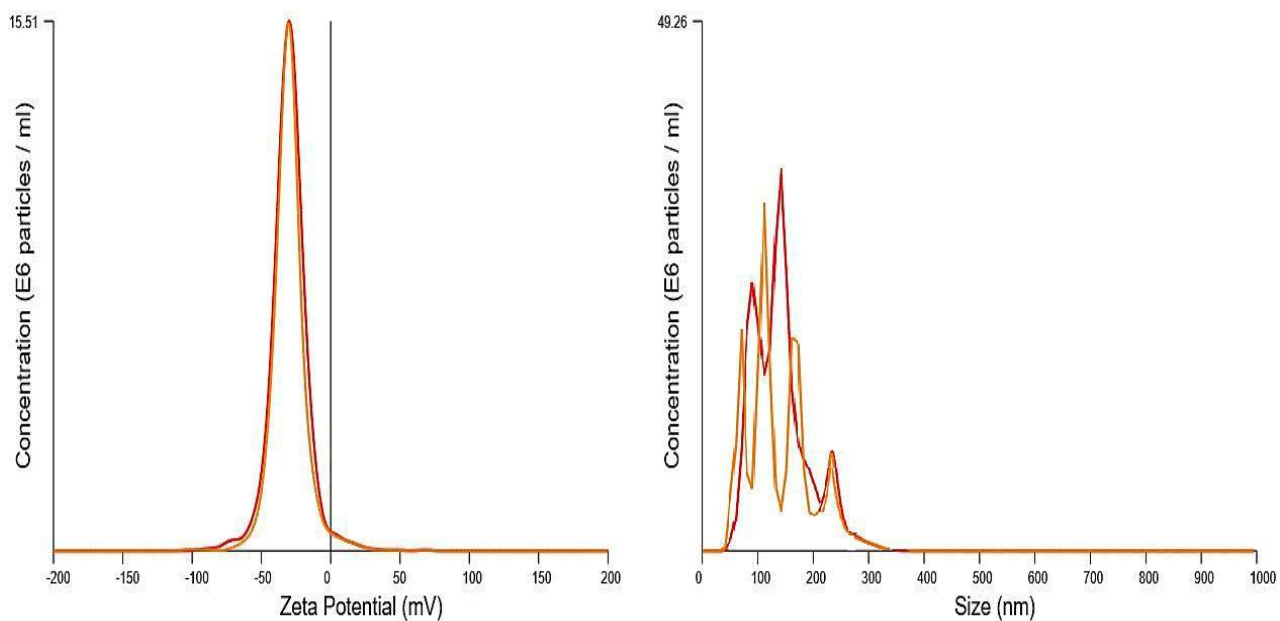


Figure 9: (a) Zeta potential (mV) of MgAl 2:1-5-Fu and (b) Size (nm) of MgAl-5-Fu.

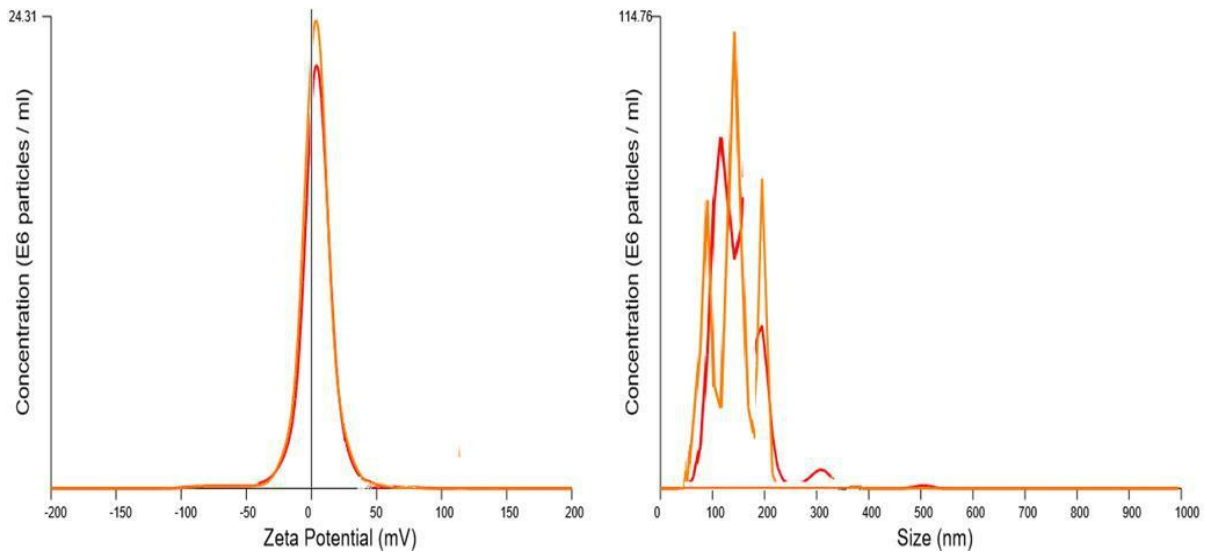


Figure 10: (a) Zeta potential (mV) of MgAl 3:1 and (b) Size (nm) of MgAl 3:1.

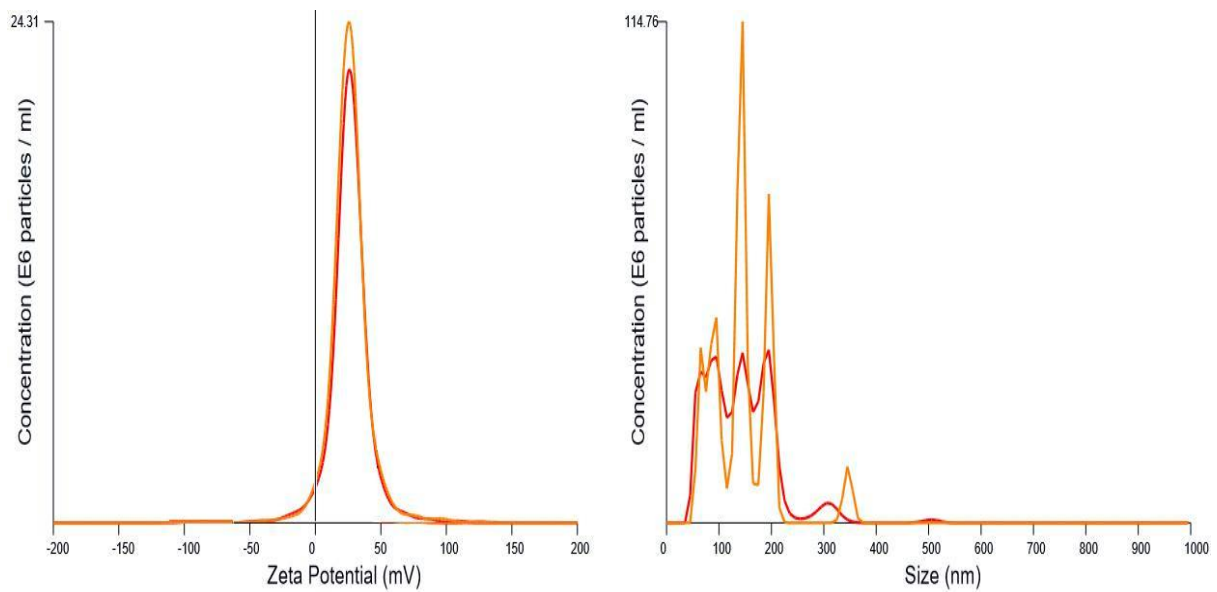


Figure 11: (a) Zeta potential (mV) of MgAl 3:1-5-Fu and (b) Size (nm) of MgAl 3:1-5-Fu.

APPENDIX B.1

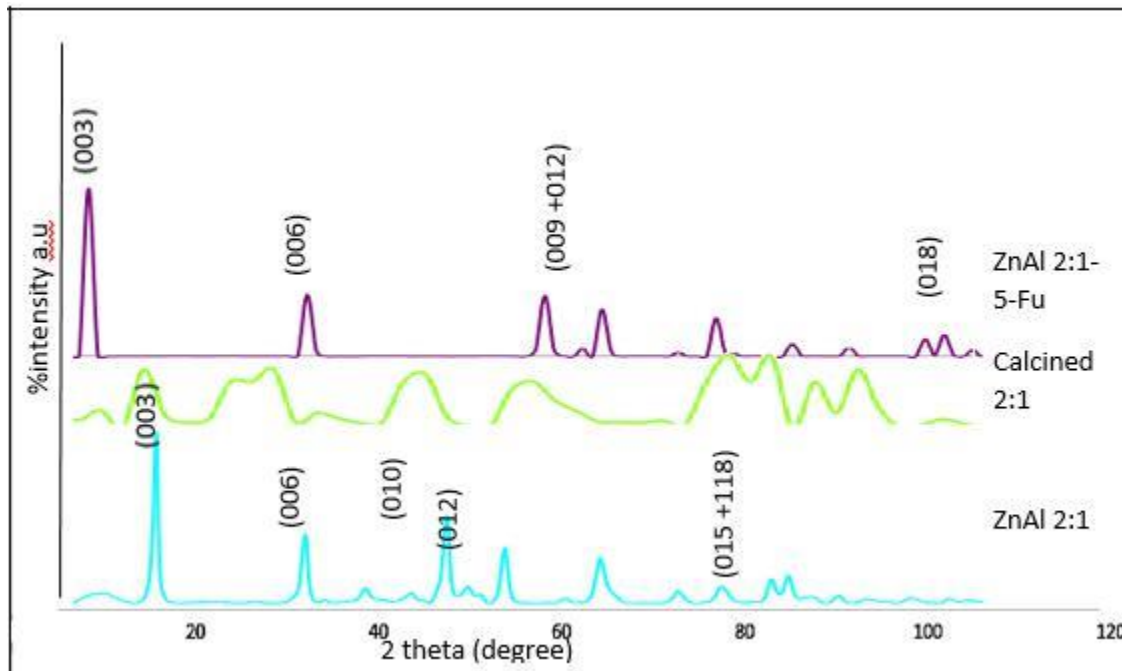


Figure 12: Xrd-spaetra (ZnAl 2:1,Calcined ZnAl 2:1 and ZnAl 2:1-5-Fu).

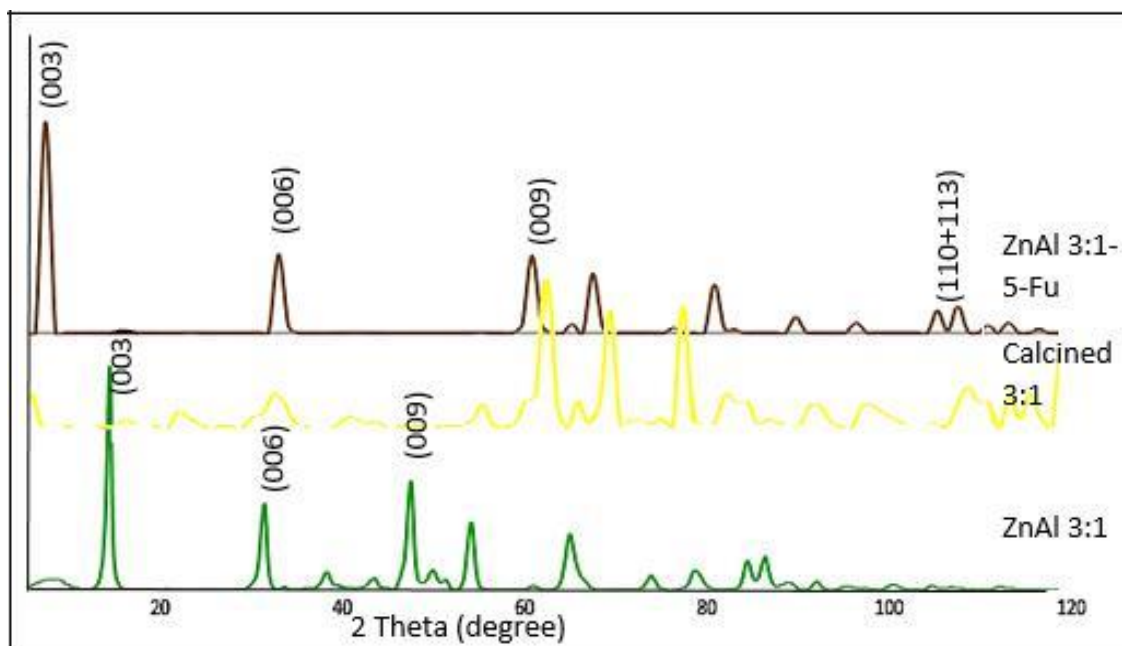


Figure 13 Xrd-spaetra (ZnAl 3:1, calcined ZnAl 3:1 and ZnAl 3:1-5-Fu).

APPENDIX B.2

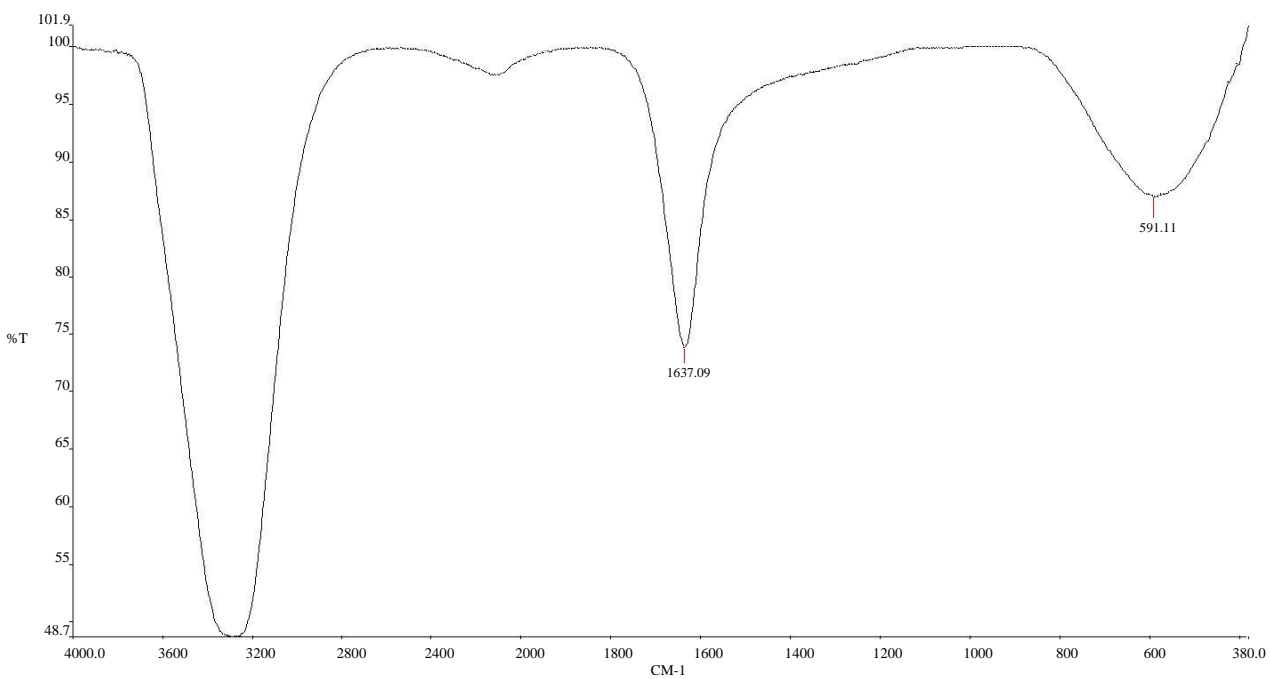


Figure 15: FTIR spectrum of 5-Fu.

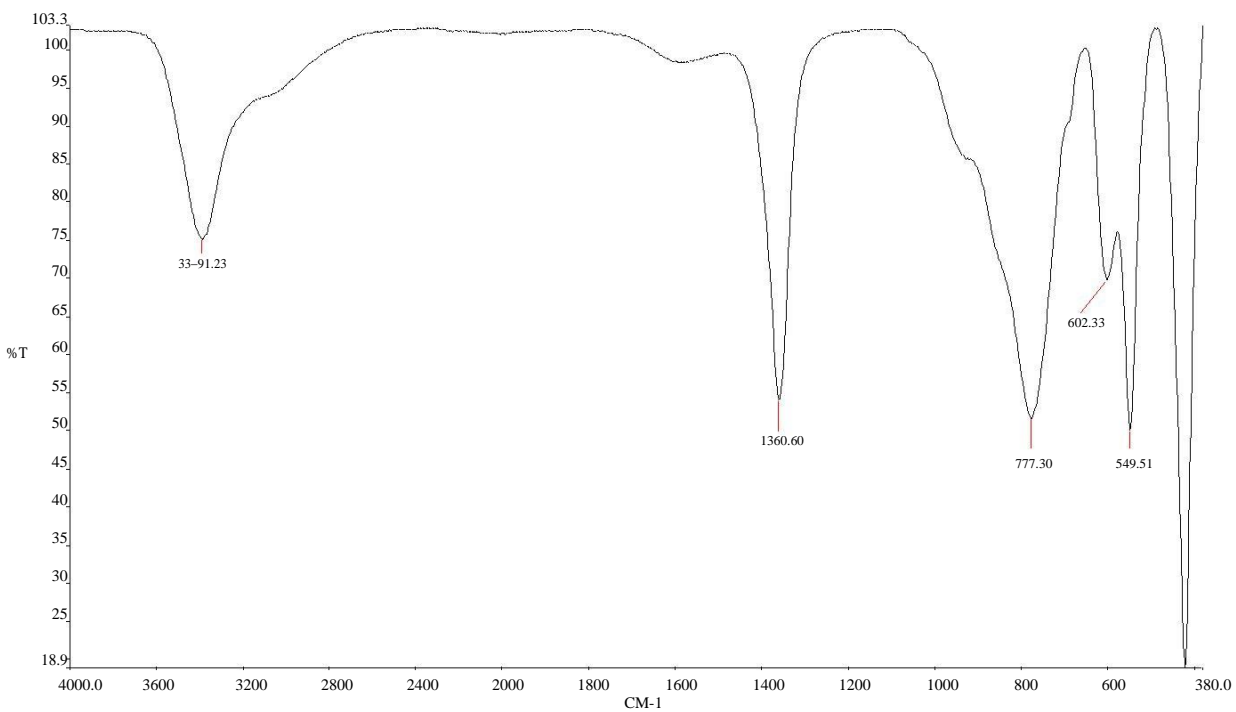


Figure 16 : FTIR spectrum of ZnAl 2:1.

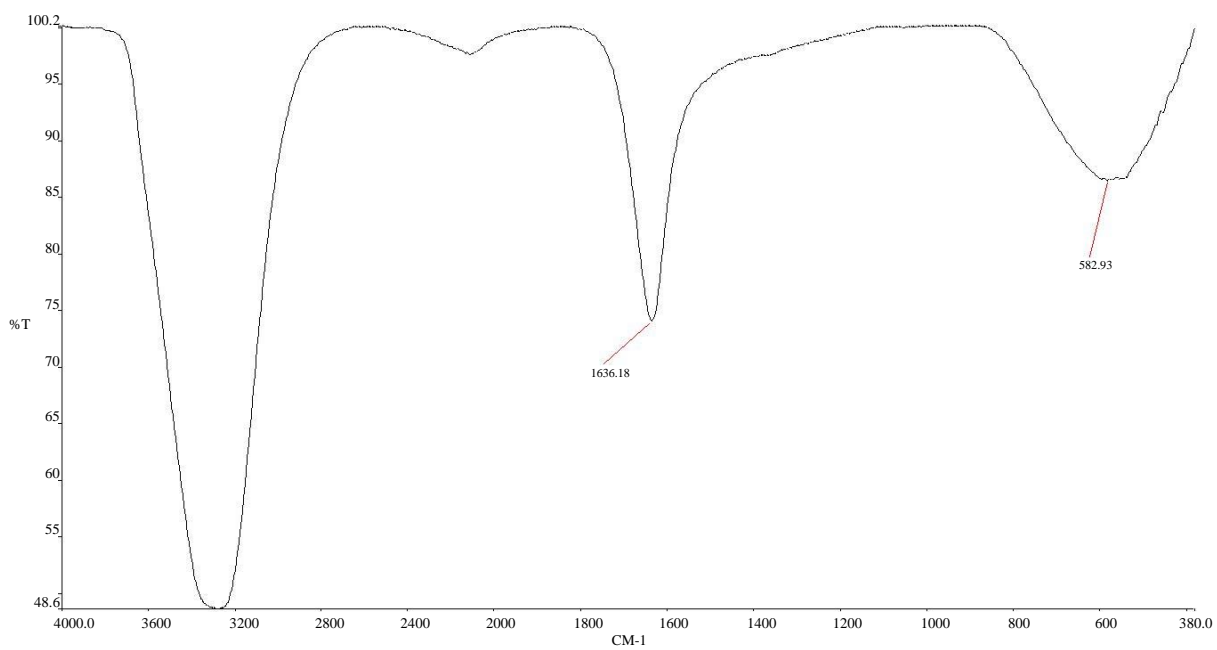


Figure 17:FTIR spectrtrum of ZnAl 2:1-5-Fu.

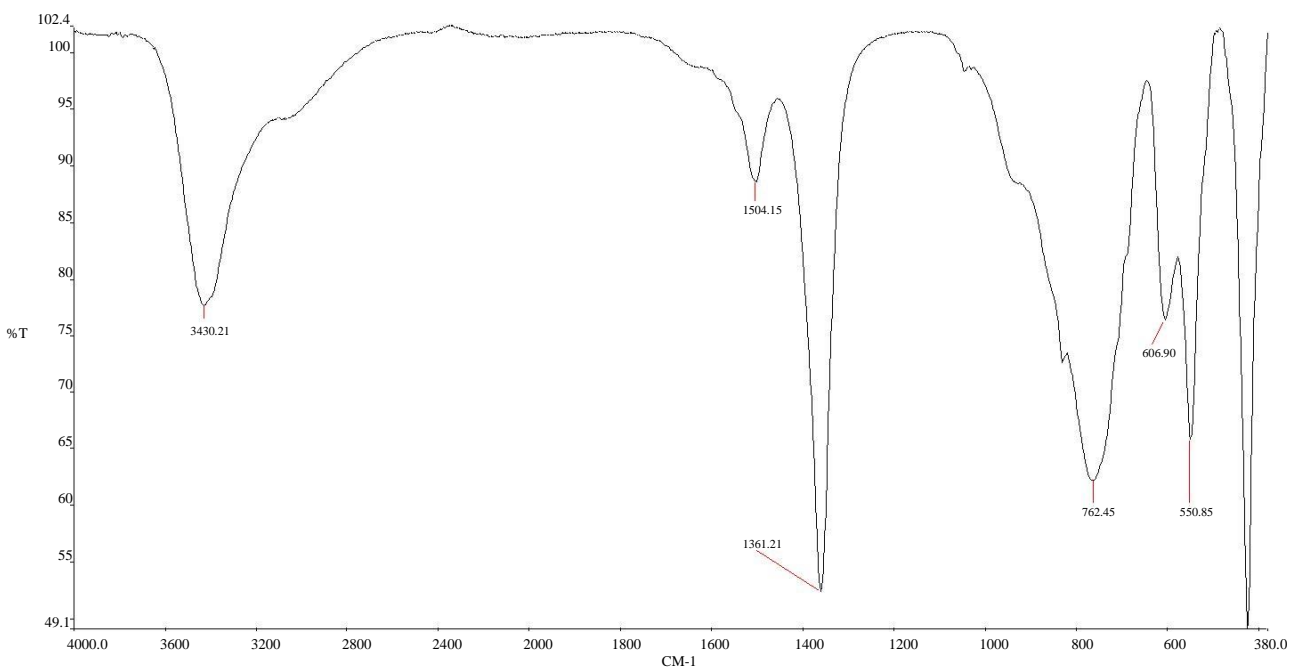


Figure 18 :FTIR spectrum of ZnAl 3:1.

ZnAl 3:1-5-Fu

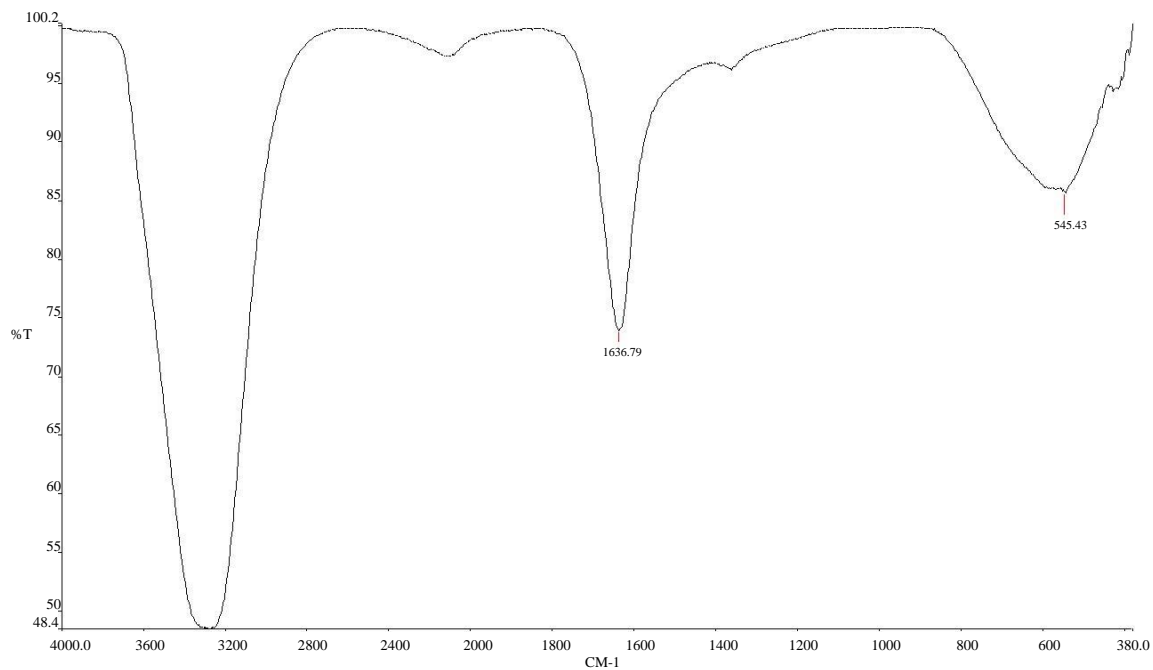


Figure 19 :FTIR spectrum of ZnAl 3:1-5-Fu.

FTIR Spectra bands of the respective LDHs and their nanohybrids.

APPENDIX B.3

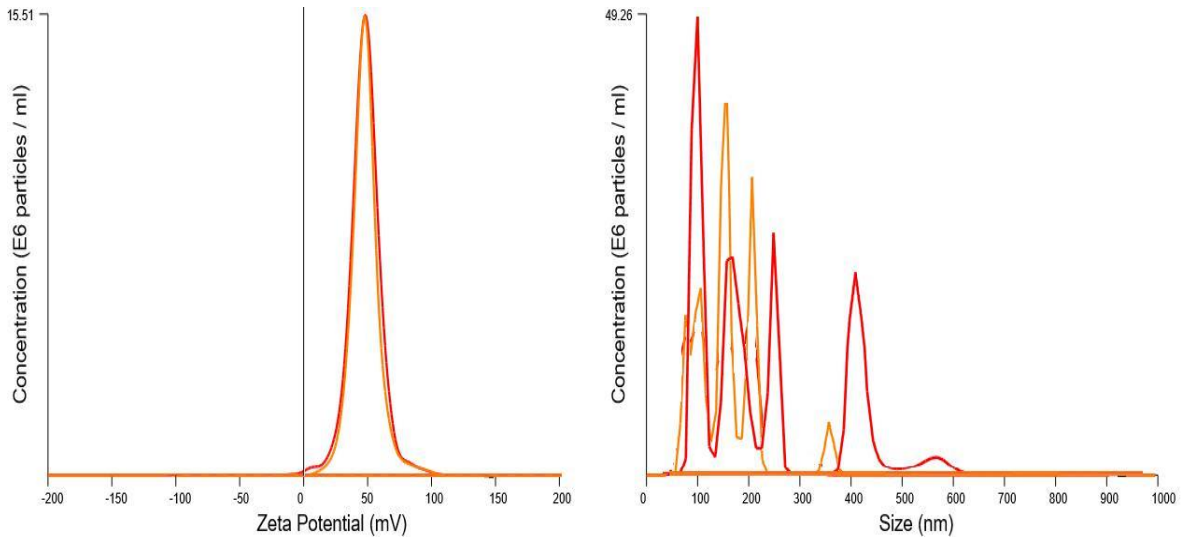


Figure 20: (a) Zeta potential (mV) of pristine ZnAl 2:1 (b) Size(nm) of ZnAl 2:1.

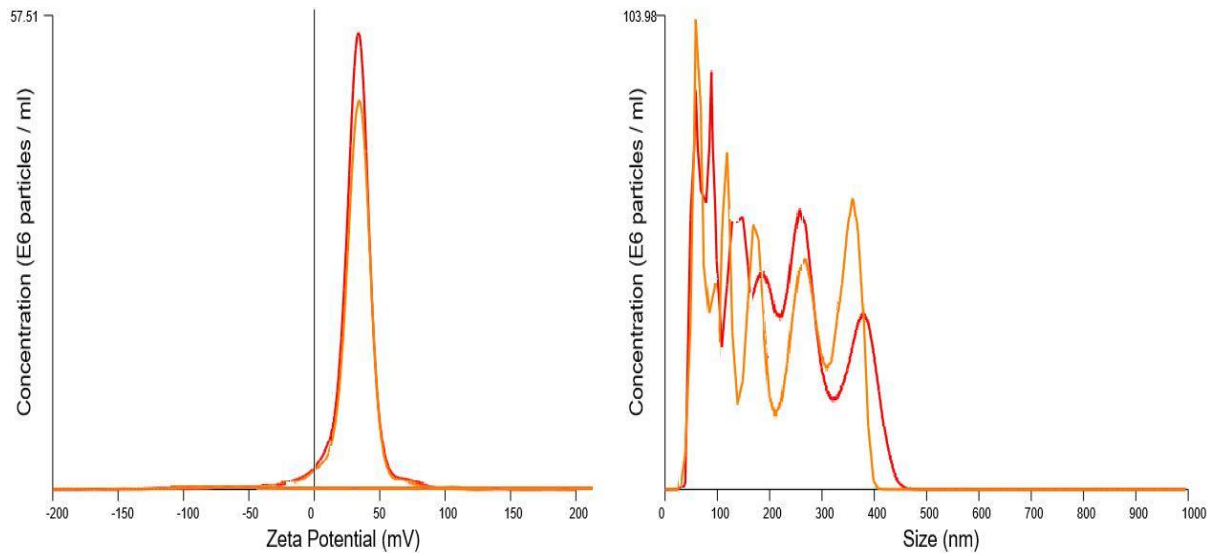


Figure 21: (a) Zeta potential (mV) of ZnAl 2:1-5-Fu (b) Size(nm) of ZnAl 2:1-5-Fu.

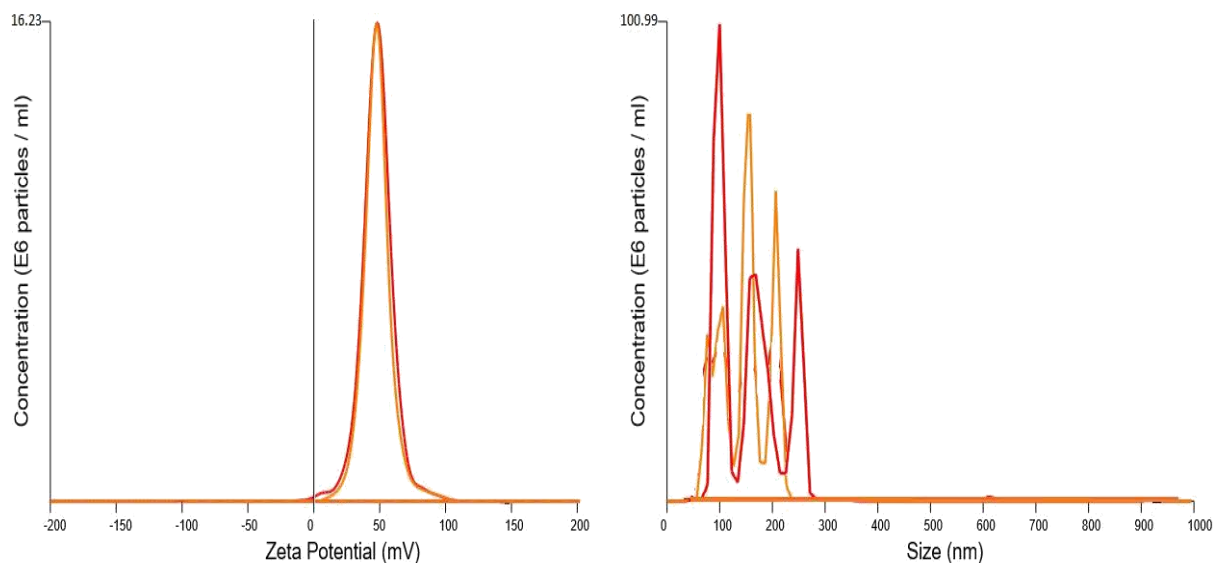


Figure 22 : (a) Zeta potential (mV) of pristine ZnAl 3:1 (b) Size(nm) of ZnAl 3:1.

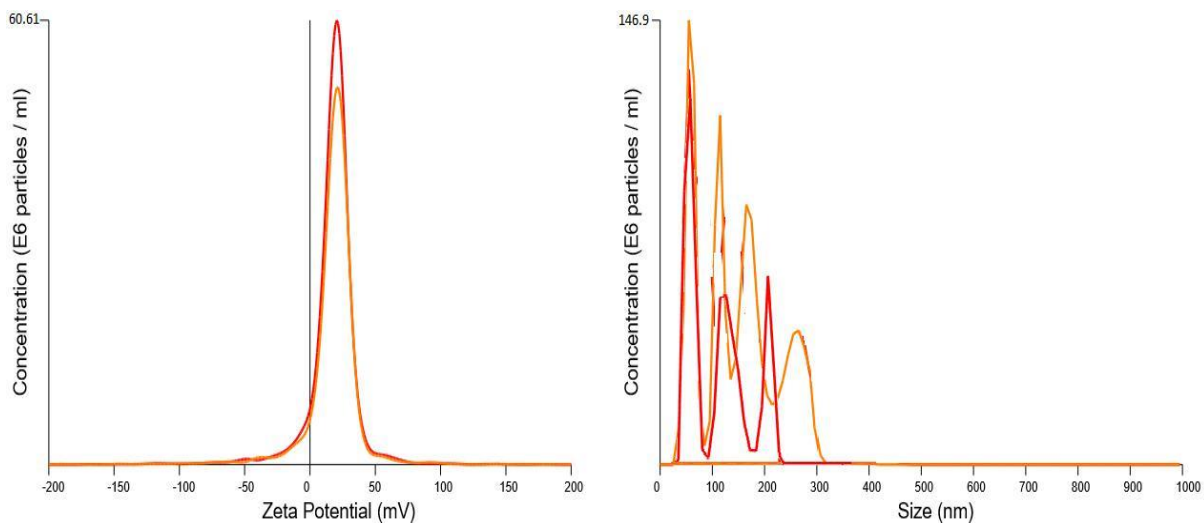


Figure 23 : (a) Zeta potential (mV) of pristine ZnAl 3:-5-Fu (b) Size(nm) of ZnAl 3:-5-Fu.

Mean Data									
ID: Calib Blank 1		Seq. No.: 1			A/S Pos: 9				
Sample Qty: g		Prep. Vol.:		Dilution:		Date: 2016/05/05 09:39:1			
Analyte	Corr. Intensity	Conc (Calib)	Std. Dev.	Calib Units	Conc (Sample)	Std. Dev.	Sample Units	RSD	
Al 396.153	232.9	[0.00]	10.37	mg/L				4.45 %	
Al 308.215	217.2	[0.00]	7.62	mg/L				3.51 %	
Al 394.401	130.9	[0.00]	5.32	mg/L				4.07 %	
Mg 285.213	411.4	[0.00]	12.33	mg/L				3.00 %	
Mg 279.077	10.3	[0.00]	6.59	mg/L				64.03 %	
Mg 280.271	1,281.3	[0.00]	22.01	mg/L				1.72 %	
Zn 206.200	60.0	[0.00]	3.59	mg/L				5.99 %	
Zn 213.857	398.9	[0.00]	22.17	mg/L				5.56 %	
Zn 202.548	115.0	[0.00]	5.99	mg/L				5.21 %	

Mean Data									
ID: Calib Std 1		Seq. No.: 2			A/S Pos: 10				
Sample Qty: g		Prep. Vol.:		Dilution:		Date: 2016/05/05 09:41:21			
Analyte	Corr. Intensity	Conc (Calib)	Std. Dev.	Calib Units	Conc (Sample)	Std. Dev.	Sample Units	RSD	
Al 396.153	130,915.0	[20]	1,250.10	mg/L				0.95 %	
Al 308.215	22,872.0	[20]	184.64	mg/L				0.81 %	
Al 394.401	60,991.4	[20]	507.12	mg/L				0.83 %	

Mean Data									
ID: Calib Std 2		Seq. No.: 3			A/S Pos: 11				
Sample Qty: g		Prep. Vol.:		Dilution:		Date: 2016/05/05 09:43:51			
Analyte	Corr. Intensity	Conc (Calib)	Std. Dev.	Calib Units	Conc (Sample)	Std. Dev.	Sample Units	RSD	
Al 396.153	191,187.3	[30]	1,714.51	mg/L				0.90 %	
Al 308.215	33,584.2	[30]	133.43	mg/L				0.40 %	
Al 394.401	89,445.3	[30]	353.72	mg/L				0.40 %	

Mean Data									
ID: Calib Std 3		Seq. No.: 4			A/S Pos: 12				
Sample Qty: g		Prep. Vol.:		Dilution:		Date: 2016/05/05 09:46:11			
Analyte	Corr. Intensity	Conc (Calib)	Std. Dev.	Calib Units	Conc (Sample)	Std. Dev.	Sample Units	RSD	
Al 396.153	255,412.9	[40]	3,698.83	mg/L				1.45 %	
Al 308.215	44,962.4	[40]	688.10	mg/L				1.53 %	
Al 394.401	119,032.4	[40]	1,637.51	mg/L				1.38 %	

Mean Data									
ID: Calib Std 4		Seq. No.: 5			A/S Pos: 13				
Sample Qty: g		Prep. Vol.:		Dilution:		Date: 2016/05/05 09:48:3			
Analyte	Corr. Intensity	Conc (Calib)	Std. Dev.	Calib Units	Conc (Sample)	Std. Dev.	Sample Units	RSD	
Al 396.153	312,322.0	[50]	1,267.58	mg/L				0.41 %	
Al 308.215	55,621.6	[50]	102.27	mg/L				0.18 %	
Al 394.401	147,351.4	[50]	344.99	mg/L				0.23 %	

Mean Data									
ID: Calib Std 5		Seq. No.: 6			A/S Pos: 14				
Sample Qty: g		Prep. Vol.:		Dilution:		Date: 2016/05/05 09:50:51			
Analyte	Corr. Intensity	Conc (Calib)	Std. Dev.	Calib Units	Conc (Sample)	Std. Dev.	Sample Units	RSD	
Al 396.153	373,543.4	[60]	1,657.44	mg/L				0.44 %	
Al 308.215	66,156.9	[60]	313.77	mg/L				0.47 %	
Al 394.401	175,304.7	[60]	553.68	mg/L				0.32 %	

n Data

Calib Std 6

Seq. No.: 7

A/S Pos: 15

APPENDIX C

Sample Qty:	g	Prep. Vol.:	Dilution:	:	Date:		
Analyte	Corr. Intensity	Conc (Calib)	Std. Dev.	Calib Units	Conc (Sample) Std. Dev.	Sample Units	RSD
Mg 285.213	435,068.8	[20]	5,584.82	mg/L			1.28 %
Mg 279.077	14,179.3	[20]	177.80	mg/L			1.25 %
Mg 280.271	1,293,720.2	[20]	18,986.22	mg/L			1.47 %

Mean Data

ID: Calib Std 7
zn al 3:1

Seq. No.: 8
Seq. No.: 19

A/S Pos: 16
A/S Pos: 27

Sample Qty:	g	Prep. Vol.:	Dilution:	:	Date:		
Analyte	Corr. Intensity	Conc (Calib)	Std. Dev.	Calib Units	Conc (Sample) Std. Dev.	Sample Units	RSD
Mg 285.213	93,981.6	[30]	4,079.84	mg/L	5.039	0.0355	0.87 %
Al 396.153	20,988.1	[20]	0.4232	mg/L	5.443	0.0232	0.69 %
Mg 279.077	6,432.1	[20]	0.0236	mg/L	5.113	0.0364	0.78 %
Mg 280.271	1,896,662.9	[20]	14,868.36	mg/L			
Mg 285.213	1,872.2	-0.557	0.0005	mg/L	-0.557	0.0005	0.08 %
Mg 279.077	64.4	0.377	0.0042	mg/L	0.377	0.0042	1.13 %

ID: Calib Std 8

Sample Qty:	g	Prep. Vol.:	Dilution:	:	Date:		
Analyte	Corr. Intensity	Conc (Calib)	Std. Dev.	Calib Units	Conc (Sample) Std. Dev.	Sample Units	RSD
Zn 206.200	20,491.4	42.15	0.282	mg/L	42.15	0.282	0.67 %
Mg 285.213	135,580.2	0.008	0.0002	mg/L	41.08	0.320	0.08 %
Mg 279.077	38,830.3	42.67	0.236	mg/L	42.07	0.236	0.55 %
Mg 280.271	2,488,130.6	[40]	23,900.00	mg/L			0.96 %

Mean Data

Sample Qty:	g	Prep. Vol.:	Dilution:	:	Date:		
Analyte	Corr. Intensity	Conc (Calib)	Std. Dev.	Calib Units	Conc (Sample) Std. Dev.	Sample Units	RSD
Al 396.153	51,547.4	7.721	0.0890	mg/L	7.721	0.0890	1.15 %
Al 308.215	9,425.4	8.157	0.0367	mg/L	8.157	0.0367	0.45 %
Al 354.401	24,915.5	7.759	0.1142	mg/L	7.759	0.1142	0.96 %
Mg 285.213	1,031,941.8	-(150)	9,734.41	mg/L	-0.400	0.0049	0.94 %
Mg 279.077	308,844.9	-(150)	2,623.56	mg/L	-0.517	0.0021	0.98 %
Mg 280.271	3,088,658.3	-(150)	28,517.71	mg/L	43.04	0.178	0.92 %
Zn 213.857	131,537.7	39.81	0.523	mg/L	39.81	0.523	1.31 %
Zn 202.548	37,538.0	41.19	0.711	mg/L	41.19	0.711	1.73 %

ID: Calib Std 10

Seq. No.: 11

A/S Pos: 19

Sample Qty:	g	Prep. Vol.:	Dilution:	:	Date:		
Analyte	Corr. Intensity	Conc (Calib)	Std. Dev.	Calib Units	Conc (Sample) Std. Dev.	Sample Units	RSD
Mg 285.213	1,231,782.4	[60]	10,747.99	mg/L			0.87 %
Mg 279.077	40,950.9	[60]	416.95	mg/L			1.02 %
Mg 280.271	3,682,762.7	[60]	37,903.83	mg/L			1.03 %

Mean Data

ID: Calib Std 11

Seq. No.: 12

A/S Pos: 20

Sample Qty:	g	Prep. Vol.:	Dilution:	:	Date:		
Analyte	Corr. Intensity	Conc (Calib)	Std. Dev.	Calib Units	Conc (Sample) Std. Dev.	Sample Units	RSD
Zn 206.200	10,722.0	[20]	27.33	mg/L			0.25 %
Zn 213.857	74,646.3	[20]	155.50	mg/L			0.21 %
Zn 202.548	20,312.4	[20]	144.20	mg/L			0.71 %

Mean Data

ID: Calib Std 12

Seq. No.: 13

A/S Pos: 21

Sample Qty:	g	Prep. Vol.:	Dilution:	:	Date:		
Analyte	Corr. Intensity	Conc (Calib)	Std. Dev.	Calib Units	Conc (Sample) Std. Dev.	Sample Units	RSD
Zn 206.200	14,688.1	[30]	160.37	mg/L			1.09 %

3.857	101,300.7	[30]	805.37	mg/L					0.80 %
02.548	27,701.8	[30]	306.66	mg/L					1.11 %

Mean Data

ID: Calib Std 13		Seq. No.: 14			A/S Pos: 22				
Sample Qty:	g	Prep. Vol.:	Dilution:		:	Date: 2016/05/05 10:09:2			
Analyte	Corr. Intensity	Conc (Calib)	Std. Dev.	Calib Units	Conc (Sample)	Std. Dev.	Sample Units	RSD	
Zn 206.200	19,787.7	[40]	107.28	mg/L					0.54 %
Zn 213.857	133,703.8	[40]	522.14	mg/L					0.39 %
Zn 202.548	37,073.2	[40]	234.43	mg/L					0.63 %

Mean Data

ID: Calib Std 14		Seq. No.: 15			A/S Pos: 23				
Sample Qty:	g	Prep. Vol.:	Dilution:		:	Date: 2016/05/05 10:11:4			
Analyte	Corr. Intensity	Conc (Calib)	Std. Dev.	Calib Units	Conc (Sample)	Std. Dev.	Sample Units	RSD	
Zn 206.200	23,990.0	[50]	6.86	mg/L					0.03 %
Zn 213.857	162,684.1	[50]	797.57	mg/L					0.49 %
Zn 202.548	44,874.5	[50]	185.07	mg/L					0.41 %

Mean Data

ID: Calib Std 15		Seq. No.: 16			A/S Pos: 24				
Sample Qty:	g	Prep. Vol.:	Dilution:		:	Date: 2016/05/05 10:14:0			
Analyte	Corr. Intensity	Conc (Calib)	Std. Dev.	Calib Units	Conc (Sample)	Std. Dev.	Sample Units	RSD	
Zn 206.200	28,700.1	[60]	260.14	mg/L					0.91 %
Zn 213.857	193,278.1	[60]	1,129.79	mg/L					0.58 %
Zn 202.548	53,621.1	[60]	335.45	mg/L					0.63 %

Mean Data

ID: mg al 3:1		Seq. No.: 17			A/S Pos: 25				
Sample Qty:	g	Prep. Vol.:	Dilution:		:	Date: 2016/05/05 10:22:3			
Analyte	Corr. Intensity	Conc (Calib)	Std. Dev.	Calib Units	Conc (Sample)	Std. Dev.	Sample Units	RSD	
Al 396.153	45,402.0	6.731	0.0454	mg/L	6.731	0.0454	mg/L		0.67 %
Al 308.215	8,546.5	7.360	0.0151	mg/L	7.360	0.0151	mg/L		0.20 %
Al 394.401	21,573.4	6.922	0.0681	mg/L	6.922	0.0681	mg/L		0.98 %
Mg 285.213	409,230.9	19.39	0.148	mg/L	19.39	0.148	mg/L		0.76 %
Mg 279.077	13,764.5	19.87	0.053	mg/L	19.87	0.053	mg/L		0.27 %
Mg 280.271	1,283,455.8	20.39	0.152	mg/L	20.39	0.152	mg/L		0.74 %
Zn 206.200	28.8	-1.051	0.0150	mg/L	-1.051	0.0150	mg/L		1.42 %
Zn 213.857	200.6	-1.471	0.0157	mg/L	-1.471	0.0157	mg/L		1.07 %
Zn 202.548	41.7	-1.246	0.0113	mg/L	-1.246	0.0113	mg/L		0.91 %

Mean Data

ID: mg al 2:1		Seq. No.: 18			A/S Pos: 26				
Sample Qty:	g	Prep. Vol.:	Dilution:		:	Date: 2016/05/05 10:25:1			
Analyte	Corr. Intensity	Conc (Calib)	Std. Dev.	Calib Units	Conc (Sample)	Std. Dev.	Sample Units	RSD	
Al 396.153	65,277.1	9.932	0.0041	mg/L	9.932	0.0041	mg/L		0.04 %
Al 308.215	12,220.5	10.69	0.045	mg/L	10.69	0.045	mg/L		0.42 %
Al 394.401	31,002.2	10.15	0.013	mg/L	10.15	0.013	mg/L		0.12 %
Mg 285.213	396,808.1	18.78	0.027	mg/L	18.78	0.027	mg/L		0.14 %
Mg 279.077	13,368.7	19.28	0.031	mg/L	19.28	0.031	mg/L		0.16 %
Mg 280.271	1,235,991.3	19.61	0.058	mg/L	19.61	0.058	mg/L		0.30 %
Zn 206.200	-9.7	-1.132	0.0052	mg/L	-1.132	0.0052	mg/L		0.46 %
Zn 213.857	-65.0	-1.554	0.0005	mg/L	-1.554	0.0005	mg/L		0.03 %
Zn 202.548	-33.2	-1.331	0.0047	mg/L	-1.331	0.0047	mg/L		0.35 %

